NAVAL POSTGRADUATE SCHOOL
Monterey, California

THESIS

SOOT PARTICLE SIZE AND CONCENTRATION DETERMINATION FROM A KEROSENE/GASEOUS OXYGEN ROCKET PLUME

by

Silvino L.C. Silva

December 1998

Thesis Advisor:	David W. Netzer
Thesis Co-Advisor:	Christopher M. Brophy
Second Reader:	Oscar Biblarz

Approved for public release; distribution is unlimited.

19990120 044

REPORT DOCUMENTATION PAGE

Form Approved
OMB No. 0704-0188

Public reporting burden for this collection of information is estimated to average 1 hour per response, including the time for reviewing instruction, searching existing data sources, gathering and maintaining the data needed, and completing and reviewing the collection of information. Send comments regarding this burden estimate or any other aspect of this collection of information, including suggestions for reducing this burden, to Washington headquarters Services, Directorate for Information Operations and Reports, 1215 Jefferson Davis Highway, Suite 1204, Arlington, VA 22202-4302, and to the Office of Management and Budget, Paperwork Reduction Project (0704-0188) Washington DC 20503.

1. AGENCY USE ONLY *(Leave blank)*	2. REPORT DATE December 1998	3. REPORT TYPE AND DATES COVERED Master's Thesis

4. TITLE AND SUBTITLE
SOOT PARTICLE SIZE AND CONCENTRATION DETERMINATION FROM A KEROSENE/GASEOUS OXYGEN ROCKET PLUME

5. FUNDING NUMBERS
NF046119800506

6. AUTHOR(S)
Silva, Silvino L. C.

7. PERFORMING ORGANIZATION NAME(S) AND ADDRESS(ES)
Naval Postgraduate School
Monterey, CA 93943-5000

8. PERFORMING ORGANIZATION REPORT NUMBER

9. SPONSORING / MONITORING AGENCY NAME(S) AND ADDRESS(ES)
Air Force Phillips Laboratory
10 East Saturn Blvd - Edwards AFB - CA 93524-7680

10. SPONSORING / MONITORING AGENCY REPORT NUMBER

11. SUPPLEMENTARY NOTES
The views expressed in this thesis are those of the author and do not reflect the official policy or position of the Department of Defense or the U.S. Government.

12a. DISTRIBUTION / AVAILABILITY STATEMENT
Approved for public release; distribution is unlimited.

12b. DISTRIBUTION CODE

13. ABSTRACT *(maximum 200 words)*

An experimental investigation was conducted to measure soot properties and concentration, and infrared signature of the plume of a kerosene/gaseous oxygen rocket motor. Multiple-wavelength measurements were used to obtain soot parameters. It was found that the multiple-wavelength technique appeared to work well for obtaining soot properties and concentration. The results implied that the soot particulate was very porous for the most fuel-rich conditions and became more compact as the O/F ratio increased. Soot mean diameter (D32) was less than 0.1 μm when the O/F ratio was less than 0.75, but increased to 0.2→0.36 μm for higher O/F ratios. The soot particle diameters obtained from the Scanning Electronic Microscope (SEM) photomicrographs of collected soot samples were in qualitative agreement with the diameters measured optically. Soot concentration in the plume was found to rapidly increase and then decrease as the O/F ratio was increased from 0.3 to 1.1, with a peak near O/F = 0.76. Infrared measurements in the 3.5-5 μm band indicated a probable shift in the dominant radiation source from gas to particulate as the soot concentration increased.

14. SUBJECT TERMS
Particle Sizing, Rocket Motors, Soot, Infrared Signature.

15. NUMBER OF PAGES 105

16. PRICE CODE

17. SECURITY CLASSIFICATION OF REPORT	18. SECURITY CLASSIFICATION OF THIS PAGE	19. SECURITY CLASSIFI- CATION OF ABSTRACT	20. LIMITATION OF ABSTRACT
Unclassified	Unclassified	Unclassified	UL

NSN 7540-01-280-5500

Standard Form 298 (Rev. 2-89)
Prescribed by ANSI Std. 239-18

Approved for public release; distribution is unlimited

SOOT PARTICLE SIZE AND CONCENTRATION DETERMINATION FROM A KEROSENE/GASEOUS OXYGEN ROCKET PLUME

Silvino L. C. Silva
Major, Brazil Air Force
B.S., Instituto Tecnologico de Aeronautica, 1980

Submitted in partial fulfillment of the
requirements for the degree of

MASTER OF SCIENCE IN AERONAUTICAL ENGINEERING

from the

NAVAL POSTGRADUATE SCHOOL
December 1998

Author: _____
Silvino L. C. Silva

Approved by: _____
David W. Netzer, Thesis Advisor

_____
Christopher M. Brophy, Thesis Co-advisor

_____
Oscar Biblarz, Second Reader

_____
Gerald H. Lindsey, Chairman
Department of Aeronautics and Astronautics

ABSTRACT

An experimental investigation was conducted to measure soot properties and concentration, and infrared signature of the plume of a kerosene/gaseous oxygen rocket motor. Multiple-wavelength measurements were used to obtain soot parameters. It was found that the multiple-wavelength technique appeared to work well for obtaining soot properties and concentration. The results implied that the soot particulate was very porous for the most fuel-rich conditions and became more compact as the O/F ratio increased. Soot mean diameter (D_{32}) was less than 0.1 μm when the O/F ratio was less than 0.75, but increased to 0.2→0.36 μm for higher O/F ratios. The soot particle diameters obtained from the Scanning Electronic Microscope (SEM) photomicrographs of collected soot samples were in qualitative agreement with the diameters measured optically. Soot concentration in the plume was found to rapidly increase and then decrease as the O/F ratio was increased from 0.3 to 1.1, with a peak near O/F = 0.76. Infrared measurements in the 3.5-5 μm band indicated a probable shift in the dominant radiation source from gas to particulate as the soot concentration increased.

TABLE OF CONTENTS

I. INTRODUCTION 1

II. THEORY AND BACKGROUND 3

A. SOOT FORMATION 3

B. MULTIPLE WAVELENGTH LIGHT EXTINCTION TECHNIQUE ... 5

1. Particle Size Distribution 5

2. Bouguer's Law 7

3. Mie Scattering Code Application 9

4. Particle Concentration Determination Method 13

5. Technique Requirements and Limitations 14

III. EXPERIMENTAL SETUP 17

A. ROCKET MOTOR 17

1. Propellant Mass Flow Control 17

2. Igniter 20

3. Injector Head 20

4. Combustion Chamber Sections 21

5. Nozzle 22

B. WHITE LIGHT SOURCE AND SENSOR SYSTEM 23

C. DATA ACQUISITION SYSTEM 24

D. INFRARED CAMERA 25

E. HELIUM-NEON LASER 25

F. VIDEO CAMERA 25

G. SOOT SAMPLING 26

H. FUEL DROPLET SIZING 26

IV. EXPERIMENTAL RESULTS 27

A. FIRING RESULTS 27

1. Performance Parameters 27

2. Transmission Parameters 29

B. SOOT SAMPLING 31
C. INFRARED EMISSIONS 37
D. VIDEO IMAGES 40
E. FUEL DROPLET SIZING 42
V. EXPERIMENTAL ANALYSIS 43
A. SOOT PROPERTIES 43
B. SOOT CONCENTRATION VERSUS O/F RATIO 45
C. UNCERTAINTY ANALYSIS FOR THE SOOT CONCENTRATION 48
D. INFRARED EMISSIONS 50
E. SOOT SAMPLING 51
VI. CONCLUSIONS AND RECOMMENDATIONS 53

APPENDIX A. MIE SCATTERING CODE LISTING 55
APPENDIX B. ROCKET MOTOR DRAWINGS 65
APPENDIX C. PRESSURE VS. TIME TRACES 71
APPENDIX D. WHITE LIGHT TRANSMISSIONS TRACES 85

LIST OF REFERENCES 91
INITIAL DISTRIBUTION LIST 93

ACKNOWLEDGEMENTS

I wish to thank my wife for her full support and patience during this research. Without her backing me up on everything this work would have been very much harder. I also wish to thank Professor David W. Netzer for his wise guidance and encouragement, Professor Christopher M. Brophy for his any time availability in guiding and supporting all the work done, and Professor Oscar Biblarz for his contribution on the final text.

On a experimental research like this most of the work depend on adequate hardware and software, and all the laboratory work was only possible due to the tireless support provided by Mr. Harry Conner, the Combustion Laboratory technician of the Department of Aeronautics and Astronautics.

I. INTRODUCTION

The use of liquid propellants for launch-vehicle propulsion systems has generally been the preferable choice due to their high specific impulse and the ease for providing throttling of the thrust level. The liquid propellant has to be sprayed into the combustion chamber, in which combustion efficiency is very dependent on intimate mixing of fuel and oxidant. Besides that, it is known that mixtures richer than stoichiometric will give best results in terms of specific impulse, because of the more rapid reduction in product molecular weight than the combustion temperature. Studies on spray combustion and its associated processes have helped designers provide for more efficient and stable combustors and to better understand the formation of several so-called pollutants such as soot, unburned fuel, nitrogen oxides (NOx) and carbon monoxide (CO). [Ref. 1] Both fuel rich conditions and/or imperfect mixing lead to undesirable residue generation, among which soot is often the element of concern since it is often associated with most of the infrared emissions from a rocket or gas turbine plume. Infrared emiting plumes are very undesirable, especially for weapon purposes (missiles and even fighter turbines), since they make it easier to detect the existence and/or location of the threat, thus facilitating the counter-attack.

The development of reliable computer codes, which can help propulsion system designers predict the amount of soot to be generated, is of high importance in looking for the least sooty conditions, as well as for analyzing the use of chemical additives in the fuel for the same purpose. These codes generally involve the use of some "reduced

kinetics" scheme together with more standard flow codes for the combustor and exhaust nozzle. To validate these codes, it is necessary to provide accurate experimental data on soot properties and concetrations over a wide range of combustor and nozzle operating conditions.

The size and concentration of soot particles from exhaust plumes have been found to significantly influence their heat signatures. Among the several methods which have been tried to accurately measure soot concentration in exhaust plumes, such as isokinetic sampling, single particle counters and light scattering, "light extinction" is likely the easiest and most reliable within a reasonable range of particle concentrations.

Cashdollar, et al [Ref. 2] gave a practical procedure for using light extinction for this purpose, even though the use of their three-wavelength light extinction technique could not provide a unique solution for the soot complex index of refraction, mean particle size and standard deviation of an assumed log-normal distribution. Four independent parameters require the use of a minimum of five wavelengths. Swenson [Ref. 3] used a five-wavelength light extinction technique with reasonable success for kerosene and gaseous oxygen. To some extent, the present work is the completion of Swenson's effort in establishing a full procedure to determine soot concentration and size.

This thesis effort has been aimed at developing and utilizing a reliable and relatively easy procedure for soot particle size and concentration determination in the exhaust plume of a small kerosene-gaseous oxygen rocket motor. The data were to be used by other investigators for validation of numerical prediction codes.

II. THEORY AND BACKGROUND

A. SOOT FORMATION

The combustion of liquid sprays occurs in liquid propellant rocket motors, gas turbines, diesel engines, industrial furnaces, etc. In all these situations, the formation of pollutant residues is a reality and soot is among the most significant of them.

> Soot is a carbonaceous solid produced in pyrolisis and combustion systems when conditions are such as to allow gas-phase condensation reactions of the fuel and its decomposition products to compete with further decompositon and oxidation. .... The formation and emission of soot are subjects of some concern for a variety of reasons. Soot particles are strongly absorbing and, within a combustor, can enhance significantly radiative heat transfer. .... The internal structure of soot particles has been examined by high-resolution phase-contrast electron microscopy. Near the edge of the particle, bent carbon layers follow the shape of the particle surface. Inside the particle, lattice structures seem to be located more or less regularly around certain centers between which the structure is less ordered. ...The density of the particles may be less than 2 g/cm3 due to large interplanar spacings. [Ref. 4]

The process of soot formation involves several phases, such as 'particle inception' (condensed phase material from the fuel-molecules via their breakdown), leading to 'surface growth' and 'coagulation'. While surface growth doesn't affect the number of particles, coagulation influences the establishment of a particle size distribution.

In Kuo [Ref. 1] we read that "it has been found from various investigations that conditions most favorable for soot formation occur when fuel-rich zones have strong temperature gradients." He also states that "the basic method of reducing soot formation in spray combustion is not only to reduce temperature gradients in fuel-rich zones but

also to reduce the size of zones where strong temperature gradients and fuel-rich concentration can arise." One can see that the flow properties should be very well determined and controlled to achieve minimum soot formation.

In rocket motors, liquid propellant atomization is often accomplished by the impingement of liquid streams which exit from small holes in the injector face. The size of the holes, the injection velocity and the liquid surface tension all influence the resulting droplet sizes.

"The rate at which the droplet evaporates and burns is generally considered to be determined by the rate of heat transfer from the flame front to the fuel droplet surface." [Ref. 5] Just as in the case of gaseous fuel diffusion flames, the burning of condensed phases often is controlled by rates of heat transfer and diffusion.

The luminosity of many flames comes from the presence of carbon particles as they radiate at the high combustion gas temperatures. Condensed phase particles present a very high emissivity when compared to gaseous combustion products.

It is commonly known that the first step for high combustion efficiency and low soot production is getting the reagents to be well mixed, which is better attained with turbulent mixing. Assuming that reasonably good mixing is achieved, soot production may still arise due to other variables, such as the difference between the chamber wall temperature and the chamber core temperature together with locally fuel-rich mixtures which may lead to unburned fuel thermal breakdown.

"Particle size and shape depend on the conditions of the flame. They may be almost spherical or in the form of filaments."[Ref. 6] The radii of these particles

range from 5 to 300 nm. Such significant variations in particle shape and size led to some of the difficulties faced by investigations of particle sizing techniques.

The words "carbon" and "soot" have been used by investigators to describe a wide variety of solid materials, many of which may contain other elements than pure carbon. Since the properties of solids change appreciably with the conditions of formation, a wide variety of soot properties has been reported. Soot concentration measurements based upon light transmission depend on soot density, a property not easy to determine.

B. MULTIPLE WAVELENGTH LIGHT EXTINCTION TECHNIQUE

1. Particle Size Distribution

Particle size is usually represented by the diameter (in microns) of a spherical particle of equivalent mass. Mie theory is based upon spherical particles and it works reasonably well if the particles are not much different from the spherical shape. For a collection of particles, size information is often given in the form of a frequency distribution plotted against particle diameter. In addition, one may define a "probability density function - P(D) " which represents statistically the distribution.

To characterize particle size distributions various diameter definitions may be adopted. They are referred to as mean, average, or equivalent diameters. If a "number distribution" N(D) is defined as $N(D) = N * P(D)$, where N is the

total number of particles in the distribution, a general mean diameter for a continuous distribution has the form:

$$D_{pq} = \frac{\int_0^\infty N(D)\, D^p\, dD}{\int_0^\infty N(D)\, D^q\, dD}$$

- (eq. 2.1)

or for a discrete distribution it would be:

$$D_{pq} = \frac{\sum N(D)\, D^p \Delta D}{\sum N(D)\, D^q \Delta D}$$

- (eq. 2.2)

where N(D) is the number per class width ΔD [Ref. 7]. Among the possible 'pq' diameter definitions, the most widely used is the so-called Sauter or Volume-to-Surface Mean Diameter (D_{32}).

From Powell, et al [Ref. 8] one can realize that for a D_{32} range up to 2.0 microns "the dependence of the intensity ratio (transmittance) upon D_{32} is nearly independent of the shape of the size distribution function… ." Often it is assumed that soot particles have a log-normal distribution. This distribution can be characterized by two parameters: the geometric mean diameter (**Dg**), which establishes the central tendency, and the geometric standard deviation (**σg**), which determines the spread about the center.

The log-normal distribution may be presented in the form [Ref. 7]:

$$P(D)=\frac{1}{\sqrt{2}\,\ln(\sigma g)D}\exp\left\{-\left[\frac{\ln(D/Dg)}{\sqrt{2}\ln(\sigma g)}\right]^2\right\}$$

- (eq. 2.3)

2. Bouguer's Law

The best way for obtaining particle size data from in a plume is certainly through some nonintrusive method, which in general leads to optical procedures. Various researchers [Ref. 9] have made use of the attenuation of monochromatic radiation to obtain the properties of particulates. These measurements have been usually based upon Bouguer's Law, also known as the Beer-Lambert Law, which states that transmission of light through a cloud of uniform (monodisperse) particles is given by: [Ref. 2]

$$T = e^{(-Q.A.n.L)} = e^{-(\frac{3}{2}\frac{Q.Cv.L}{D})}$$

- (eq. 2.4)

where:

A	-	cross-sectional area of the particle
Cv	-	volume concentration of particles
D	-	particle diameter
L	-	path length containing the particles
n	-	number concentration of particles
Q	-	dimensionless extinction coefficient

It should be noted that Bouguer's Law is defined for monodispersed particulate which almost never is the real situation. The extinction coefficient (Q) includes loss of light due to both absorption and scattering.

Dobbins [Ref. 9] revised Bouguer's Law to apply to a polydisperse system:

$$T = \exp\left[-\left(\frac{3 Q_{bar} C_v L}{2 D_{32}}\right)\right]$$

- (eq. 2.5)

where Q_{bar} is the average extinction coefficient found for a <u>continuous</u> distribution by:

$$Q_{bar} = \frac{\int_0^\infty Q(D) N(D) D^2 dD}{\int_0^\infty N(D) D^2 dD}$$

- (eq. 2.6)

or for a discrete distribution by:

$$Q_{bar} = \frac{\sum Q(D) N(D) D^2 \Delta D}{\sum N(D) D^2 \Delta D}$$

- (eq. 2.7)

Even when the log-normal particle distribution is assumed, the extinction coefficient (Q) needs to be calculated for each particle diameter. Mie theory is often applied [Ref. 2] to light scattering by a single spherical particle in order to obtain the extinction coefficient (Q). Q is a function of wavelength (λ) , particle diameter (D) and its complex index of refraction (m= a – i.b). The imaginary part

(b) is the absorption index. Cashdollar [Ref. 2] also adds that "even though the Q values are calculated on the basis of single scattering, it is valid to use these values in Bouguer's Law for the multiple-scattering case at high concentration of particles. The law breaks down only when particles are spaced closer than a few particle diameters and interact electromagnetically, thus changing the Q values."

3. Mie Scattering Code Application

Cashdollar, et al assumed the particle index of refraction to be one of the values previously reported in the literature. Swenson [Ref. 3] made use of their method but let the complex index of refraction vary over all possible values. From Cashdollar's three-wavelength transmission experiments, Swenson had to increase to five wavelengths which could provide the four independent ratios required for obtaining values for the four variables: index of refraction (m= **a** – i.**b**), geometric standard deviation (**σg**) and Sauter Diameter (**D_{32}**). Cashdollar's Mie code was adapted by Swenson to handle five wavelengths. This Mie scattering code (Appendix A) was used to generate the Q's and Q_{bar}'s for the set of five wavelengths. The wavelengths were 0.3650μm, 0.4047μm, 0.4358μm, 0.5461μm and 0.5770 μm, which represent well defined light emission power peaks from a white-light mercury lamp.

Forming the ln-transmittance ratio for two wavelengths using equation 2.5, results in:

$$\left[\frac{\ln(T(\lambda_i))}{\ln(T(\lambda_j))}\right]=\left[\frac{Q_{bar}(\lambda_i,D_{32},m,\sigma_g)}{Q_{bar}(\lambda_j,D_{32},m,\sigma_g)}\right]$$

- (eq. 2.8)

(experiment) **(theory)**

where the transmittances (T) are found experimentally for each wavelength through the ratio of light intensities (I) as follows:

$$T_{exp} = \frac{I_{(w\,/\,plume)} - I_{(no\,..\,light)}}{I_{(no\,..\,plume)} - I_{(no\,..\,light)}}$$

- (eq. 2.9).

As Swenson [Ref. 3] observed, " ...For five wavelengths, there are ten ln-transmittances ratios, but only four are independent"... " required to solve for the four unknowns $\mathbf{D_{32}}$, σ**g**, and m= **a** – i. **b** ." The "best values" for the four variables are found by obtaining the best fit for Equation 2.8 . Therefore, the Mie code sweeps through reasonable ranges on all the four variables until it gets the best combination, which is the one that best falls over a 45-degree line through the origin when plotting for all cases:

$$\left(\ln T_i / \ln T_j\right) vs. \left(Qbar_i / Qbar_j\right)$$

The actual check used by the Mie code for the best fit is the minimization of the sum of the squared deviations (**SSD**) between the natural log-transmittance ratios and the average extinction coefficient ratios.

Once the best fit was attained for a set of transmittance values all four variables were saved by the code, and it was run again for that specific condition to obtain the average extinction coefficient.

For best understanding of the whole method we now assume a fictitious experiment for which Table 2.1 expresses the experimental results. Figure 2.1 shows how the evaluation of the best fit correlated the data.

Wavelength (micron)	0.3650	0.4047	0.4536	0.5461	0.5770
Transmittance (0 to 1)	0.242	0.383	0.460	0.651	0.691

Table 2.1 - Transmittance values from a fictious experiment

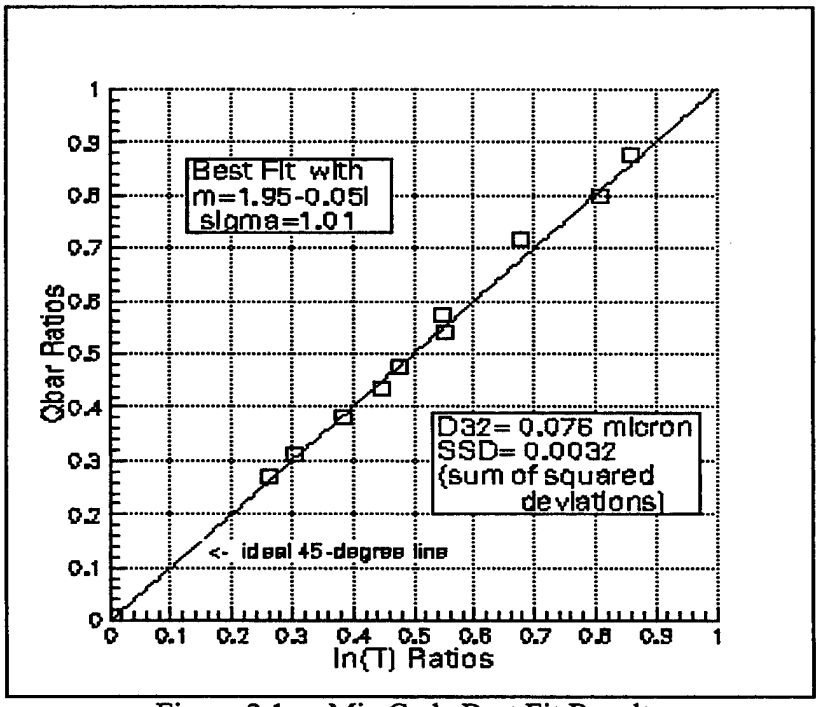

Figure 2.1 - Mie Code Best Fit Results

Once the best fit gave the index of refraction, D32 and σ_g for the case run (e.g. Figure 2.1), a second run for this specific case gave the average extinction coefficient as a function of the Sauter Mean Diameter (D32), shown at Figures 2.2 and 2.3.

Picking one of the wavelengths, 0.5770 micron for example, a Q_{bar} of 0.05333 is found for the best fit D_{32} value of 0.076 microns. These value of Q_{bar} and D_{32}, as well as the respective wavelength transmittance value (T=0.691) were then used in the Beer-Lambert formula (eq. 2.5) to get the desired particle concentration.

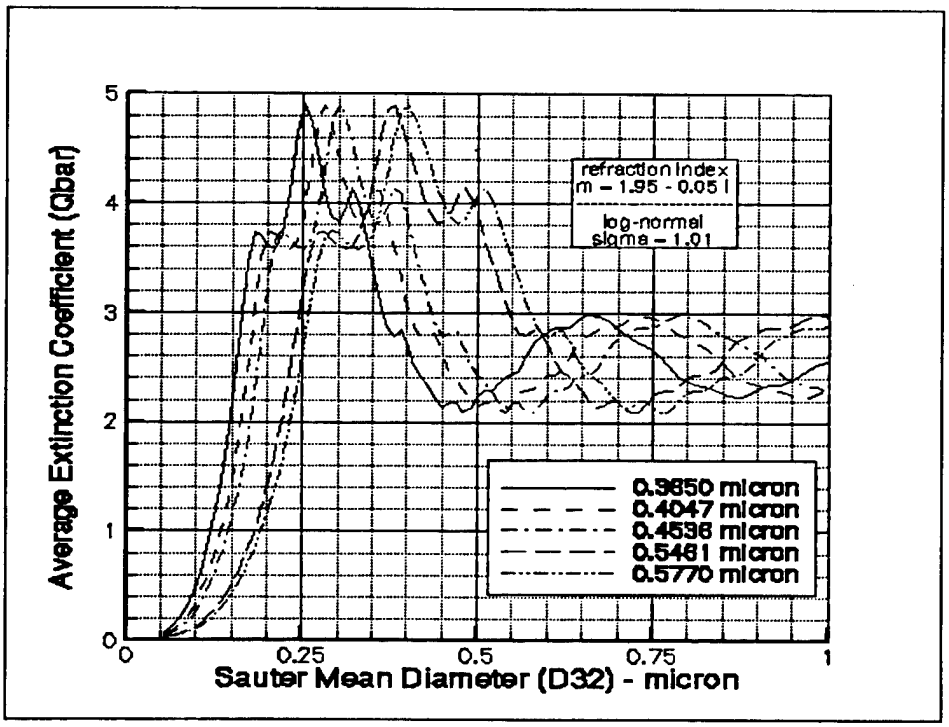

Figure 2.2 – Q_{bar} vs. D_{32} for 5 wavelengths (overall)

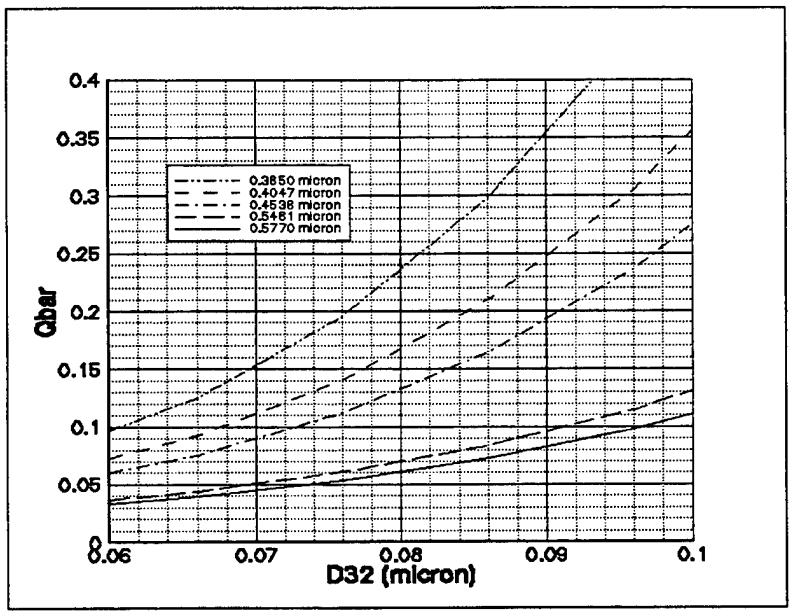

Figure 2.3 – Q_{bar} vs. D_{32} for 5 wavelengths (detail)

4. Particle Concentration Determination Method

After determining the light beam path length through the exit plume, Equation 2.5 can finally be solved for particle volume concentration (Cv). However, the plume code that was used to predict soot levels utilized a particle mass concentration defined as:

$$Cm = \frac{mass_{soot}}{mass_{gas}} = Cv \left(\frac{\rho_{soot}}{\rho_{gas}} \right) \qquad \text{- (eq. 2.10)}$$

The soot density (ρ_{soot}) was taken as 1.5 g/cm3 [Ref. 3]. The gas density was obtained from the perfect gas law, assuming that the plume pressure (P_e) was 1 atm. The plume exhaust gas temperature (T_e) and molecular weight (M_e) were obtained at the nozzle exit from a Thermochemical Equilibrium (TEP) code

[Ref. 10] using the actual nozzle expansion ratio and measured chamber pressure. T_e was corrected for the C* efficiency (discussed below). The kerosene fuel was asssumed to be similar to RP-1/JP-4 fuel. Thus, Cm was obtained by:

$$Cm = Cv\left(\frac{\rho_{soot} R\, T_e}{P_e M_e}\right)$$

- (eq. 2.11)

To finally get the ratio between soot (carbon) mass and the total mass coming out of the nozzle (soot + gas) we use the definition of Carbon Mass Percentage (**%C(gr)**):

$$\%\ C\ (gr) = \left(\frac{mass_{soot}}{mass_{total}}\right) x100\% = \left(\frac{Cm}{1+Cm}\right) x100\%$$

---- (eq. 2.12)

5. Technique Requirements and Limitations

For accurate extinction measurements the detector must view only the transmitted light, that is, the detector should never see the forward scattered light from relatively large particles. Hodkinson [Ref. 11] suggested that the detector half-angle field of view be limited to less than one-tenth the angle of the first angular minimum in the Fraunhofer diffraction pattern:

$$\theta_{1/2} \leq (7.0)\frac{wavelength}{diameter_{particle}}$$

- (eq. 2.13)

Fortunately this was not a hard condition to achieve since the light beam that passed through the plume to the detector was collected into a small enough slit located relatively far from the plume.

Running the Mie code for a best fit using a set of measured transmittance values sometimes led to multiple solutions with nearly identical values of SSD. Some of these solutions gave unreasonable results for particle index of refraction (m). This may be related to the fact that the particle distribution may not be log-normal and the particles may not be perfect spheres as Mie theory assumes. When a solution resulted in a value for 'm' far from those which have been reported in the literature, it was discarded.

III. EXPERIMENTAL SETUP

A. ROCKET MOTOR

1. Propellant Mass Flow Control

Propellants were commercial kerosene (liquid fuel) and gaseous oxygen. The mass flow control of oxygen was performed through the upstream pressure of a sonically choked nozzle. A nozzle throat diameter of 0.0635 inch was chosen to cover the whole range needed for the experiments. The sonically choked nozzle equation is:

$$\dot{m} = C_d P_{up} A_{th} \sqrt{\frac{\gamma \left(\frac{2}{\gamma+1} \right)^{\frac{\gamma+1}{\gamma-1}}}{R\, T_{up}}} = C_d \frac{P_{up} A_{th}}{\sqrt{R\, T_{up}}} f(\gamma)$$

- (eq. 3.1)

where:

$\dot{m}$ - Gas Mass Flow Rate

C_d - Choked Throat Discharge Coefficient

P_{up} - Choked Nozzle Upstream Absolute Pressure

A_{th} - Choked Nozzle Throat Cross Sectional Area

R - Gas Constant for Oxygen

T_{up} - Choked Nozzle Upstream Gas Absolute Temperature

$f(\gamma)$ - Function of Specific Heat Ratio for Oxygen

The discharge coefficient (C_d) was experimentally measured as 0.97 using an ASME nozzle with a discharge coefficient of 0.98 . Taking 'γ'=1.4, which is the room temperature specific heat ratio for oxygen, then f(γ)=0.68473, and Eq. 3.1 can be easily solved for $\dot{m}$ to get the oxygen mass flow rate.

To make sure the oxygen nozzle is choked, $P_{downstream}$ must be less than (0.52828)* $P_{upstream}$, the sonic choking condition when the specific heat ratio (γ) is 1.4 .

Fuel mass flow rate control was provided using cavitating venturis. These devices provide repeatable, stable flow rates that are independent of the downstream pressure, enabling gross simplifications of otherwise complex flow regulating systems. The fluid medium is accelerated through the venturi throat where its vapor pressure is reached, at which point instantaneous 'flashing' or 'cavitation' occurs. The vapor is then recondensed in the venturi diffuser with low pressure loss and no erosive damage. Flow rate is thereby fixed solely by upstream pressure and is unaffected by fluctuations downstream. With a fixed feed pressure, cavitating venturis act as 'hard' flow regulators, which means flow rate is only dependent on upstream pressure and fluid properties.

To cover the whole range of kerosene mass flow rates needed for the experiments, four venturis were used, each with different throat diameter. The throat diameters were 0.029", 0.034", 0.043", and 0.052". Just as the sonic choke, the cavitating venturi has a minimum upstream-downstream pressure difference to

make sure cavitation happens. This pressure differential (typically a minimum of 200 psi) was established along with the calibration of each venturi using kerosene (Figure 3.1) . These calibrations were performed with the aid of a laboratory balance and video recorded timing, so that they gave a very reliable measurement of the fuel mass flow rate for each upstream venturi pressure tested. A turbine flowmeter was also used in the kerosene line as a check for the cavitating venturis.

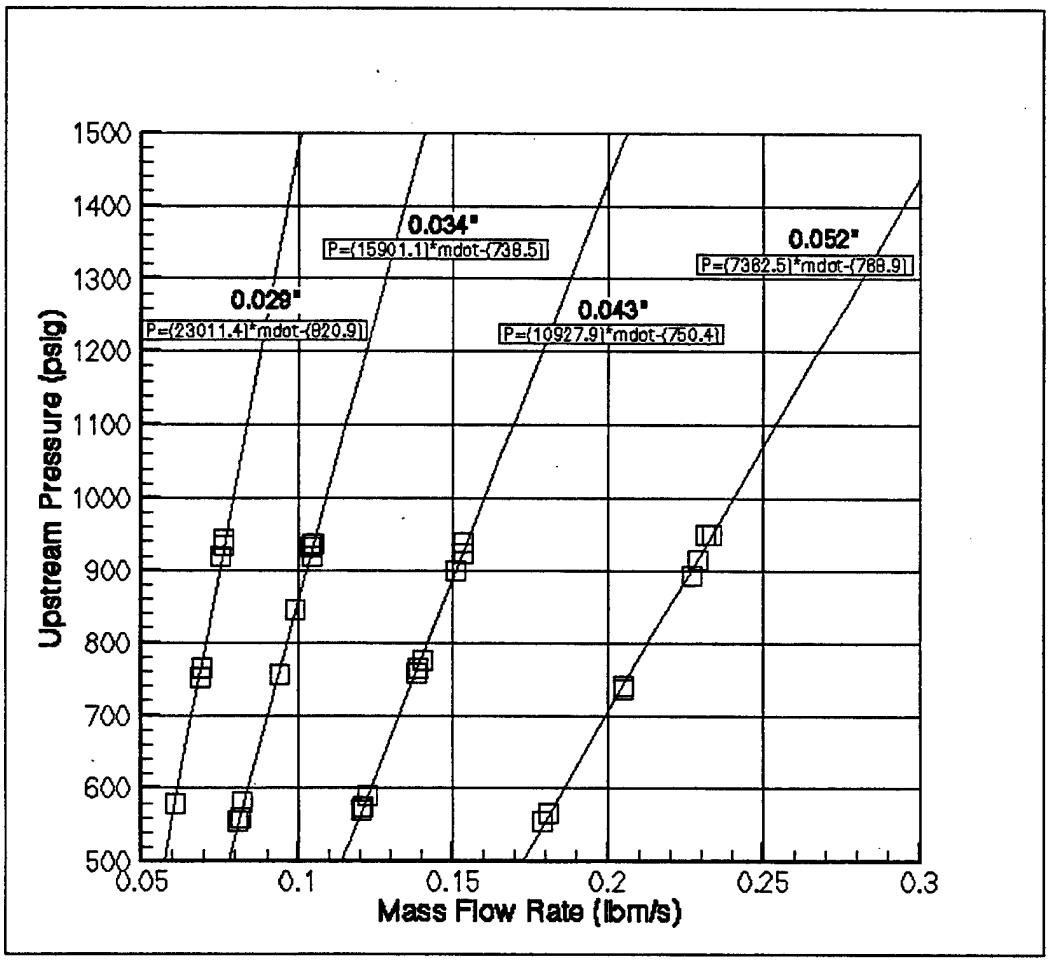

Figure 3.1 - Cavitating Venturi Calibration for Kerosene

From upstream pressure measurements taken from fuel and oxygen lines, both mass flow rates could be obtained and each (O/F) ratio was accurately determined.

2. Igniter

Kerosene is not easily ignitable at fuel-rich conditions, even when mixed with pure oxygen. This became clear when an ethylene-oxygen torch was used for igniting the kerosene-oxygen mixture. To provide a more constant and reliable ignition, a hydrogen-oxygen torch was used on all firings. Solenoid valves were used to turn the torch gases on and off. Adjusted to a blue flame condition through needle valves this torch provided a rapid ignition in almost all the firings. The hot gas from the torch flowed through the rocket motor injector head into the combustion chamber. Figure 3.2 shows the overall experimental setup used in all firings.

3. Injector Head

Three similar injector heads were designed and fabricated with one central (oxygen) and 8, 6, or 5 peripherical (fuel) orifices. Appendix B shows the rocket motor drawings in detail, including the injector head sketch. The purpose of different numbers of identical orifices was to have an average fuel droplet size on the order of 50μm with geometric standard deviation of 2.3 (assumed log-normal distribution) for all the fuel mass flow rates required to provide the (O/F) range studied. The injector design was driven by keeping its "Penetration Parameter"

[Ref. 12] within the optimum range (0.5 to 0.8). With this same intention, the 8-hole and the 6-hole injector heads were later turned into 4 and 3-hole injectors by welding shut alternating holes. Water was flowed through each injector to insure proper impingement of the fuel streams.

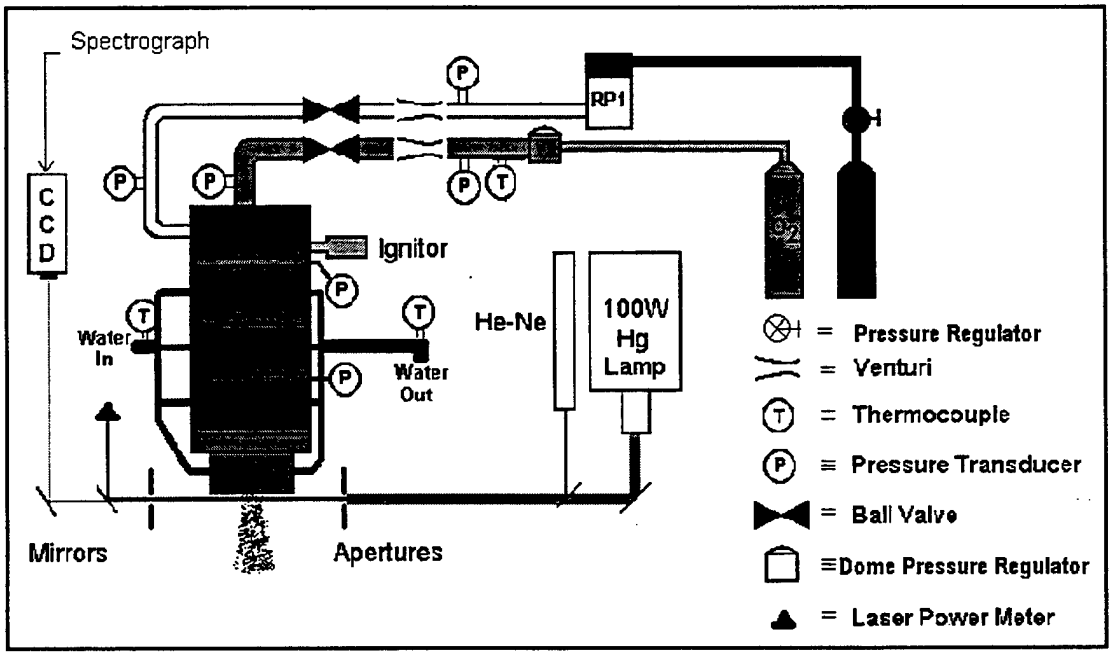

Figure 3.2 - Firings Experimental Setup

4. Combustion Chamber Sections

Three water cooled combustion chamber sections were mounted as shown in Figure 3.3 . Detailed drawings of the combustion sections can be found also in Appendix B.

Between the injector head and the first chamber section a thin solid ring was used for pressure measurement in the very upstream chamber channel where the propellant mixing occurred. An identical ring was used between the second and

third chamber sections for a mid-chamber pressure measurement. Between the first and second chamber sections a thin solid turbulence ring was used to turn the first chamber section into a pre-chamber where the mixing and most of the combustion were expected to occur. The actual purpose of the turbulence ring was to provide a uniform soot distribution in the exhaust plume.

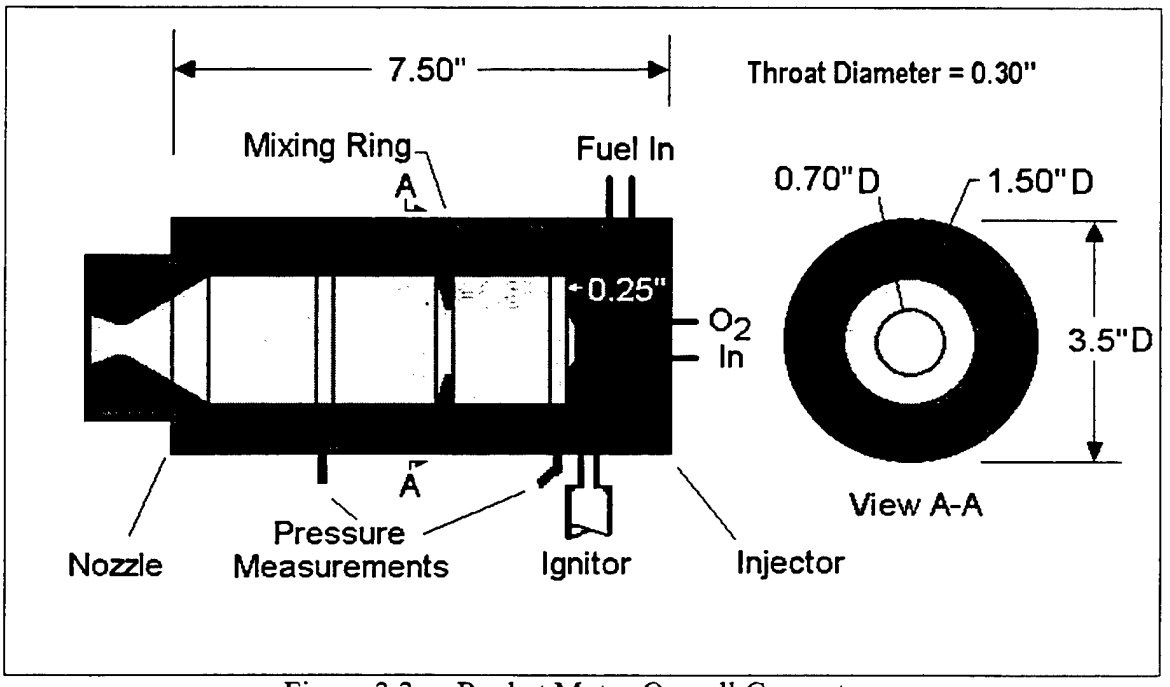

Figure 3.3 - Rocket Motor Overall Geometry

5. Nozzle

A water cooled nozzle was designed and fabricated with conical convergent and divergent sections. Detailed drawing of this device can be found also in Appendix B. All parts of the rocket motor were made of stainless steel 304L. The cooling system flowed water independently through the nozzle and each of the three chamber sections. The water exits were joined together downstream, where water flow rate and temperature were measured for each firing. The measured

water flow rate and temperature rise were used to calculate the heat loss from the combustor. The heat loss was used to correct the theoretical characteristic velocity (C*) obtained from the TEP code. A nozzle discharge coefficient of 0.96 was experimentally determined using a choked ASME nozzle with a discharge coefficient of 0.98.

B. WHITE LIGHT SOURCE AND SENSOR SYSTEM

The white light source used was an ORIEL model 66002 100W Hg lamp with a set of 1.5 inch diameter condensing lenses. This Hg lamp provides a set of five very well defined power peaks centered at the wavelengths of 365.0 , 404.7 , 435.8 , 546.1 , and 577.0 nm. The collimated white light beam was reduced to an 0.125 inch diameter by a pinhole aperture and passed through the rocket plume. A second pinhole apperture with a diameter of 0.0625 inch was used after the beam crossed the plume to prevent the measurements from being contaminated by forward scattering. Finally the white light beam went through a 25μm slit of an ORIEL 77400 1/8 meter spectrograph. The beam then spread into its spectrum components and was imaged on an ORIEL Instaspec IV CCD detector with 1024x256 pixels on 25μm centers. Typically, about 50 center rows were binned to minimize any beam steering problems as well as to have a proper average power transmission for each wavelength. There was negligible variation in power across the 50 diodes. Figure 3.4 shows a normalized transmission plot produced by this system, from which the transmittances were calculated. Background correction was possible through the system software.

The wavelength calibration of the Hg lamp power peaks was performed with specially designed Melles Griot optical filters matching the desired wavelengths. In all the runs the white light beam crossed the rocket plume at a plane 3 mm away from the nozzle exit and almost in all cases through the rocket centerline.

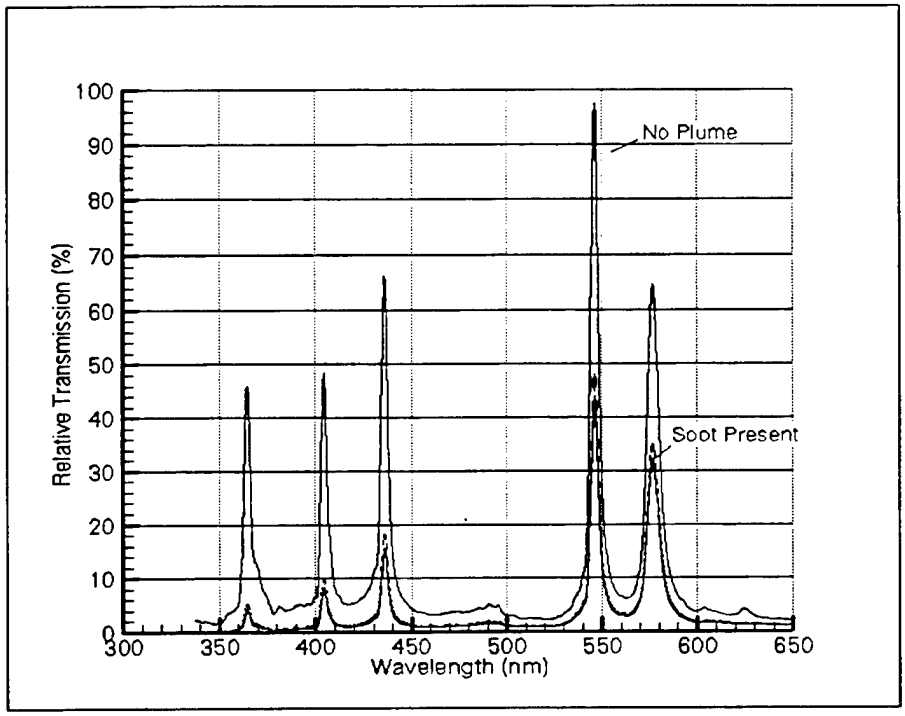

Figure 3.4 - Typical Transmission Plot

C. DATA ACQUISITION SYSTEM

A Microsoft Visual Basic 5.0 Code was developed to perform the control of the whole firing procedure, which included user defined torch time, propellant flow times, chamber purge time, and delay between starting torch and starting propellant flow. The desktop computer running the Visual Basic Flow Control was coupled with a National Instruments BNC-2090 Analog Breakout Box, a PCI-MIO-16E-4 500Ks/s Data Acquisition Board and a relay box. This provided the control of all valves as well

as the 10Hz digitization of all the analogical device readings, such as pressures, temperatures, flow measurements, and laser diode voltage.

D. INFRARED CAMERA

An AGEMA 870 Infrared (IR) thermal imaging camera was used to view the rocket plume and measure its IR emissions from a point of view perpendicular to the rocket axis. The IR camera contained a glass filter with a bandpass of 3.5 to 5 μm. Images from the IR camera were recorded at 25 Hz and saved into a microcomputer harddisk. With an assumed emissivity of the plume, the temperature profile could be obtained from the measured irradiance. Conversely, the emissivity of the source can be calculated with a known temperature.

E. HELIUM-NEON LASER

Besides the white light beam, a Melles Griot 6 mW helium-neon laser beam was passed through the rocket plume and directed onto a power meter with a laser line interference filter attached. This provided an additional wavelength (632.8 nm) to get transmission values if needed for the calculations. On all runs the He-Ne laser beam crossed the rocket plume in a plane 3 mm away from the nozzle exit and through the rocket plume centerline.

F. VIDEO CAMERA

A conventional CCD camera set at a $1/10000^{th}$ shutter speed was used to record the plume image at a standard framing rate of 30 Hz.

G. SOOT SAMPLING

Soot samples were collected with probes connected to a vacuum line. The probes utilized 0.2μm paper filters. Two ¼-inch diameter tube probes with individual filters were positioned 4 feet (fore position) and 20 feet (aft position) downstream from the rocket nozzle. Both were oriented toward the nozzle exhaust. The purpose of the soot sampling was to obtain qualitative data for comparison with the calculated particle diameters. Soot samples were sucessfully obtained only in the last four firings, thus not covering the whole O/F range tested. The paper filters were gold plated (after the exposure to soot) using a gold plasma and a Scanning Electronic Microscope (SEM) was used to obtain photomicrographs.

H. FUEL DROPLET SIZING

A Malvern Mastersizer system with 100mm lens was used in an attempt to measure the droplet size distribution of the fuel. This system uses a 18mm diameter, 2mW helium-neon laser beam. For this experiment the injector head was exhausted into ambient air and the laser beam was positioned 1.75 inches aft of the injector face, which was the gap between the injector face plane and the turbulence ring.

IV. EXPERIMENTAL RESULTS

A. FIRING RESULTS

1. Performance Parameters

More than 70 firings were conducted with the 5, 4, and 3-hole injector heads covering an (O/F) range from 0.330 to 1.115, from July through October 1998 . Not all the firings were successful. Some presented problems mostly related to ignition difficulties when an ethylene-oxygen torch was used and others would not ignite when the mixture was too fuel-rich (lower O/F ratios). It was believed that the introduction of the 'turbulence ring' introduced stagnation conditions in the pre-chamber which led twice to combustor failures. These failures partially destroyed the rocket motor, requiring new chamber sections and turbulence rings to be fabricated. There were also some initial firings when the white light system was not yet available and only the helium-neon laser was used. These runs will not be referred to since they were used to test the whole apparatus and firing control hardware and software. Table 4.1 shows the performance parameters from the firings. The first digit of the run number was the number of orifices in the injector. Theoretical characteristic exhaust velocities were calculated with the TEP code including a correction for the heat loss to the water cooling system. Experimental C* was calculated as:

$$C^{*}_{\exp} = \left(P_C A_{th} C_d \Big/ \dot{m}_t \right) \qquad \text{- (eq. 4.1)}$$

where Pc was taken as pressure downstream of the mixing ring and $\dot{m}_t$ is the total mass flow rate. Ignition delays were occasionally encountered but steady state conditions were still reached during these rocket firings. Appendix C shows the pressure-time traces including upstream oxygen choked nozzle, upstream fuel venturi, and chamber pressures and the helium-neon laser transmission diode voltages (background corrected).

Run #	(O/F) Ratio	O2 Mass Flow (lbm/s)	Kerosene Mass Flow (lbm/s)	$P_{chamber}$ (psig)	C^*_{exp} (ft/s)	C^*_{theor} (ft/s)	C^*_{eff} (%)	Comments
5-28	0.721	0.07043	0.0977	338	4390	4256	103.1	Normal Burning
5-29	0.744	0.06870	0.0924	328	4446	4284	103.8	Normal Burning
5-32	0.658	0.06826	0.1037	326	4140	4172	99.2	Normal Burning
5-34	0.658	0.06735	0.1023	328	4222	4172	101.2	Normal Burning
5-35	0.338	0.06893	0.2037	323	2587	3638	71.1	Normal Burning
5-37	0.469	0.07337	0.1564	342	3250	3891	83.5	Ignition Delay
5-39	0.494	0.07428	0.1505	355	3449	3935	87.6	Normal Burning
5-40	0.497	0.07533	0.1516	367	3532	3941	89.6	Normal Burning
5-41	0.330	0.06840	0.2070	323	2561	3621	70.7	Normal Burning
5-49	0.510	0.07774	0.1525	380	3604	3963	90.9	Ignition Delay
4-01	0.575	0.07947	0.1381	400	4015	4066	98.7	Normal Burning
4-02	0.566	0.07820	0.1382	393	3966	4052	97.9	Normal Burning
4-03	0.581	0.08008	0.1378	401	4019	4075	98.6	Normal Burning
4-10	0.660	0.08015	0.1215	395	4278	4185	102.2	Ignition Delay
4-13	0.647	0.07947	0.1228	397	4286	4167	102.9	Normal Burning
4-14	0.750	0.07443	0.0992	362	4553	4297	106.0	Normal Burning
4-15	0.754	0.07578	0.1005	363	4497	4302	104.5	Normal Burning
3-01	0.895	0.07865	0.0879	375	4917	4475	109.9	Normal Burning
3-02	0.909	0.07986	0.0879	372	4842	4491	107.8	Ignition Delay
3-03	0.894	0.07986	0.0893	377	4867	4474	108.8	Normal Burning
3-04	1.080	0.09018	0.0835	416	5230	4699	111.3	Normal Burning
3-05	1.097	0.09153	0.0834	421	5256	4719	111.3	Normal Burning
3-06	1.115	0.09131	0.0819	420	5295	4741	111.7	Partial Failure

Table 4.1 - Performance Parameters

Figure 4.1 shows how characteristic velocity efficiency (C^*_{eff}) behaved for the O/F ratios tested. The data from Table 4.1 indicate that the 4 and 5-orifice injectors had nearly the same performance at the same O/F ratio. For O/F ratios lower than 0.8 C^*_{eff} decreased significantly.

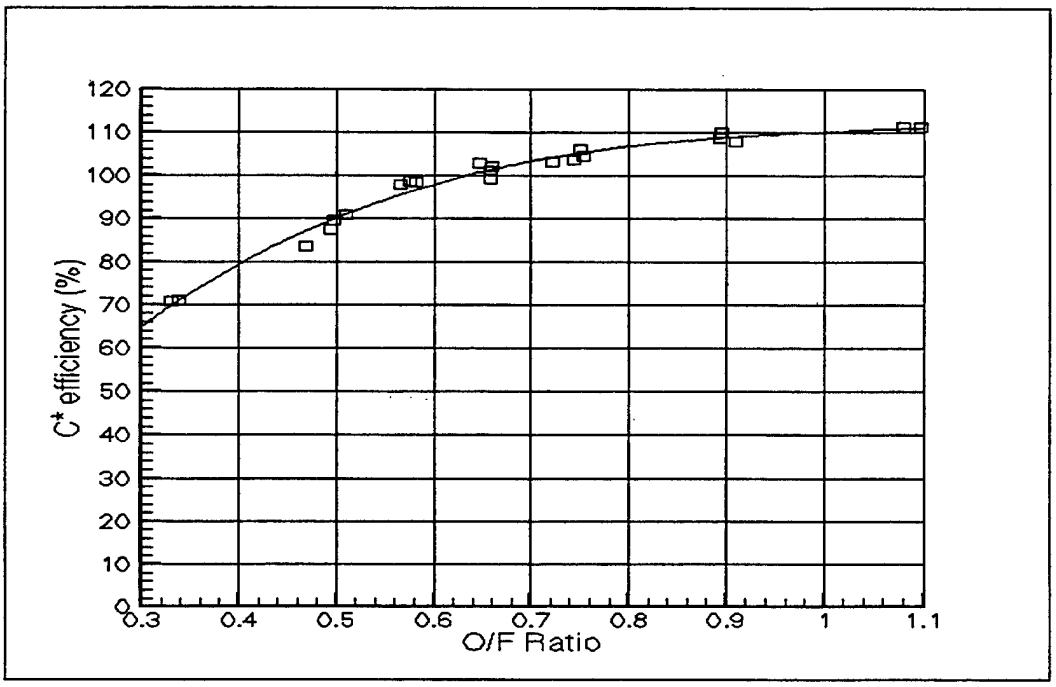

Figure 4.1 - Characteristic Velocity Efficiency vs. O/F Ratios

2. Performance Parameters

The transmittances, or the ratios between with-fire and without-fire transmissions (with background correction) for all five wavelength peaks measured are presented in Table 4.2 for all the above runs.

The transmittance results were calculated for the part of every run when the transmission values reached a relatively steady value, away from the influence of the torch ignition. On all the runs the 1/8 inch diameter white light beam crossed the rocket plume at its centerline, except for runs 4-10 through 4-15, and runs 3-01 through 3-06, when it crossed the plume about 80% and 50% of

Run #	Wavelength (micron)				
	0.3650	0.4047	0.4358	0.5461	0.5770
5-28	0.0022	0.0039	0.0065	0.0178	0.0221
5-29	0.0022	0.0044	0.0068	0.0226	0.0278
5-32	0.0054	0.0131	0.0203	0.0656	0.0760
5-34	0.0050	0.0111	0.0176	0.0539	0.0682
5-35	0.5391	0.6741	0.7322	0.8529	0.8800
5-37	0.3309	0.4765	0.5502	0.7181	0.7532
5-39	0.2420	0.3830	0.4600	0.6510	0.6910
5-40	0.1979	0.3361	0.4170	0.6310	0.6701
5-41	0.5392	0.6591	0.7160	0.8230	0.8332
5-49	0.1671	0.2810	0.3489	0.5360	0.5420
4-01	0.0081	0.0226	0.0369	0.1282	0.1523
4-02	0.0081	0.0224	0.0364	0.1261	0.1500
4-03	0.0046	0.0106	0.0160	0.0534	0.0598
4-10	0.0050	0.0090	0.0131	0.0310	0.0421
4-13	0.0120	0.0201	0.0260	0.0580	0.0710
4-14	0.0140	0.0230	0.0290	0.0590	0.0750
4-15	0.0130	0.0180	0.0220	0.0450	0.0540
3-01	0.0171	0.0204	0.0247	0.0422	0.0476
3-02	0.0169	0.0180	0.0238	0.0396	0.0450
3-03	0.0160	0.0197	0.0214	0.0376	0.0425
3-04	0.0763	0.0806	0.0838	0.1034	0.1607
3-05	0.0810	0.0898	0.1062	0.1479	0.1629
3-06	0.0910	0.0988	0.1158	0.1803	0.1819

Table 4.2 - Measured Transmittances

the plume width radially away from the centerline, respectively. The offset was employed to increase the transmittance for the plumes with the highest opacities in order to be more confident of the applicability of the Beer-Lambert law. For

example, compare run 5-29 (O/F=0.744 $T_{0.365}$ = 0.0022) to runs 4-14 (O/F=0.750 $T_{0.365}$ = 0.0140) and 4-15 (O/F=0.754 $T_{0.365}$ = 0.0130). The plume width 3mm aft from the nozzle exit plane was 16.2mm, while for the 80% and the 50% locations the plume widths were calculated as 9.7mm and 14.0mm, respectively.

On runs 3-04, 3-05, and 3-06 plume afterburning occurred, e.g. exhaust gases re-ignited when mixed with ambient air. This significantly contaminated the helium-neon laser transmittance, and probably also the white light five-peak transmission counts.

B. SOOT SAMPLING

Soot sampling was introduced only on the latest runs (runs 3-03 through 3-06). Figures 4.2 through 4.12 show the SEM pictures taken of the filter papers. On all SEM pictures the small dash on the lower right corner is the size scale for 0.5 micron.

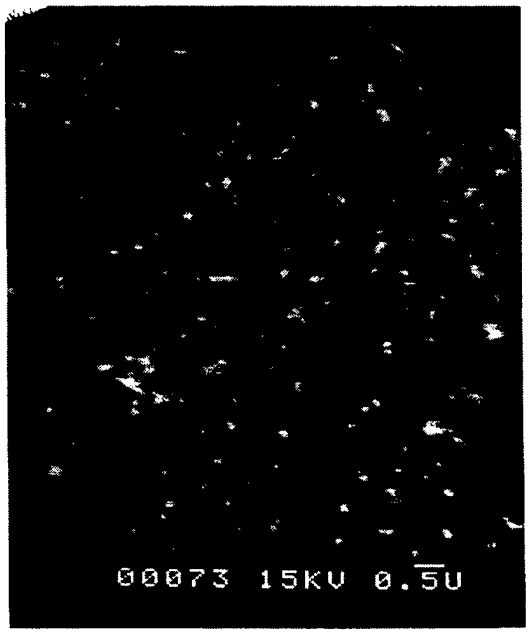

Figure 4.2 - Run 3-03 - Fore Tube Soot Sample

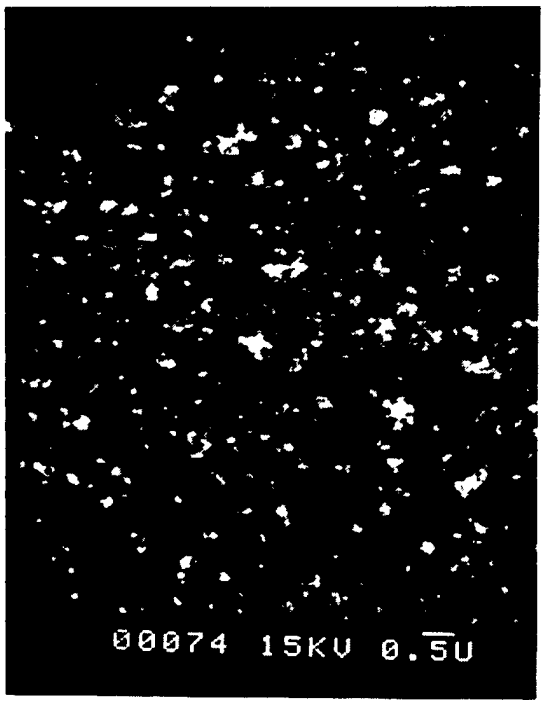

Figure 4.3 - Run 3-03 - Fore Tube Soot Sample

Figure 4.4 - Run 3-04 - Fore Tube Soot Sample

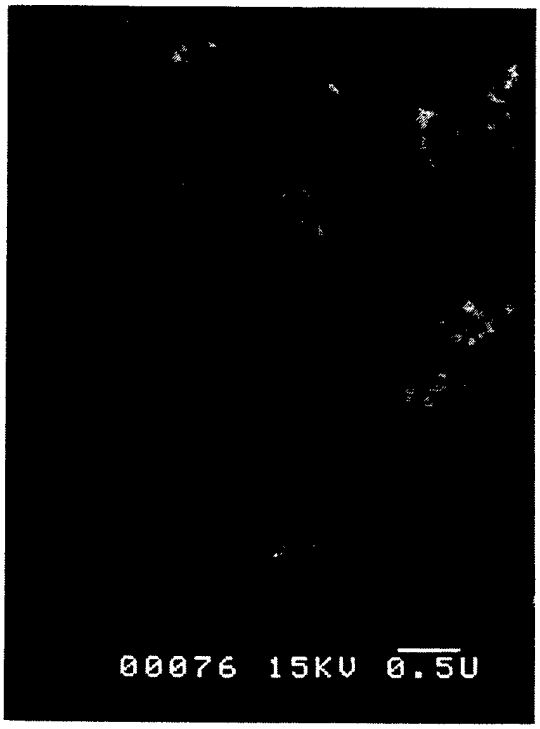

Figure 4.5 - Run 3-04 - Fore Tube Soot Sample

Figure 4.6 - Run 3-05 - Fore Tube Soot Sample

Figure 4.7 - Run 3-05 - Fore Tube Soot Sample

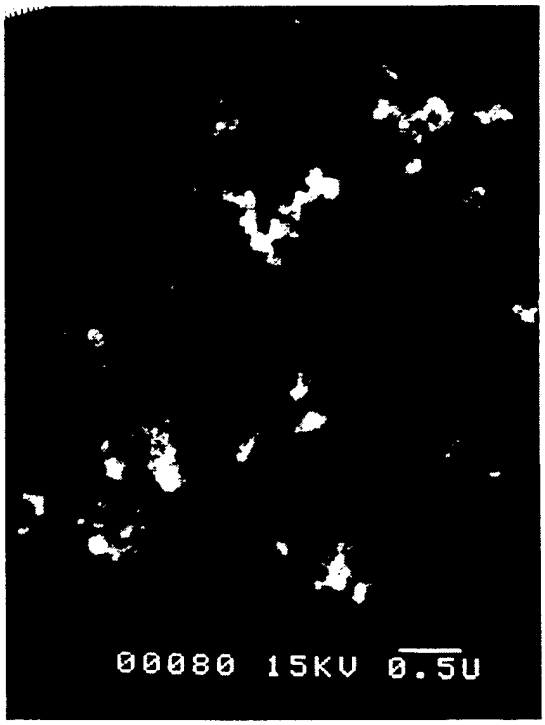

Figure 4.8 - Run 3-05 - Fore Tube Soot Sample

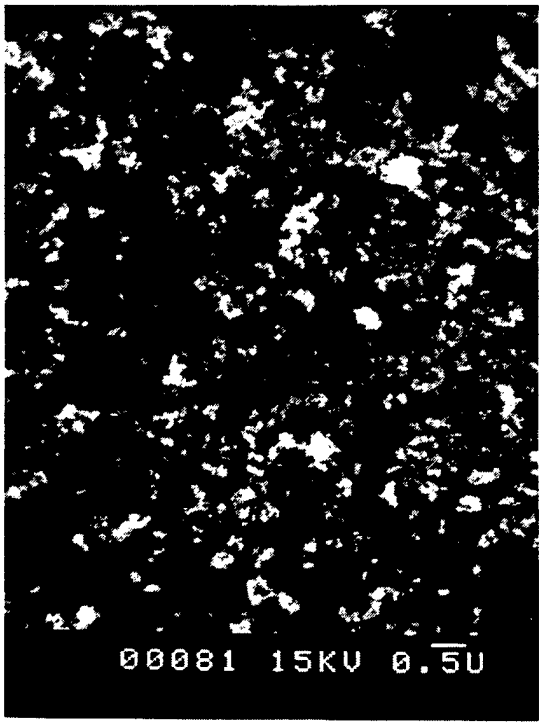

Figure 4.9 - Run 3-05 - Aft Tube Soot Sample

Figure 4.10 - Run 3-06 - Fore Tube Soot Sample

Figure 4.11 - Run 3-06 - Fore Tube Soot Sample

Figure 4.12 - Run 3-06 - Aft Tube Soot Sample

C. INFRARED EMISSIONS

Five infrared images are shown below on Figures 4.13, 4.14, 4.15, 4.16 , and 4.17 for (O/F) ratios 0.338, 0.494, 0.658, 0.895, and 1.115, respectively. For each run the total radiance from the plume to about 30 nozzle exit diameters was measured (Table 4.3). In addition the nozzle exit temperature was calculated for each run using TEP and corrected for C^*_{eff}. The plume emissivity was varied in the AGEMA software until the plume exit temperature matched the calculated temperature. The resulting axial variation in centerline temperature profiles are also shown in Figures 4.13 through 4.17, plotted versus distance in nozzle exit diameters downward from the nozzle exit plane.

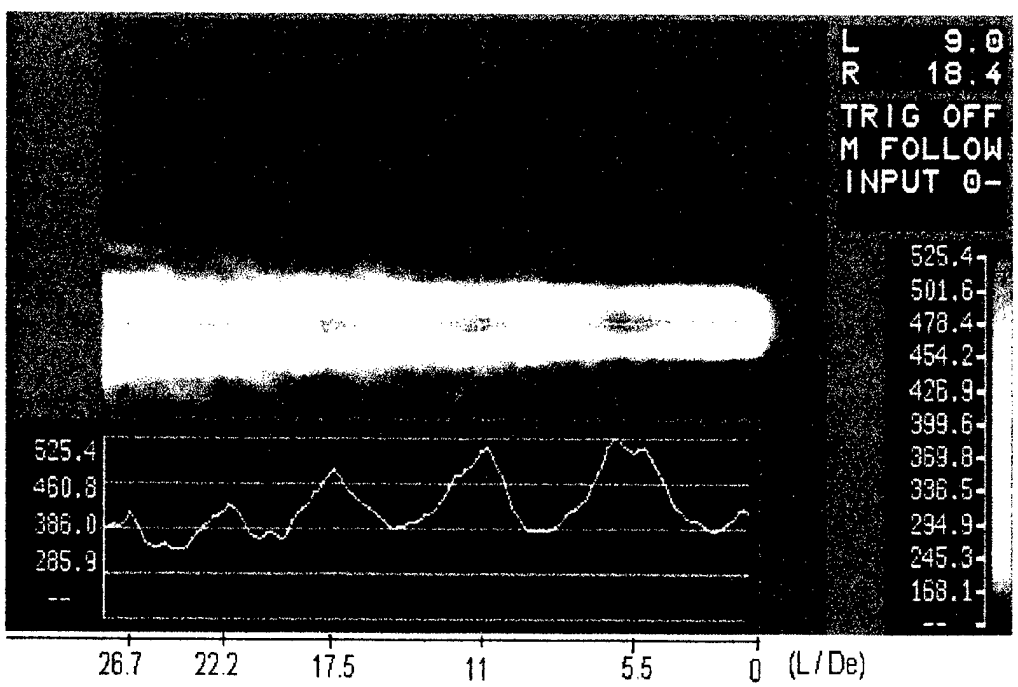

Figure 4.13 - Plume Temperature (K) Distribution for (O/F) = 0.338

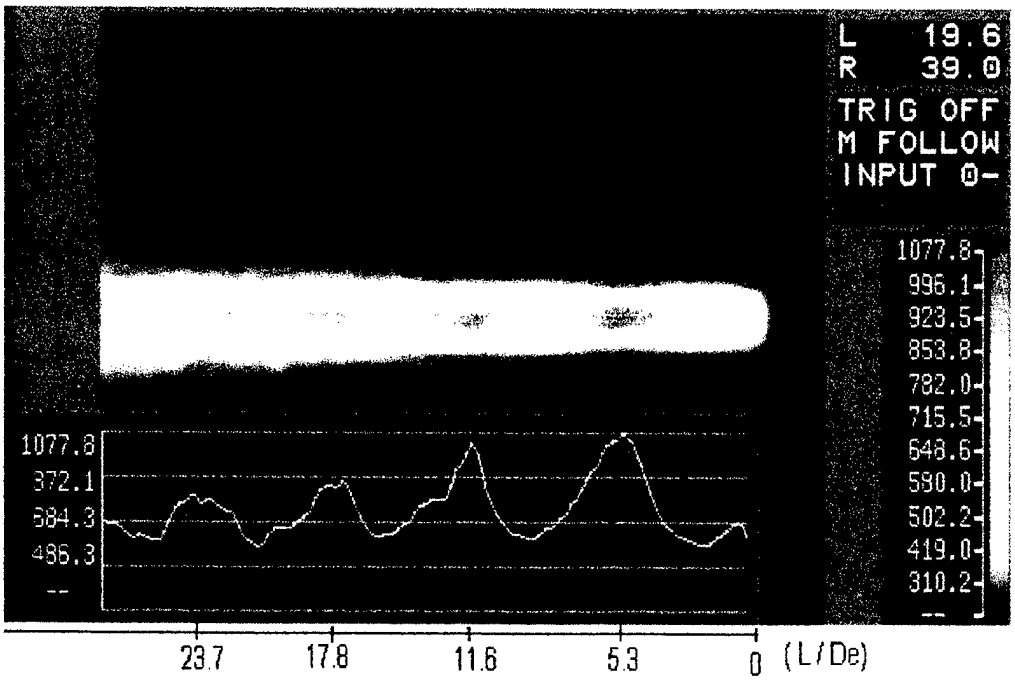

Figure 4.14 - Plume Temperature (K) Distribution for (O/F) = 0.494

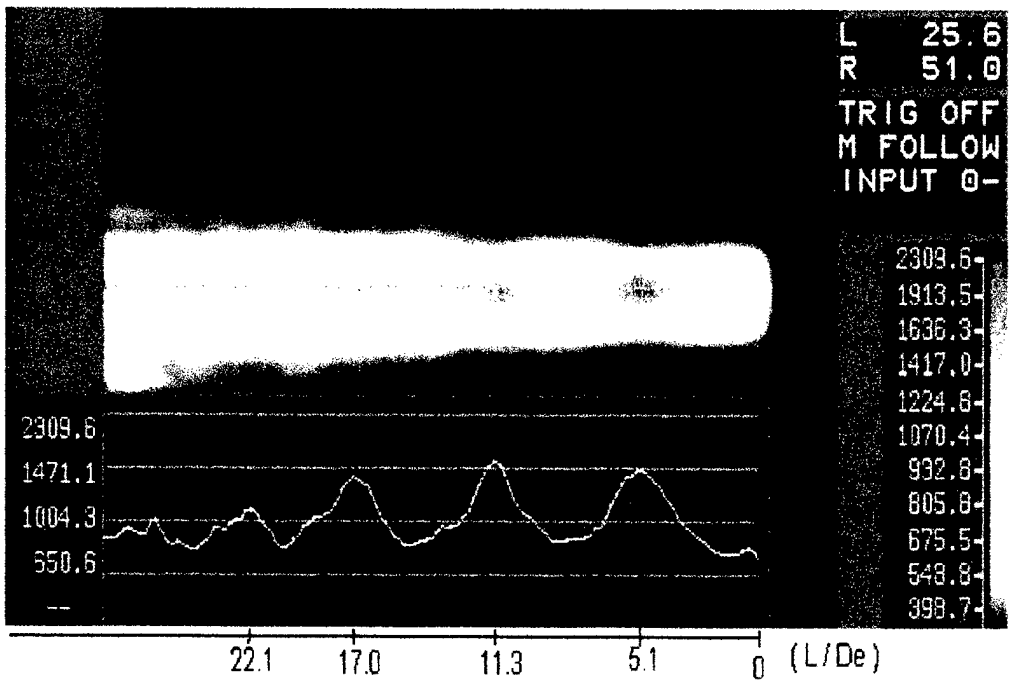

Figure 4.15 - Plume Temperature (K) Distribution for (O/F) = 0.658

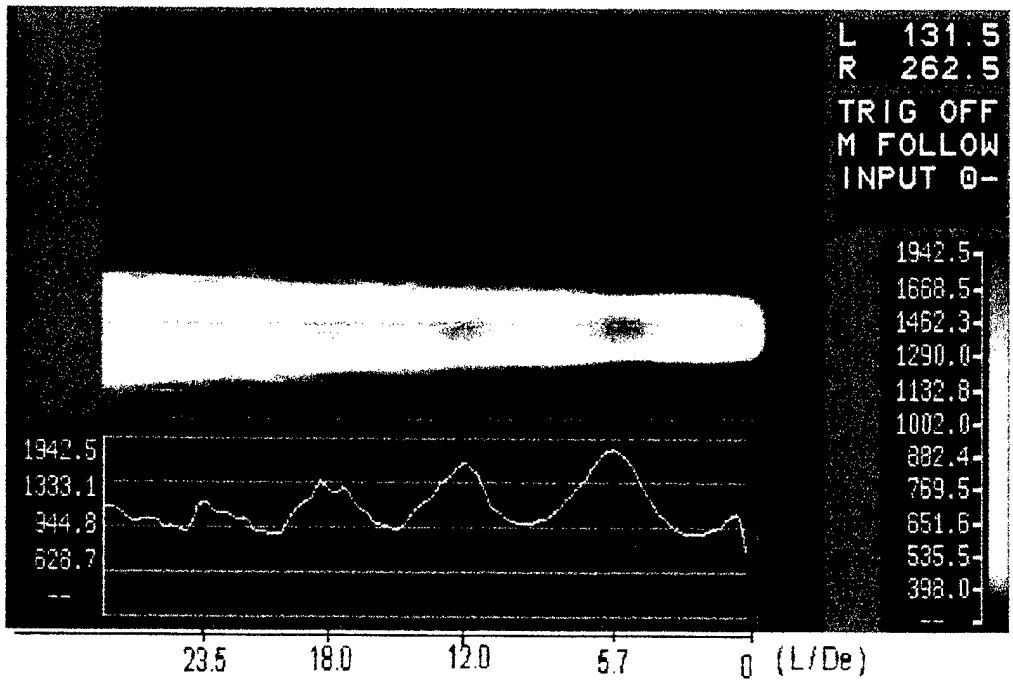

Figure 4.16 - Plume Temperature (K) Distribution for (O/F) = 0.895

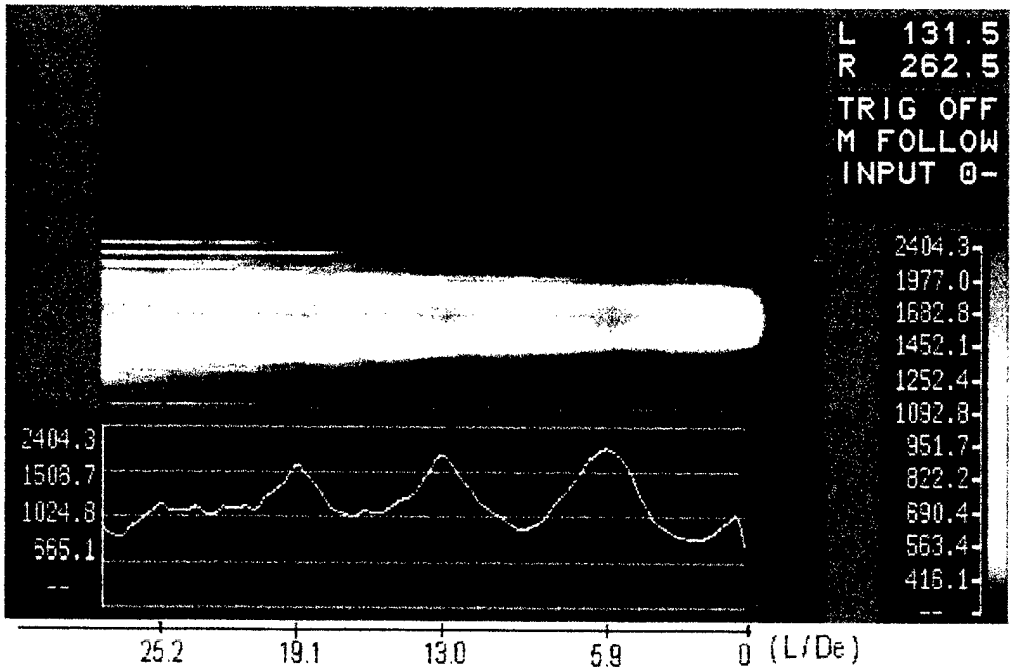

Figure 4.17 - Plume Temperature (K) Distribution for (O/F) = 1.115

Run #	O/F ratio	Calculated Equilibrium Nozzle Exit Temperature (K)	Emissivity (ε)	Total Radiance (W) (average)
5-35	0.338	411	0.072	23.8
5-39	0.494	645	0.045	33.6
5-34	0.658	845	0.032	80.2
3-01	0.895	996	0.182	173.5
3-06	1.115	1010	0.163	176.6

Table 4.3 - Total Radiance Measurements

D. VIDEO IMAGES

Figures 4.18, 4.19, and 4.20 show the effect of O/F ratio on the plume opacity.

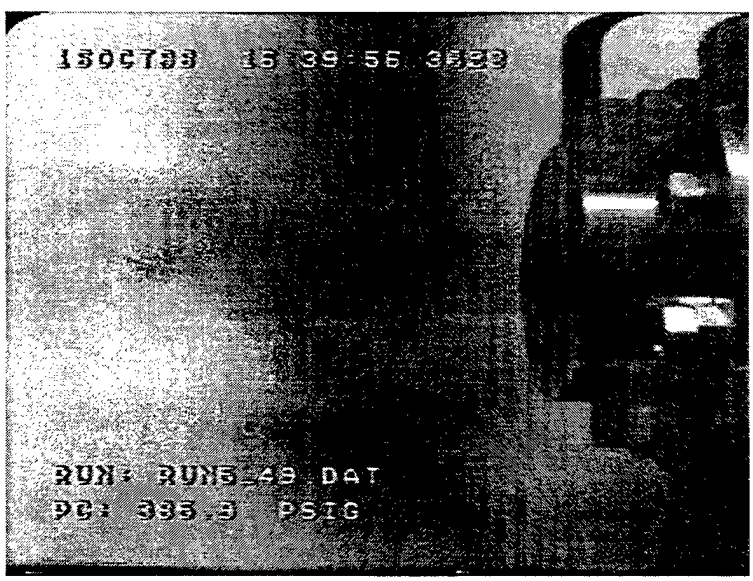

Figure 4.18 - Visible Plume Image for O/F=0.510

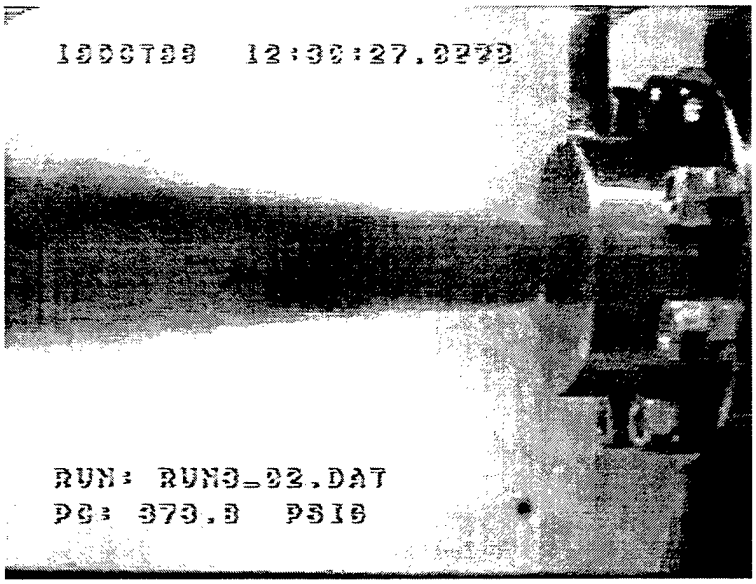

Figure 4.19 - Visible Plume Image for O/F=0.909

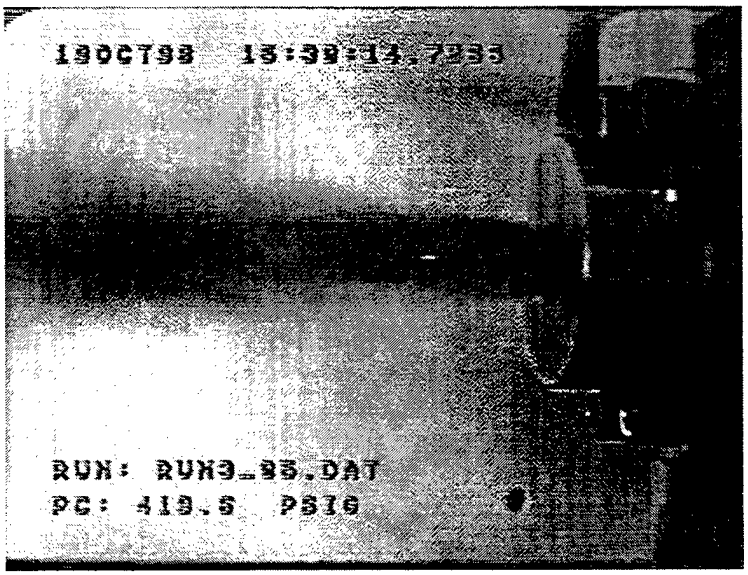

Figure 4.20 - Visible Plume Image for O/F=1.097

E. FUEL DROPLET SIZING

Several attempts were made to obtain the droplet size distributions with the Malvern Mastersizer system placed from 1.75 inch to 5 inches away from the injector head face. Unfortunately all of them presented transmittance values of about 1%, which made the analysis throroughly unreliable. Therefore, no good data could be obtained from these experiments. Future efforts will utilize a phase-Doppler particle analyzer (PDPA) to measure the spatial variation in the particle size distribution.

V. EXPERIMENTAL ANALYSIS

A. SOOT PROPERTIES

For each firing the transmittance values were run on the Mie code whose results are presented in Table 5.1. The parameter SSD (Sum of Squared Deviations)

Run #	(O/F) Ratio	Index of Refraction (m = a + b. i) (a +/- 0.02) (b +/- 0.01)	Log-Norm. Sigma (σg) (+0.04/-0.16)*	Sauter Diameter D_{32}(μm) (+/- 0.010)	SSD
5-41	0.330	2.53 – 0.03 i	1.01	0.411	0.04422
5-35	0.338	1.81 – 0.03 i	1.01	0.171	0.00509
5-42	0.360	2.05 – 0.03 i	1.17	0.060	0.01644
5-37	0.469	2.08 – 0.03 i	1.37	0.050	0.00390
5-39	0.494	1.95 – 0.05 i	1.01	0.076	0.00324
5-40	0.497	1.95 – 0.05 i	1.11	0.080	0.00213
5-49	0.510	2.30 – 0.13 i	1.41	0.050	0.01295
4-02	0.566	1.70 – 0.19 i	1.21	0.100	0.00086
5-33	0.572	2.05 – 0.21 i	1.12	0.100	0.00085
4-01	0.575	1.75 – 0.19 i	1.31	0.090	0.00087
4-03	0.581	1.65 – 0.35 i	1.21	0.070	0.00021
4-13	0.647	1.50 – 0.06 i	1.16	0.040	0.00068
5-32	0.658	1.80 – 0.29 i	1.32	0.060	0.00096
5-34	0.658	1.75 – 0.37 i	1.42	0.060	0.00026
4-10	0.660	1.73 – 0.15 i	1.01	0.271	0.00048
5-28	0.721	1.37 – 0.41 i	1.05	0.031	0.00066
5-29	0.744	1.37 – 0.47 i	1.06	0.090	0.00014
4-14	0.750	1.73 – 0.16 i	1.01	0.271	0.00093
4-15	0.754	1.40 – 0.29 i	1.21	0.270	0.00012
3-03	0.894	1.42 – 0.19 i	1.01	0.360	0.00050
3-01	0.895	1.32 – 0.32 i	1.01	0.320	0.00018
3-02	0.909	1.85 – 0.22 i	1.01	0.271	0.00082
3-04	1.080	2.36 – 0.20 i	1.04	0.200	0.00690
3-05	1.097	1.69 – 0.27 i	1.01	0.282	0.00079
3-06	1.115	1.55 – 0.20 i	1.01	0.330	0.00551

Table 5.1 - Mie Code Results (* σ_{min} = 1.00)

defined how well the values for index of refraction, log-normal sigma and D_{32} resulted in the best agreement between lnT-ratios and Q_{bar}-ratios. A perfect fit would yield SSD = 0. The results of Table 5.1 represent the minimum SSD values that could be obtained for each set of transmittance values. In general, values of SSD which represented very good fits had orders of magnitude of $10^{-3} to 10^{-4}$. Some of the SSD values were greater and were mostly the ones with greater value for the real part of the index of refraction.

The variation of "a" (index of refraction real part) with O/F ratios did not present a significant trend. The values were typical of those reported in the literature [Ref. 2,13]. Values of "a">1.95 generally occurred when the data correlation was poor. The absorption coefficient ("b") was quite low for the most fuel-rich conditions. As the O/F ratio was increased the absorption coefficient approached values most often measured for soot (0.3 – 0.7) [Ref. 2,13]. The low "effective" values of "b" were also observed by Powell & Zinn [Ref. 13] and Santoro, et al [Ref. 14]. They report that the effect was due to the particulate consisting of loosely packed soot. Powell & Zinn [Ref. 13] determined that for a measured value of "b"=0.075 the fraction of optical mean volume occupied by particulate was only 0.184. The current data appear to indicate that very fuel-rich conditions result in very porous soot particulate which becomes more dense as the O/F ratio is increased. Except for three values, when the O/F ratio was less than 0.75, D_{32} was smaller than 0.1μm. When the O/F ratio was higher than 0.75 D_{32} was 0.20→0.36μm, which is more typical of the sizes observed in gas turbine engine plumes. The relatively

high uncertainty on σ_g shows that even for the very low values (e.g., 1.01) the actual particle distribution may be far from monodisperse.

The uncertainties presented in Table 5.1 for index of refraction (real and imaginary part) and geometric standard deviation (σg) were obtained using the Mie code. Each variable was individually varied away from the optimal solution until the calculated D_{32} had a significant variation (usually 10%). A similar approach was used for the D_{32} uncertainty, using a variation in SSD to three times the best-case value.

B. SOOT CONCENTRATION VERSUS O/F RATIO

With the methodology presented in Chapter II, the soot mass concentration was calculated. The results are presented in Table 5.2 and plotted in Figure 5.1.

The achievement of low values of SSD was in most cases relatively easy. However, for some transmittance sets, if the ranges for index of refraction (m) that the Mie code swept through were not limited to reasonable values, even lower values of SSD could be obtained for higher (>3.0) values of the real part of 'm'. These over-calculated values for the real part of 'm' were far from those presented anywhere in the literature for soot and were not used. The next best fits were taken, still with very low SSD values. It should be noted that %C(gr) was obtained using ρ_{soot}=1.5 g/cm3. As pointed out in the previous section the particulate density may have been considerably less for the most fuel-rich conditions. This would decrease %C(gr) below the values shown in Table 5.3 , giving a much steeper rise on %C(gr) in Figure 5.1.

Run #	O/F ratio	%C(gr)	Run #	O/F ratio	%C(gr)
5-28	0.721	18.19	4-03	0.581	15.98
5-29	0.744	14.36	4-10	0.660	15.81
5.32	0.658	19.89	4-13	0.647	15.40
5-34	0.658	16.38	4-14	0.750	13.89
5-35	0.338	0.96	4-15	0.754	21.46
5-37	0.469	10.64	3-01	0.895	18.18
5-39	0.494	11.54	3-02	0.909	18.34
5-40	0.497	11.31	3-03	0.894	17.58
5-41	0.330	1.17	3-04	1.080	4.56
5-49	0.510	12.61	3-05	1.097	8.03
4-01	0.575	16.22	3-06	1.115	9.58
4-02	0.566	15.71	---	---	---

Table 5.2 - Soot Mass Concentration vs. O/F Ratios

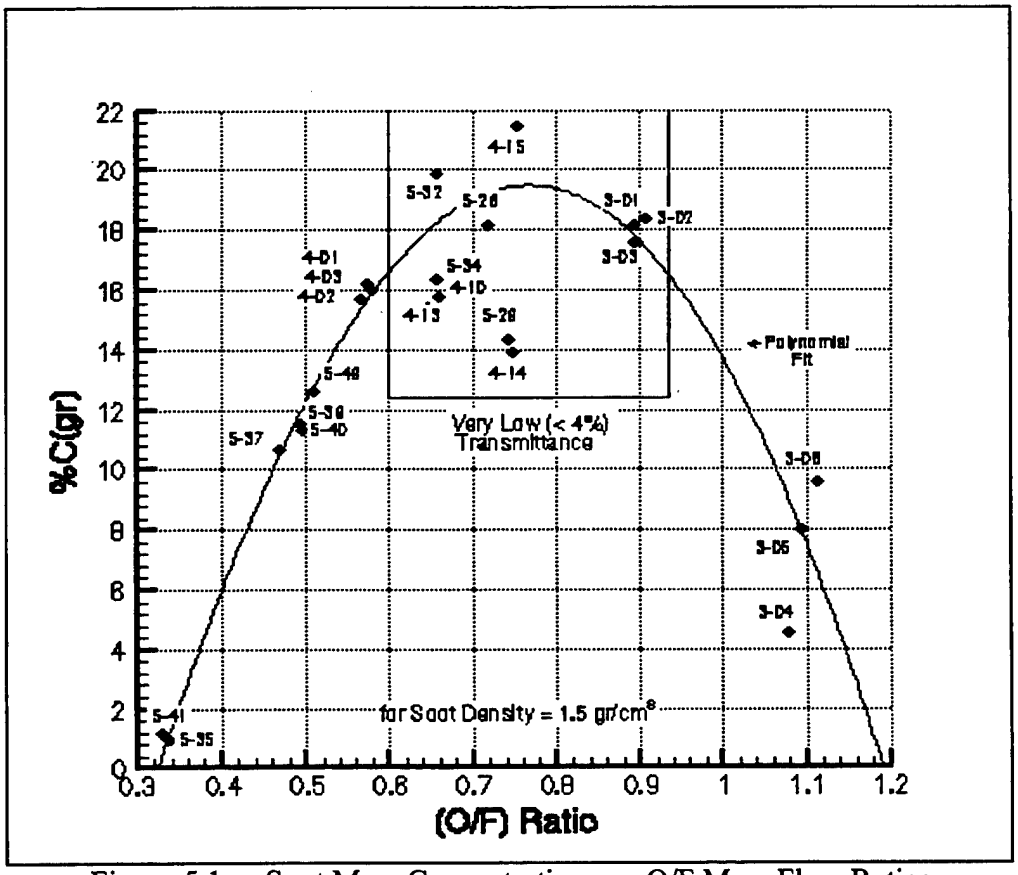

Figure 5.1 - Soot Mass Concentration vs. O/F Mass Flow Ratios

Using a simple average of the transmittance for all five wavelengths as a parameter, it was observed that when it was lower than 4% (which happened for O/F ratios between 0.6 and 0.90, as shown in Figure 5.1) there was considerable scatter in the soot concentration values, except for runs 3-01 through 3-03. Outside this O/F ratio range soot concentrations were significantly repeatable. Runs 3-04 through 3-06 seeemed to have been significantly affected by the plume afterburning. Unfortunately this O/F ratio condition could not be repeated in time due to the combustion chamber failure, but the transmittance values were very stable. For the most fuel-rich condition tested (O/F ~ 0.33) it was hard to get good results from the Mie Code, which may have been related to a significant portion of unburned fuel mixed with the soot particles in the plume or to the probable porosity of the soot particle. These were relatively cold firings and it would be likely that condensed fuel droplets could exist in the plume. The particulate analysis assumed that only soot particles were present in the plume.

Figure 4.1 shows C* efficiencies over 100%. This behavior comes possibly from the theoretical C* values given by the TEP code, which assumes perfect mixing and instantaneous chemical equilibrium. These assumptions may give lower chamber stagnation temperature and C*'s than actually exists because of incomplete combustion. It is believed that a significant portion of the fuel could actually be going through the rocket motor without any chemical reaction. Thus, for the fuel-rich conditions of this investigation, combustion would occur closer to stoichiometric conditions. This would increase the chamber pressure and, thus, the experimental C* value above those obtained assuming chemical equilibrium of all combustion products.

C. UNCERTAINTY ANALYSIS FOR THE SOOT CONCENTRATION

An uncertainty analysis was conducted on the O/F ratios and on the %C(gr) values. O/F ratios obviously depended on the oxygen and fuel mass flow rates. Oxygen mass flow rate uncertainties were calculated for a +/- 0.0005" tolerance on the choked throat diameter, a +/- 2K accuracy on oxygen temperature, +/- 2 psi on upstream pressure, and 0.5% on choked throat discharge coefficient. This resulted in a +/-2.53% uncertainty in oxygen mass flow rate values. On the fuel side, accuracies were +/- 2 psi on upstream venturi pressure, +/-0.94% for the 0.052"venturi throat diameter venturi and +/-0.65% for all other venturis used. The accuracies resulted in a +/-2.1% uncertainty in O/F ratio for runs using the 0.052" venturi and +/-1.8% uncertainty in O/F ratio for runs using all other venturis. Figure 5.2 shows the previous plot with these O/F uncertainties included. Considering now the uncertainties on %C(gr) one of the runs was picked for full analysis. Run 4-02 was selected for its relatively low SSD and for being outside the lower-than-4% transmittance O/F range. For the mean transmittance values for each wavelength obtained from the Oriel system we originally had a best fit of:

$m=1.70-0.19i$, $\sigma g=1.21$, $D_{32}=0.1002$ micron, SSD=0.0008649, $Q_{bar}(577nm)=0.26413$ $T(577nm)=0.1500$, %C(gr)= 15.71%.

The uncertainties in %C(gr) may come from the uncertainties in transmission values read by the Oriel system, and from uncertainties of the index of refraction, geometric standard deviation and soot mean diameter (expressed in Table 5.1). It was found that the transmission readings were very steady and presented a negligible

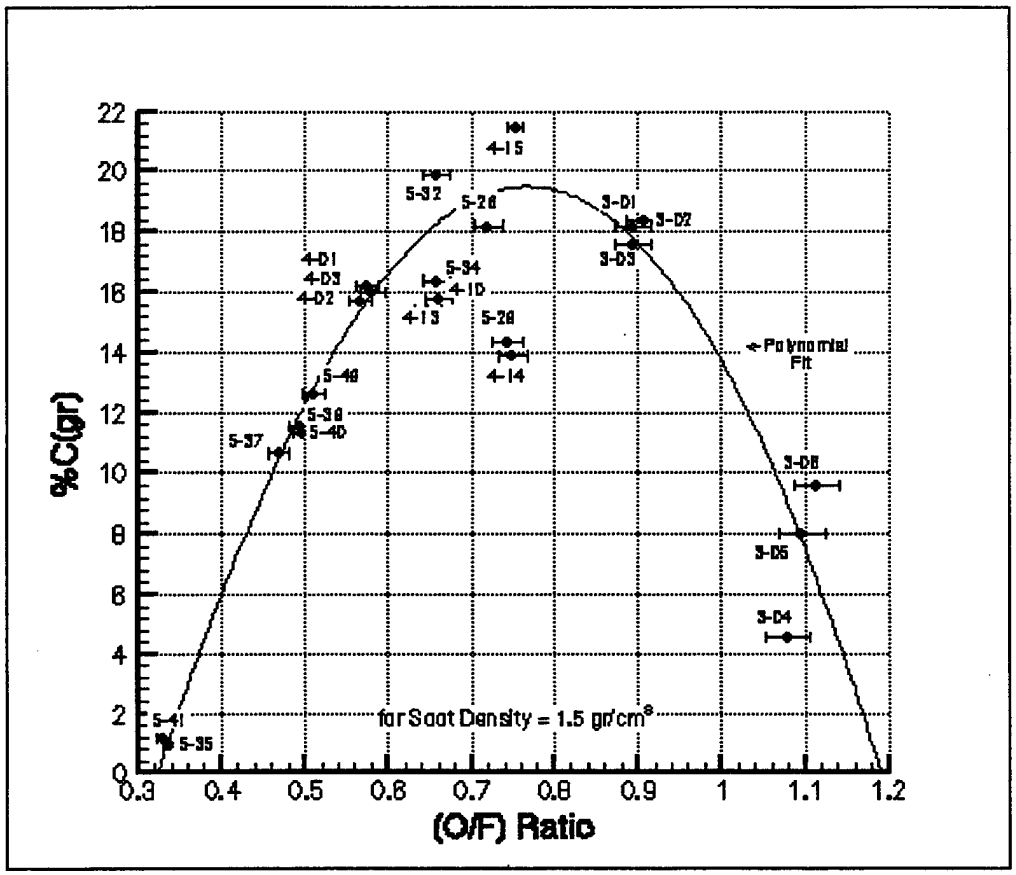

Figure 5.2 - Soot Concentration vs. O/F Ratio with Uncertainties

uncertainty. The influence on %C(gr) was calculated independently for the uncertainties in "a","b", σg and D_{32}. Uncertainty in "a" was +/- 0.02, which gave a +/- 4.80% uncertainty in %C(gr). Uncertainty in "b" was +/- 0.01, which gave a +/- 3.55% uncertainty in %C(gr). Uncertainty in σg was –0.16/+0.04, which gave a +3.12%/-1.23% uncertainty in %C(gr). Uncertainty in D_{32} was +/- 0.010μm, which gave a +/- 5.6% uncertainty in %C(gr). The uncertainty, when considered altogether, may increase above the independent uncertainty figures, and the unprobable worst case cennario (all pluses/all

minuses) would give a maximum uncertainty on %C(gr) of +/- 16.1%. It would be safe to say the overall uncertainty on %C(gr) was probably lower than +/- 5%. As discussed above, the variation in soot particulate density would have a one-to-one influence on %C(gr).

D. INFRARED EMISSIONS

Figures 4.13 through 4.17 showed temperature distributions along the plume centerline. Temperatures in the plume ranged approximately from 600K to 2200K. The Mach disks resulted in a significant part of the total radiation. It should be noted that the Mach disks are highly visible both optically and by the temperature profile, even for the most opaque plumes. Table 4.3 presented the total plume radiance measured to 28 nozzle exit diameters (D_e) downward from the nozzle exit plane. Even though the centerline temperature distribution seemed to behave as if no afterburning was occurring for the O/F ratio of 1.115, it was observed in the video image aft of 28 D_e. The measured radiance for O/F=1.115 was expected to be significantly lower than for O/F=0.895 (a significant drop in soot concentration), which was not obtained. This was probably due to the significant radiation from the downstream afterburning that reached the camera lens. If this occurred, the temperature would have been much higher than the value of 1010 K used in Table 4.3, and would result in a lower emissivity. The low values of emissivity are more typical of those for gases and the higher values to those of particulate, possibly indicating the dominant radiation mechanism shifts as the soot concentration increased.

E. SOOT SAMPLING

Figures 4.2 through 4.12 showed the photomicrographs of runs 3-03, 3-04, 3-05, and 3-06 which had D_{32} values of 0.3602μm (σg=1.01), 0.2001μm (σg=1.04), 0.2815μm (σg=1.01), and 0.3301μm (σg=1.01), respectively. These low values of σg would indicate a nearly monodisperse distribution. However, it has already been shown that the uncertainties were high on σg, which is supported by the photomicrographs. Figures 4.2 and 4.3 (run 3-03 – fore tube) showed that spherical particles were a significant presence with diameters ranging approximately from 0.1 to 0.4μm. It also showed some filiform particles and particle agglomerates. Figures 4.4 and 4.5 (run 3-04 – fore tube) showed not as many spherical particles, with diameters ranging approximately from 0.1 to 0.3μm, but a greater amount of irregular but compact particle agglomerates as big as 0.75μm. Figures 4.6, 4.7, and 4.8 (run 3-05 – fore tube) showed not only a significant presence of spherically shaped particles with diameters ranging approximately from 0.1 to 0.4μm, but also filiform agglomerates of particles within this diameter range. Figure 4.9 (run 3-05 – aft tube) showed basically the same particle diameter range except that the presence filiform particles and agglomerates was more significant. Figures 4.10 and 4.11 (run 3-06 – fore tube) showed a significant amount of spherically shaped particles with diameters ranging from 0.1 to 0.6μm. Not a significant amount of agglomerates nor filiform particles were observed. Figure 4.12 (run 3-06 – aft tube) showed some particles as big as 1μm which may not have been soot, but the picture quality did not allow a better analysis.

It is not known whether the filiform particles and agglomerates existed in the flow or were a result of the collection process. The larger size of the spherical particles from these runs were in qualitative agreement with the 0.20→0.36 μm values of D_{32} obtained optically.

VI. CONCLUSIONS AND RECOMMENDATIONS

The multiple-wavelength light extinction technique was generally successful for obtaining soot concentration and properties in a plume of a kerosene/gaseous oxygen rocket motor over the fuel-rich O/F ratio range where the soot concentration was predicted to have a rise-peak-drop behavior.

The results implied that the soot particulate was very porous for the most fuel-rich conditions and became more compact as the O/F ratio increased. Soot mean diameter (D_{32}) was less than 0.1 μm when the O/F ratio was less than 0.75, but increased to 0.2→0.36 μm for higher O/F ratios. The soot particle diameters obtained from the SEM photomicrographs of collected soot samples were in qualitative agreement with the diameters measured optically. Soot concentration in the plume was found to rapidly increase and then decrease as the O/F ratio was increased from 0.3 to 1.1 , with a peak near O/F = 0.76. Infrared measurements in the 3.5-5 μm band indicated a probable shift in the dominant radiation source from gas to particulate as the soot concentration increased.

The turbulence ring combustor design apparently could not withstand the conditions imposed by the higher O/F ratios and should be improved or re-designed. The Malvern Mastersizer was inadequate for the spray particle sizing. A phase Doppler particle analyzer (PDPA), which can typically measure particles down to a minimum diameter of 0.5μm with a dynamic range (d_{max}:d_{min}) of 50:1, could be used with much better chances of getting reliable results.

The experimental technique developed in this investigation is basically ready to go to the next step in the planned study, which would analyze the influence of fuel additives on soot generation. For better results it is recommended: to shield the light sensors from background radiation such as afterburning using a ducted light beam; to possibly increase burning time to get very stable transmission results, away from torch gas influence and transients; to increase the white-light lamp power and then use selective optical filters to equalize the 5 wavelength power peaks to minimize the influence of noise, especially on the ultraviolet range.

APPENDIX A. MIE SCATTERING CODE LISTING

The Mie Scattering Code listed hereafter is a modified version of the miescat4.for code used by Swenson [Ref. 3]. The data reduction process (i.e., finding the best combination of complex index of refraction, geometric standard deviation and Sauter mean diameter for the measured transmittances) was initially modified to be run on a microcomputer using Microsoft Fortran Powerstation, but the attempt was not successful due to a problem with this software which could not be solved in time. So the version presented here was run on the NPS Aeronautics Department's Silicon Graphics Powerstation in a Unix environment. The final version was checked for proper results against the original Cashdollar program [Ref. 2]. The code allows iteration starting values, step sizes, and the number of loops to be input in the data file for complex index of refraction and geometric standard deviation. The difference between the current miescat5.for and Swenson's miescat4.for was that miescat5.for did three loops instead of two, sweeping through real and immaginary parts of the index of refraction besides the geometric standard deviation. Another new feature was that when all numbers of loops were set to 1 in the data file, the program generated and saved Q vs D, and Qbar vs. D32 for the specified index of refraction and geometric standard deviation. If any of the number of loops was not 1, then the code understood it was a search for the best case, did not save Q vs. D nor Qbar vs. D32, but saved all the best cases for each set of index of refraction and geometric standard deviation. This made the program run faster and generate only those files necessary for each situation.

```
c  **********  PROGRAM MIESCAT5.F   FOR  5 WAVELENGTHS  **********

C
C                BY KENNETH CASHDOLLAR,  1976
C                REVISED BY THOMAS WELDON, JULY, 1977
C                  BASED ON PROGRAM MICOEF BY C D LITTON AND Z J FINK
C
C   modified by Silvino L.C. SILVA to obtain the best
c                   index of refraction,log-normal sigma and
c                   respective D32, for a given set of transmission
c                   coefficients (from 5 wavelengths)
C
C      QBAR CALCULATES ABSORPTION AND EXTINCTION COEFFICIENTS FOR LIGHT
C    TRANSMISSION THROUGH DUST PARTICLES WITH COMPLEX REFRACTIVE INDEX
C    AND A LOG-NORMAL SIZE DISTRIBUTION, THEN PLOTS THE RESULTS
C
C
C
C
C****************  DATA INPUT FORMAT  **********************************
C
C
C         VARIABLE NAMES AS IN PROGRAM
C
C   ROW 1 ... T1,T2,T3,T4,T5
C   ROW 2 ... WAV(1),WAV(2),WAV(3),WAV(4),WAV(5)
C   ROW 3 ... NUMR,STEPR
C   ROW 4 ... NUMI,STEPI
C   ROW 5 ... NUMS,STEPS
C   ROW 6 ... RDUST,RMED
C   ROW 7 ... L2,L3,DS,DELDS
C   ROW 8 ... ND,SIGMA,SD32,SDL32
C
C        FORMATS AND VARIABLE DESCRIPTION

C*********************************************************************
C
C
C
C
      PROGRAM MIESCAT5

      COMPLEX R,RDUST,RSUST1,DI,DELDI,RX,RINDX(5),DIS,DELIS
      COMPLEX COEFR,DPR,XJR,DJR,PR,OPTRDUST
      DIMENSION DPR(1000),XJR(1000),DJR(1000),PR(1000)
      REAL X,D,DELD,DS,DELDS,CO,COE,COEF,QEXT,QABS,QSCA,XM,AREL,XMINT
      REAL SD32,SDL32,SIGMA,STEPR,STEPI,STEPS,RDUST1R,RDUST1I,WAVE
      REAL WAVL(5),QBARCHK,DQ,DIAM32
      INTEGER M,NPTS1,MINT,K,NUMR,NUMI,NUMS,L
      INTEGER ND,NBEST
      REAL XY(1000),WAV(5),SMALLEST
      REAL DP(1000),XK(1000),XJ(1000),DJ(1000),P(1000)
      REAL RAT51(1000),RAT52(1000),RAT53(1000),RAT54(1000)
      REAL RAT41(1000),RAT42(1000),RAT43(1000)
      REAL RAT31(1000),RAT32(1000),RAT21(1000)
      REAL RAT51A(1000),RAT52A(1000),RAT53A(1000),RAT54A(1000)
```

```
      REAL RAT41A(1000),RAT42A(1000),RAT43A(1000)
      REAL RAT31A(1000),RAT32A(1000),RAT21A(1000),SSD(1000)
      REAL GAMMA,BETA
      COMPLEX A(1000),B(1000),C(1000),RDUST1
      COMPLEX ALPH,XH(1000),DH(1000),E(1000),DE(1000)
      COMMON/ADQ/DQ(1000,2)
      COMMON ALLQ(10000,4,5)
      COMMON/AVG1/DIAM32(1000),WAV(5)


      OPEN(UNIT=1, FILE='mie5inp.dat', STATUS='UNKNOWN')
      OPEN(UNIT=2, FILE='QLnTRatios.dat', STATUS='UNKNOWN')
      OPEN(UNIT=3, FILE='QvsD.dat',   STATUS='UNKNOWN')
      OPEN(UNIT=4, FILE='QbarD32.dat',STATUS='UNKNOWN')
      OPEN(UNIT=5, FILE='BestD32.dat',STATUS='UNKNOWN')

C-----------------------------------------------------------------------

C
C    RDUST IS COMPLEX REFRACTIVE INDEX OF DUST PARTICLES, WITH MINUS
C    RMED IS REAL REFRACTIVE INDEX OF MEDIUM

      READ(1,102)T1,T2,T3,T4,T5
      WRITE(*,102)T1,T2,T3,T4,T5
102   FORMAT(F7.5,2X,F7.5,2X,F7.5,2X,F7.5,2X,F7.5)
      READ(1,103)WAV(1),WAV(2),WAV(3),WAV(4),WAV(5)
      WRITE(*,103)WAV(1),WAV(2),WAV(3),WAV(4),WAV(5)
103   FORMAT(F6.4,2X,F6.4,2X,F6.4,2X,F6.4,2X,F6.4)
      write(5,801)wav(1),t1,wav(2),t2,wav(3),t3,wav(4),t4,wav(5),t5
      READ(1,104)NUMR,STEPR
      write(5,103)t1,t2,t3,t4,t5
      write(5,103)wav(1),wav(2),wav(3),wav(4),wav(5)
      write(5,104)numr,stepr
      WRITE(*,104)NUMR,STEPR
      READ(1,104)NUMI,STEPI
      write(5,104)numi,stepi
      WRITE(*,104)NUMI,STEPI
      READ(1,104)NUMS,STEPS
      write(5,104)nums,steps
      WRITE(*,104)NUMS,STEPS
104   FORMAT(I3,2X,F4.3)

      READ(1,32)RDUST,RMED
      write(5,32)rdust,rmed
      WRITE(*,32)RDUST,RMED
32    FORMAT (2F6.3,2X, F6.3)

      READ(1,34)L2,L3,DS,DELDS
      write(5,34)L2,L3,ds,delds
      WRITE(*,34)L2,L3,DS,DELDS
34    FORMAT(I3,2X,I3,2X,F6.4,2X,F6.4)

      READ(1,12)ND,SIGMA,SD32,SDL32
      write(5,12)nd,sigma,sd32,sdL32
      WRITE(*,12)ND,SIGMA,SD32,SDL32
12    FORMAT(I3,2X,F5.3,2X,F5.3,2X,F5.3)

      RDUST1=RDUST
      RDUST1R=REAL(RDUST1)
      RDUST1I=IMAG(RDUST1)
```

```
      SMALLEST=1000.
      OPTSSD=1000.
C=====================================================================

      DO 9 INDEX1=1,NUMS
      RDUST1R=REAL(RDUST)
      write(*,655)index1,nums
655   format(/,'ON Sigma loop Index1=',i3,' /',i3)
C                        (STARTING OVERALL LOOP ON SIGMA)
      DO 8 INDEX2=1,NUMR
      RDUST1I=IMAG(RDUST)
      write(*,656)index2,numr
656   format('  On RdustR loop Index2=',i3,' /',i3)
C                         (STARTING OVERALL LOOP ON RDUSTR)
      DO 6 INDEX3=1,NUMI
      write(*,657)index3,numi
657   format('    on RdustI loop Index3=',i3,' /',i3)
C                          (STARTING OVERALL LOOP ON RDUSTI)
C ---------------------------------------------------------------------
C     IMAGINARY PART OF R CHANGED TO POSITIVE TO CONFORM TO EXPANSION
C                                        FORMULA IN PROGRAM
      RDUST1=CMPLX(RDUST1R,0.0)+CMPLX(0.0,RDUST1I)
      RX=RDUST1/RMED
      R=CONJG(RX)
      RINDX(1)=RX
      RINDX(2)=RX
      RINDX(3)=RX
      RINDX(4)=RX
      RINDX(5)=RX
C-------------------------------------------------------------
C      INITIAL VALUES FOR ARRAY
      DO 51 K=1,5
      DO 52 J=1,2
      ALLQ(1,J,K)=0.0
      ALLQ(1,J+2,K)=0.0
      DO 53 I= 2,10000
      ALLQ(I,J,K)=100.0
      ALLQ(I,J+2,K)=1.0
   53 CONTINUE
   52 CONTINUE
   51 CONTINUE
C----------------
      DO 54 I=1,1000
      DIAM32(I)=0.0
      RAT51(I)=0.0
      RAT52(I)=0.0
      RAT53(I)=0.0
      RAT54(I)=0.0
      RAT41(I)=0.0
      RAT42(I)=0.0
      RAT43(I)=0.0
      RAT31(I)=0.0
      RAT32(I)=0.0
      RAT21(I)=0.0
      RAT51A(I)=0.0
      RAT52A(I)=0.0
      RAT53A(I)=0.0
      RAT54A(I)=0.0
      RAT41A(I)=0.0
      RAT42A(I)=0.0
```

```
      RAT43A(I)=0.0
      RAT31A(I)=0.0
      RAT32A(I)=0.0
      RAT21A(I)=0.0
      SSD(I)=0.0
   54 CONTINUE
C-----------------------------------------------------------------
      DO 4 NI=1,5
C                                (STARTING OVERALL LOOP ON WAVELENGTHS)
C      WRITE(2,106) Wav(NI)
C      WRITE(*,106) Wav(NI)
C  106 FORMAT(/,' Entering the Wavelenth loop for Lambda=',F7.4)

      WAVE=WAV(NI)
      WAVL(NI)=WAVE*10000.0
C
C      INITIAL VALUES SET
C
C    MAX VALUE FOR D IS (1000*WAVE)/(1.3*PI*RMED) = 244*WAVE/RMED
C    D IS REAL DIAMETER IN MICRONS,DELD IS INCREMENT
C    DI=I*D IS COMPLEX DIAMETER, DELDI IS INCREMENT
C    X IS REAL SIZE PARAMETER  X= PI*DIAMETER*RMED/WAVELENGTH
C    ALPH IS COMPLEX SIZE PARAMETER, ALPH=I*X

      D=DS
      DELD=DELDS
      DI=DIS
      DELDI=DELIS
C
C-----------------------------------------------------------------------
C
      M=1
      DO 3 J=1,L3
      DO 2 I=1,L2
      X=3.14159*D/WAVE*RMED
      ALPH=3.14159*DI/WAVE*RMED
      XJ(1)= SIN(X)/X
      XJ(2)= SIN(X)/(X**2)- COS(X)/X
      XJR(1)=CSIN(R*X)/(R*X)
      XJR(2)=CSIN(R*X)/((R*X)**2)-CCOS(R*X)/(R*X)
      XH(1)=CEXP(ALPH)/ALPH
      XH(2)=((-CEXP(ALPH))/X)-((0.,1.)*CEXP(ALPH)/(X**2))
      DJ(1)= COS(X)/X- SIN(X)/(X**2)
      DJR(1)=CCOS(R*X)/(R*X)-CSIN(R*X)/((R*X)**2)
      DH(1)=CEXP(ALPH)/X+((0.,1.)*CEXP(ALPH)/(X**2))
      QEXT=0.0
      QSCA=0.0
C
C        L1 = ITERATIONS FOR SPHERICAL FUNCTIONS,  L1=1.3*X
      L1=1.3*X
      IF(L1.LE.10)  L1=10
      DO 1 L=1,L1
      CO=(FLOAT(L))/(2*L+1)
      COE=(FLOAT(L+1))/(2*L+1)
      COEF=(FLOAT(2*L+1))/X
      COEFR=(FLOAT(2*L+1))/(R*X)
      XJ(L+2)=COEF*XJ(L+1)-XJ(L)
      XJR(L+2)=COEFR*XJR(L+1)-XJR(L)
      XH(L+2)=COEF*XH(L+1)-XH(L)
      DJ(L+1)=CO*XJ(L)-COE*XJ(L+2)
```

```
      DJR(L+1)=CO*XJR(L)-COE*XJR(L+2)
      DH(L+1)=CO*XH(L)-COE*XH(L+2)
      P(L)=X*XJ(L+1)
      PR(L)=(R*X)*XJR(L+1)
      DP(L)=XJ(L+1)+X*DJ(L+1)
      DPR(L)=XJR(L+1)+(R*X)*DJR(L+1)
      E(L)=X*XH(L+1)
      DE(L)=XH(L+1)+X*DH(L+1)
      A(L)=((DPR(L)*P(L))-(R*PR(L)*DP(L)))/((DPR(L)*E(L))-(R*PR(L)*DE(L
     1)))
      B(L)=((R*DPR(L)*P(L))-(PR(L)*DP(L)))/((R*DPR(L)*E(L))-(PR(L)*DE(L
     1)))
      C(L)=A(L)+B(L)
      GAMMA=CABS(A(L))
      BETA=CABS(B(L))
      XK(L)=(FLOAT(2*L+1))*(2./(X**2))*((GAMMA**2)+(BETA**2))
      XY(L)=(FLOAT(2*L+1))*(2./(X**2))*(REAL(C(L)))
      QEXT=QEXT+XY(L)
      QSCA=QSCA+XK(L)
    1 CONTINUE
      QABS=QEXT-QSCA
      DQ(M,1)=D
      DQ(M,2)=QEXT
C      WRITE(2,22)X,DQ(M,1),QABS,DQ(M,2),M
C 22  FORMAT(9X,2HA=,F8.3,4X,2HD=,F7.3,4X,5HQABS=,F6.3,4X,5HQEXT=,F6.3,4
C     1X,I3)


C=====================================================================
C     D AND QEXT FOR MONODISPERSE PUT INTO PLOTTING ARRAY
C     EVERY FOURTH POINT CALCULATED IS PUT INTO ARRAY- ALLQ
C
C      XM=M
C      AREL=XM/4.0
C      MINT=M/4
C      XMINT=MINT
C      IF (AREL.NE.XMINT) GO TO 60
C      IF (D.GT.1.20) GO TO 60
C      NUMBER OF POINTS FOR PLOTS 1 AND 3 IS NPTS1
C      NPTS1=MINT
C=====================================================================
      ALLQ(M,1,NI)=D
      ALLQ(M,3,NI)=QEXT
C----------------------------
C    INCREMENT SIZE PARAMETERS        D=DIAMETER
      D=D+DELD
      DI=DI+DELDI
      M=M+1
    2 CONTINUE
C              (end loop on L2)
C---------------------------------------------------------------------

      DELD=2.0*DELD
      DELDI=2.0*DELDI
    3 CONTINUE
C              (end loop on L3)
C---------------------------------------------------------------------
      CALL QAVG(M,NI,ND,SIGMA,NPTS2,SD32,SDL32)
      K1=ND+1
```

```
    4 CONTINUE
C                (end loop on NI)
C-----------------------------------------------------------------------
C       This  DO(600) is to print out QvsD  , when it is
 the case of running a single value for index of refraction(m) and sigma
(in this case, m and sigma should be set the wanted value and  all the
variables numr,numi and nums made equal to 1)

C       DO 600 I=1,M-1
C      WRITE(3,601)ALLQ(I,1,1),ALLQ(I,3,1),ALLQ(I,3,2),ALLQ(I,3,3),ALLQ(I
C      1,3,4),ALLQ(I,3,5)
601    FORMAT(6(F11.5))
C600    CONTINUE
C------------saving list of D, and Qext for the 5 wavelengths for
plotting....
       IF(numi.ne.1) GOTO  702
       DO 700 J=2,K1
       WRITE(4,601)ALLQ(J,2,1),ALLQ(J,4,1),ALLQ(J,4,2),ALLQ(J,4,3),ALLQ(J
      1,4,4),ALLQ(J,4,5)
700    CONTINUE
702    CONTINUE


C------------saving list of D32, and Qbar for the 5 wavelengths for
plotting...
C  ==================================================================
C          EVALUATING THE TRANSMISSION LOG RATIOS AND SSD's
C
c       SMALLEST=1000.
       K=ND+1
       DO 650 N=2,K
       RAT51(N)=ALLQ(N,4,5)/ALLQ(N,4,1)
       RAT52(N)=ALLQ(N,4,5)/ALLQ(N,4,2)
       RAT53(N)=ALLQ(N,4,5)/ALLQ(N,4,3)
       RAT54(N)=ALLQ(N,4,5)/ALLQ(N,4,4)
       RAT41(N)=ALLQ(N,4,4)/ALLQ(N,4,1)
       RAT42(N)=ALLQ(N,4,4)/ALLQ(N,4,2)
       RAT43(N)=ALLQ(N,4,4)/ALLQ(N,4,3)
       RAT31(N)=ALLQ(N,4,3)/ALLQ(N,4,1)
       RAT32(N)=ALLQ(N,4,3)/ALLQ(N,4,2)
       RAT21(N)=ALLQ(N,4,2)/ALLQ(N,4,1)
       RAT51A(N)=(RAT51(N)-ALOG(T5)/ALOG(T1))**2
       RAT52A(N)=(RAT52(N)-ALOG(T5)/ALOG(T2))**2
       RAT53A(N)=(RAT53(N)-ALOG(T5)/ALOG(T3))**2
       RAT54A(N)=(RAT54(N)-ALOG(T5)/ALOG(T4))**2
       RAT41A(N)=(RAT41(N)-ALOG(T4)/ALOG(T1))**2
       RAT42A(N)=(RAT42(N)-ALOG(T4)/ALOG(T2))**2
       RAT43A(N)=(RAT43(N)-ALOG(T4)/ALOG(T3))**2
       RAT31A(N)=(RAT31(N)-ALOG(T3)/ALOG(T1))**2
       RAT32A(N)=(RAT32(N)-ALOG(T3)/ALOG(T2))**2
       RAT21A(N)=(RAT21(N)-ALOG(T2)/ALOG(T1))**2
       SSD(N)=RAT51A(N)+RAT52A(N)+RAT53A(N)+RAT54A(N)+RAT41A(N)+RAT42A(N)
       SSD(N)=SSD(N)+RAT43A(N)+RAT31A(N)+RAT32A(N)+RAT21A(N)

       IF(SSD(N).LT.SMALLEST) NBEST=N
       IF(SSD(N).LT.SMALLEST) SMALLEST=SSD(N)

650    CONTINUE
```

```
C ===========collecting the optimum results along all the best ones
      IF(SSD(NBEST).LT.OPTSSD) OPTRDUST=RDUST1
      IF(SSD(NBEST).LT.OPTSSD) OPTSIGMA=SIGMA
      IF(SSD(NBEST).LT.OPTSSD) OPTD32=ALLQ(NBEST,2,1)
      IF(SSD(NBEST).LT.OPTSSD) OPTSSD=SSD(NBEST)
c=====================================================================
C                 PRINTOUT OF TRANSMISSION RATIOS AND LOG QBAR RATIOS
      IF(NUMI.NE.1)GOTO 715
      WRITE(2,705)RDUST1,SIGMA,ALLQ(NBEST,2,1),SSD(NBEST)

      T51=ALOG(T5)/ALOG(T1)
      T52=ALOG(T5)/ALOG(T2)
      T53=ALOG(T5)/ALOG(T3)
      T54=ALOG(T5)/ALOG(T4)
      T41=ALOG(T4)/ALOG(T1)
      T42=ALOG(T4)/ALOG(T2)
      T43=ALOG(T4)/ALOG(T3)
      T31=ALOG(T3)/ALOG(T1)
      T32=ALOG(T3)/ALOG(T2)
      T21=ALOG(T2)/ALOG(T1)
      WRITE(2,714)T51,RAT51(NBEST),T51
714   FORMAT(3(1X,F12.8))
      WRITE(2,714)T52,RAT52(NBEST),T52
      WRITE(2,714)T53,RAT53(NBEST),T53
      WRITE(2,714)T54,RAT54(NBEST),T54
      WRITE(2,714)T41,RAT41(NBEST),T41
      WRITE(2,714)T42,RAT42(NBEST),T42
      WRITE(2,714)T43,RAT43(NBEST),T43
      WRITE(2,714)T31,RAT31(NBEST),T31
      WRITE(2,714)T32,RAT32(NBEST),T32
      WRITE(2,714)T21,RAT21(NBEST),T21
715   CONTINUE

c -------------- recording all the best ones in file BestD32.dat  ------
c      goto 383
      WRITE(5,705)RDUST1,SIGMA,ALLQ(NBEST,2,1),SSD(NBEST)
705   FORMAT(' m=',2f6.4,'i  Sigma=',f5.3,
     1'  gives best  D32=',f6.4,' w/  SSD=',F12.7)

c   printing into screen SSD values to follow the run...
      WRITE(*,707)SSD(NBEST)
707   FORMAT(35X,'SSD= ',f12.7)

383   continue
      RDUST1I=RDUST1I-STEPI
6     CONTINUE
c-------------------------------end loop on RDUST1I -----
      RDUST1R=RDUST1R+STEPR
8     CONTINUE
c-------------------------------end loop on RDUST1R ----------
      SIGMA=SIGMA+STEPS
9     CONTINUE
c------------------------------ end loop on SigmaG -----------------
c
=====================================================================
c     ------------ recording and printing the optimum results -----
      WRITE(*,801)WAV(1),T1,WAV(2),T2,WAV(3),T3,WAV(4),T4,WAV(5),T5
      WRITE(5,801)WAV(1),T1,WAV(2),T2,WAV(3),T3,WAV(4),T4,WAV(5),T5
801   FORMAT(/,' for T(',f6.4,')=',f6.4,'  T(',f6.4,')=',f6.4,
     1'  T(',f6.4,')=',f6.4,' T(',F6.4,')=',F6.4,' T(',F6.4,')=',F6.4)
```

```
      WRITE(*,802)OPTRDUST,OPTSIGMA,OPTD32,OPTSSD
      WRITE(5,802)OPTRDUST,OPTSIGMA,OPTD32,OPTSSD
802   FORMAT(/,'THE OPTIMUM RESULTS ARE:',/,'m=',2f6.4,'i ',
     1'with SigmaG=',f5.3,' which gives D32=',f6.4,' and SSD=',
     1f12.7)

      STOP
      END

C-----------------------------------------------------------------------
      SUBROUTINE QAVG(M,NI,ND,SIGMA,NPTS2,SD32,SDL32)
C
C                BY KENNETH CASHDOLLAR, 1976
C
C    QAVG CALCULATES D32 AND QBAR FOR A GIVEN QEXT VS D AND
C    A GIVEN LOG-NORMAL SIZE DISTRIBUTION
C
C
C    INPUT DATA = ND,SIGMA,D32,DEL32
C
      INTEGER M
      INTEGER ND
      REAL ALLQ,DQ,DIAM32
      COMMON ALLQ(10000,4,5)
      COMMON/ADQ/DQ(1000,2)
      COMMON/AVG1/DIAM32(1000),WAV(5)


C        DQ(I,1)=D,  DQ(I,2)=QEXT
C     NI=WAVELENGTH OR REFRACTIVE INDEX CHANGE
C    ND IS NUMBER OF D32,QBAR CALCULATIONS
C    SIGMA IS THE GEOMETRIC STANDARD DEVIATION
C    D32 IS THE SURFACE WEIGHTED MEAN DIAMETER
C    DEL32 IS INCREMENT FOR D32
C    DIST IS SURFACE WEIGHTED LOG-NORMAL SIZE DISTRIBUTION
C      M IS THE MAXIMUM NUMBER OF POINTS IN Q-ARRAY FOR MONODISPERSE
C
C      PRINT 240
C  240 FORMAT(8X,'D32
',7X,'DMIN',7X,'DMAX',5X,'NMBR',6X,'D10X',7X,'D32X'
C    1,8X,'QBAR',7X,'I'/)
C
C      WRITE(*,1000)WAV(NI)
C1000  FORMAT('  ENTERING SUBROUTINE QAVG FOR LAMBDA=',F7.4,' MICRON')
C
      D32=SD32
      DEL32=SDL32
C

C      NUMBER OF POINTS FOR PLOTS 2 AND 4 IS NPTS2
      NPTS2=ND+1
      DO 17 NN=1,ND
C
      DMIN=D32/SIGMA**3.
      DMAX=D32*SIGMA**2.5
      AS=ALOG(SIGMA)**2.
      DG=EXP(ALOG(D32)-2.5*AS)
      QSUM=0.0
      DSUM=0.0
```

```
      XSUM=0.0
      DHOLD=0.0
      DNSUM=0.0
      XNSUM=0.0
      NMBR=0
      MM=M-2
      DO 13  N=1,MM
C
      IF (DQ(N,1).LT.DMIN) GO TO 13
      IF (DQ(N,1).GT.DMAX) GO TO 15
      IF (NMBR.GT.0) GO TO 242
      DMINZ=DQ(N,1)
C
  242 CONTINUE
      DD=DQ(N+1,1)-DQ(N,1)
      AA=(ALOG(DQ(N+1,1)/DG))**2/(2.0*AS)
      DIST=EXP(-AA)*DQ(N+1,1)/SQRT(6.2832*AS)
      QSUM=QSUM+(DIST*DQ(N+1,2)+DHOLD*DQ(N,2))*DD/2.0
      DSUM=DSUM+(DIST*DQ(N+1,1)+DHOLD*DQ(N,1))*DD/2.0
      XSUM=XSUM+(DIST+DHOLD)*DD/2.0
      XNSUM=XNSUM+(DIST/DQ(N+1,1)**2+DHOLD/DQ(N,1)**2)/2.0*DD
      DNSUM=DNSUM+(DIST/DQ(N+1,1)+DHOLD/DQ(N,1))/2.0*DD
      XHOLD=DQ(N+1,1)
      DHOLD=DIST
      NMBR=NMBR+1
   13 CONTINUE
   15 CONTINUE
      QBAR=QSUM/XSUM
      D32X=DSUM/XSUM

      D10X=DNSUM/XNSUM
      ALLQ(NN+1,2,NI)=D32X
      ALLQ(NN+1,4,NI)=QBAR

      DIAM32(NN+1)=D32

C      QBARCHK(NN+1,1,NI)=D32X
C      QBARCHK(NN+1,2,NI)=QBAR

      D32=D32+DEL32
   17 CONTINUE
C      WRITE(*,1001)WAV(NI)
C1001  FORMAT('  Leaving  Subroutine QAVG for Lambda=',F7.4,' micron')

      RETURN
      END
c=================================================================
c typical input file (mieinp.dat) should be like...
c
c  0.8000  0.7000  0.6000  0.5000  0.4000
c  0.3130  0.4600  0.6328  0.7200  0.8500
c   04  .100
c   10  .050
c   11  .050
c   1.700-0.050  1.0000
c  250  001  0.0060  0.0050
c  120  1.010  0.030  0.010
.
```

APPENDIX B. ROCKET MOTOR DRAWINGS

Four basic pieces formed the rocket motor: injector head, chamber section, turbulence ring, and nozzle. In this appendix all four drawings are given in this same sequence. The injector head drawing was the same, for 8, 6, 5, 4, 3 and 2-fuel elements. This part was not water cooled. The injector head's central orifice was meant for the oxygen flow and the peripherical orifices for the kerosene. Three water cooled chamber sections were used to provide the desired combustor length. The turbulence ring was a solid disk with internal diameter smaller than the chamber section internal diameter, and was mounted between the first and the second chamber sections. The nozzle was also water cooled and employed conical convergent and divergent sections. The rocket motor also utilized two extra rings, just like the turbulence ring except that the internal diameter was equal to the chamber section internal diameter. They had a radial, 1/16" diameter hole to provide measurement of the chamber pressure. These two rings were mounted adjacent to the injector head and between the second and third chamber sections, one on each side of the turbulence ring.

INJECTOR HEAD DRAWING

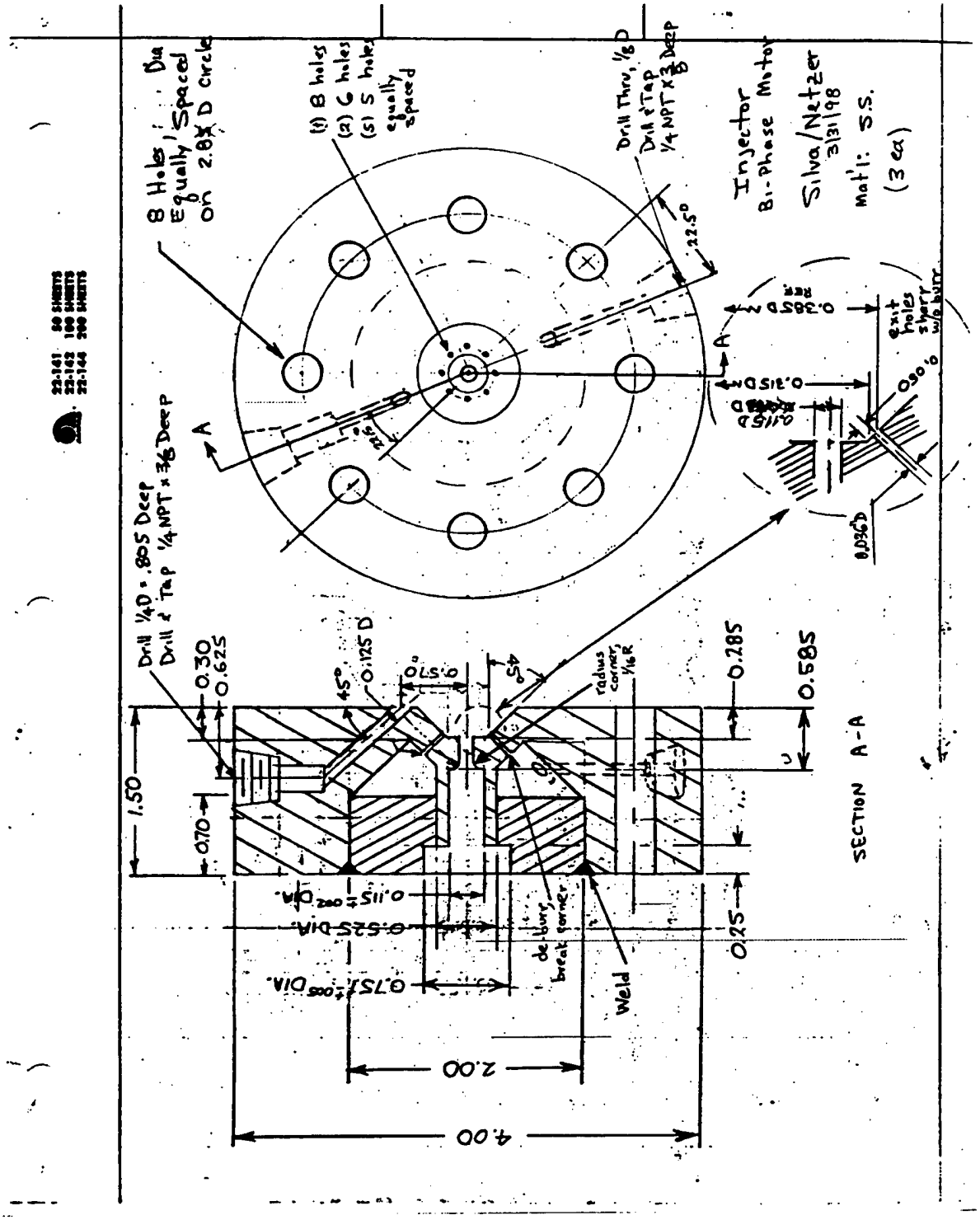

CHAMBER SECTION DRAWING

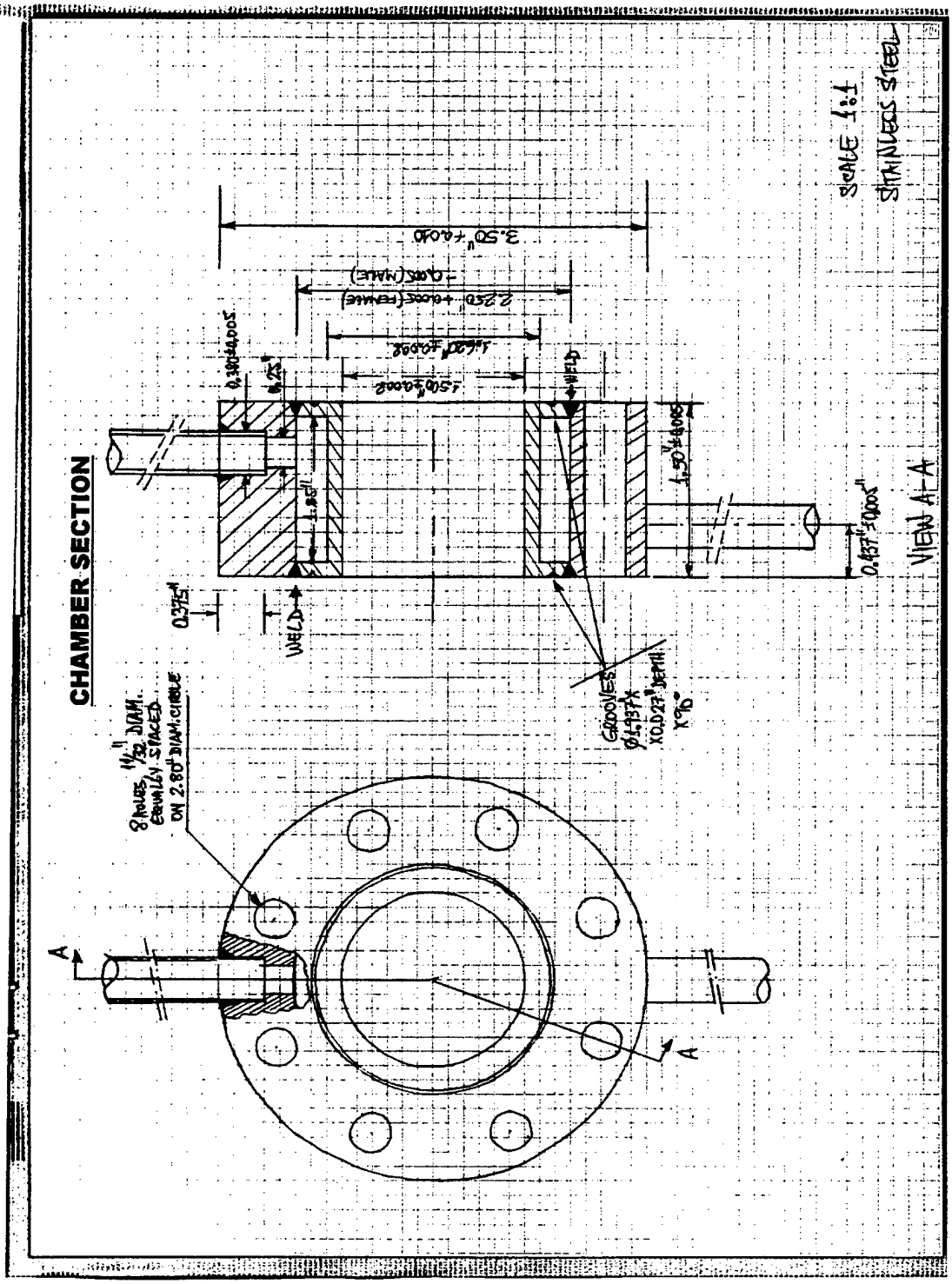

TURBULENCE RING

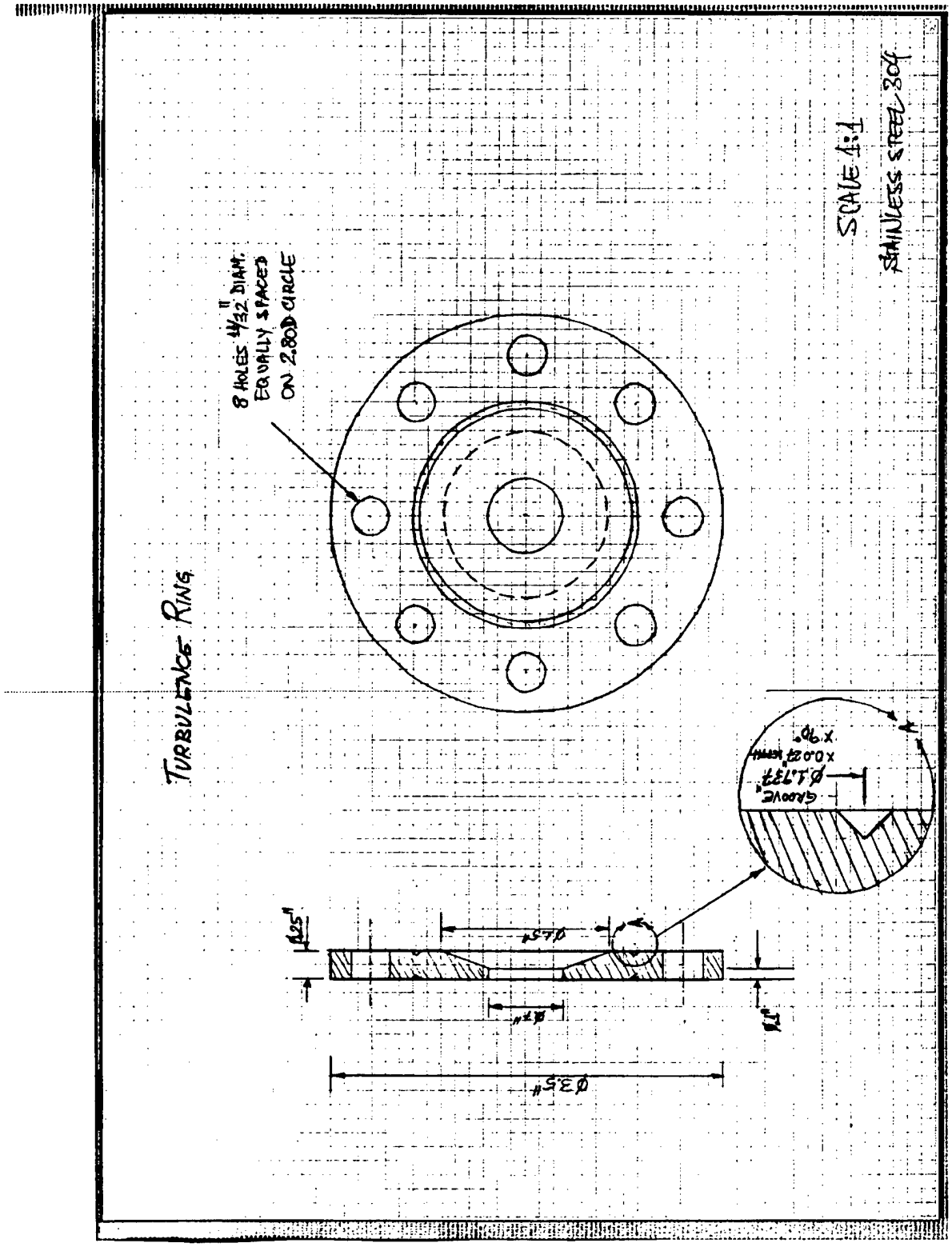

NOZZLE

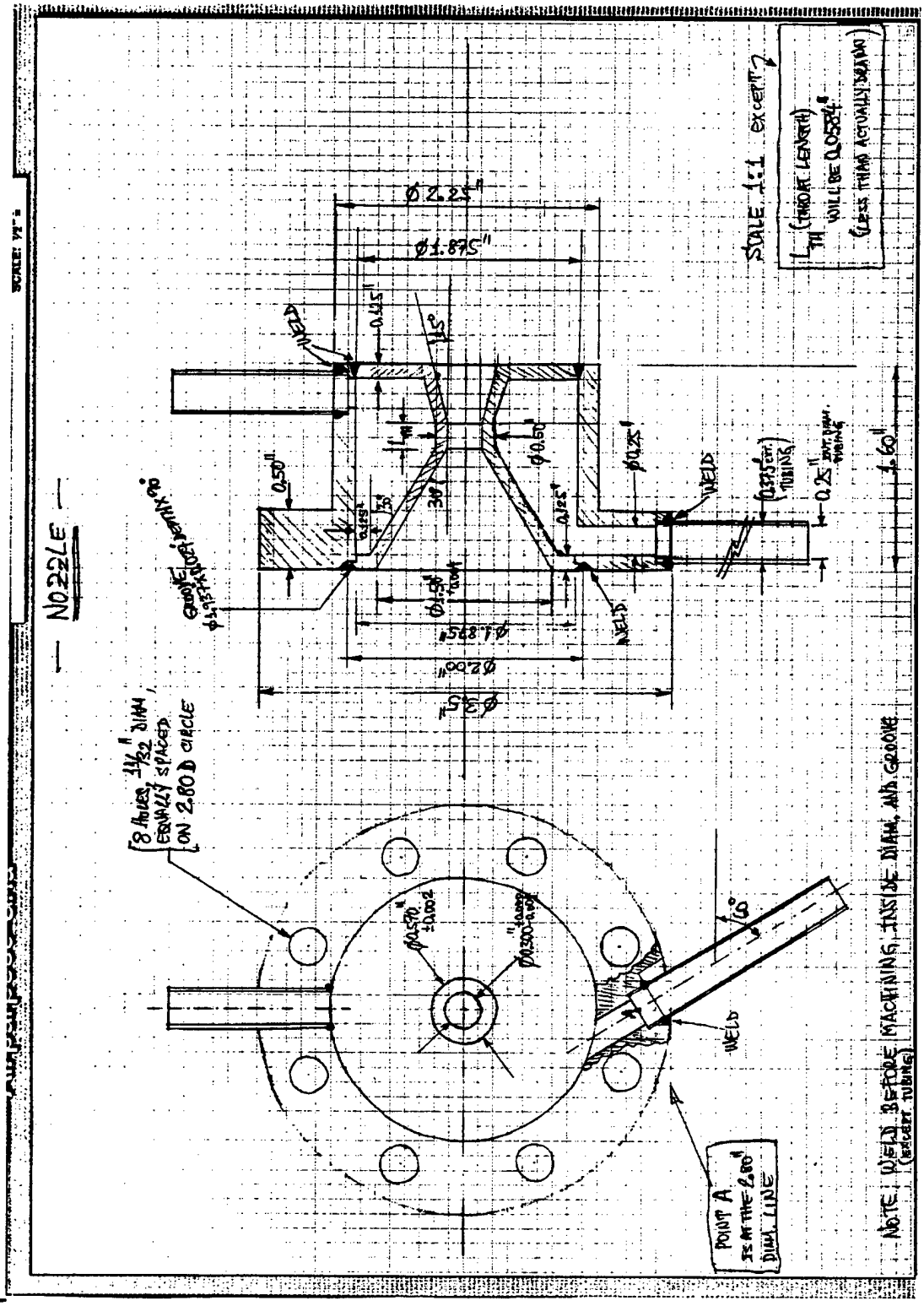
NOZZLE
SCALE 1:1 EXCEPT
(THROAT LENGTH) WILL BE 0.0584" (LESS THAN ACTUALLY DRAWN)
Ø2.25"
Ø1.875"
Ø2.00"
Ø3.5"
WELD
8 HOLES, 11/32" DIAM EQUALLY SPACED ON 2.80 D CIRCLE
POINT A IS AT THE 2.80" DIAM. LINE
NOTE: WELD BEFORE MACHINING, INSIDE DIAM. AND GROOVE (EXCEPT TUBING)

APPENDIX C. PRESSURE VS. TIME TRACES

The following pressure transducer and diode voltage traces are from the actual firings whose soot concentration results were plotted in Chapter V. All plots have a run number on the top. Variables plotted were:

P_{O2}Choke – the oxygen sonically choked throat upstream pressure

P_{fuel}Venturi – the kerosene cavitating venturi upstream pressure

P_{O2}Low – the oxygen line pressure immediately before entering the injector head

P_{fuel}Low – the kerosene line pressure immediately before entering the injector head

$P_{chamber}$ – two lines for chamber pressure (at the injector head and at mid-chamber)

He-Ne Voltage – the diode voltage from the helium-neon laser beam

Also given are the venturi orifice diameters used in the fuel (kerosene) line and the actual (O/F) ratio for each firing. It should be noticed that for some runs (those with too low pressure difference between P_{fuel}Venturi and P_{fuel}Low) the venturi calibration formula will not match the (O/F) shown. That was because in these cases the venturi did not actually cavitate and the calibration did not apply. For these cases specific extra fuel flow calibrations were done reproducing upstream and downstrem venturi pressures to get reliable mass flow rates.

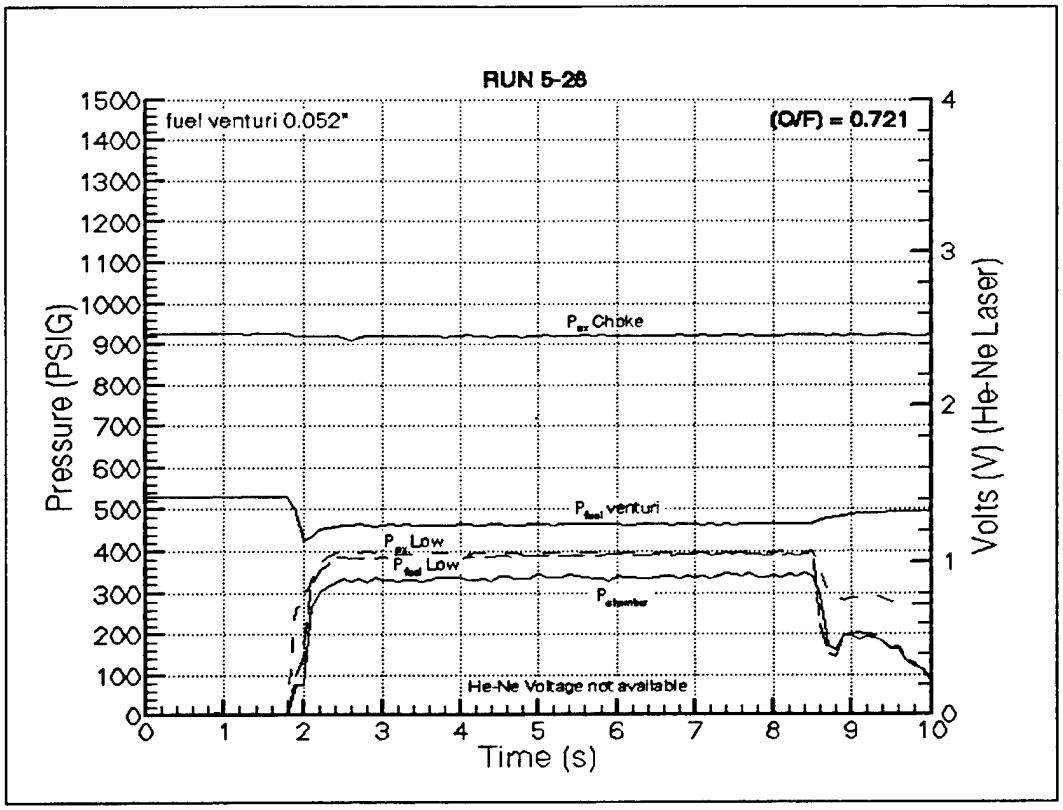
RUN 5-28
fuel venturi 0.052"
(O/F) = 0.721
Pressure (PSIG)
Volts (V) (He-Ne Laser)
Time (s)
P_ox Choke
P_fuel venturi
P_ox Low
P_fuel Low
P_chamber
He-Ne Voltage not available

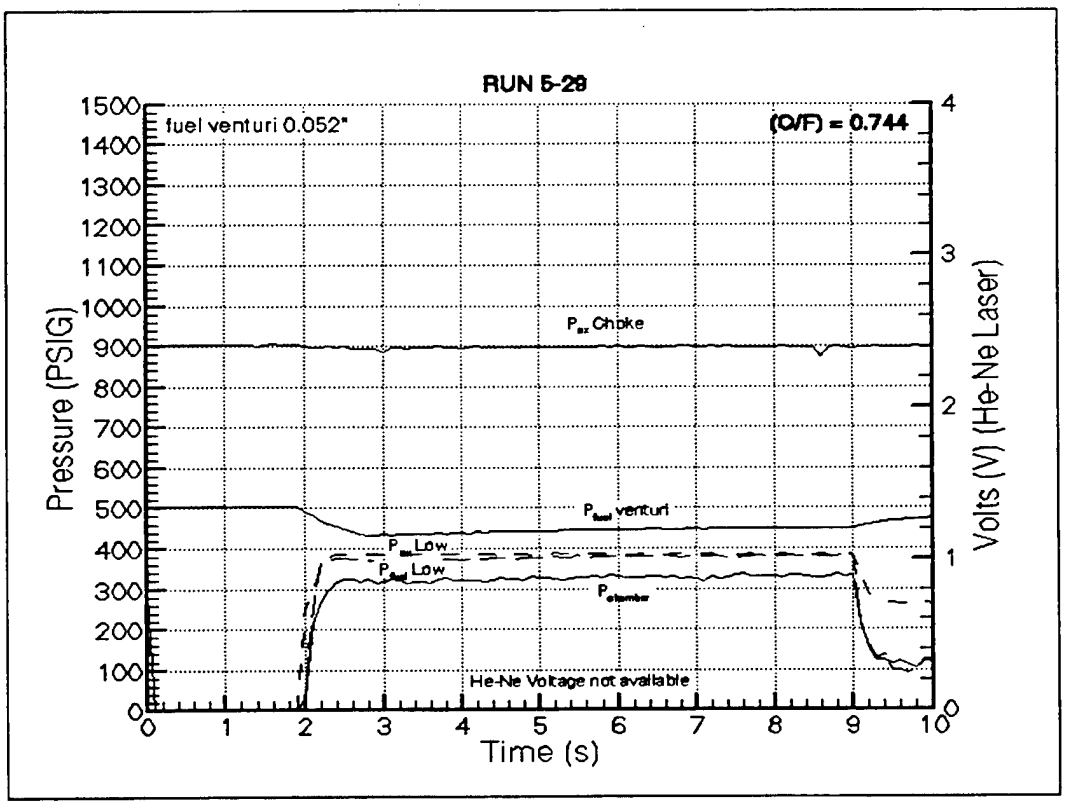
RUN 5-29
fuel venturi 0.052"
(O/F) = 0.744
Pressure (PSIG)
Volts (V) (He-Ne Laser)
Time (s)
P_ox Choke
P_fuel venturi
P_ox Low
P_fuel Low
P_chamber
He-Ne Voltage not available

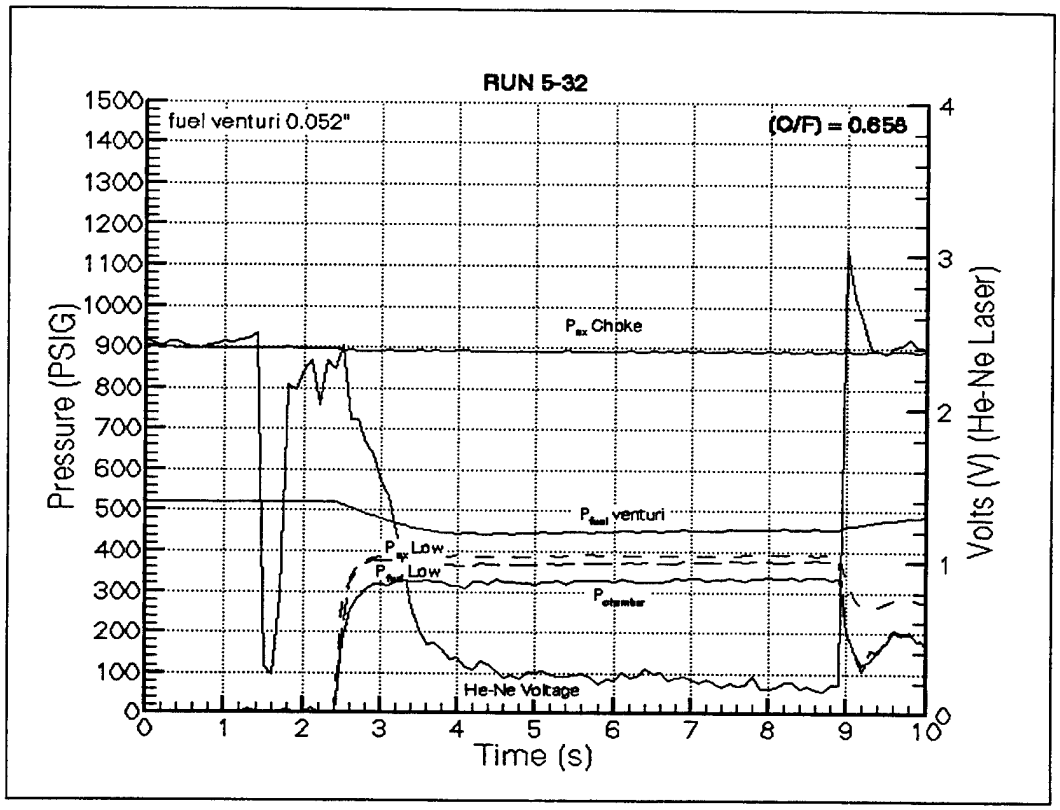
RUN 5-32
fuel venturi 0.052"
(O/F) = 0.658
Pressure (PSIG)
Volts (V) (He-Ne Laser)
Time (s)
P_ox Choke
P_fuel venturi
P_ox Low
P_fuel Low
P_chamber
He-Ne Voltage

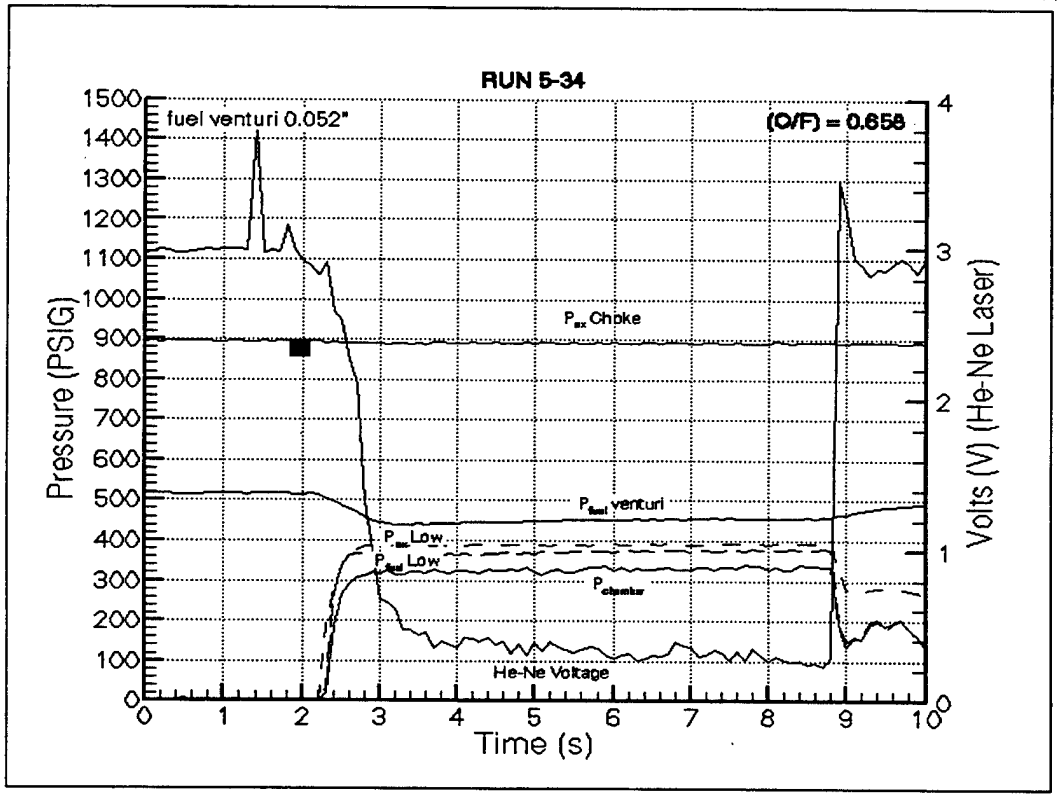
RUN 5-34
fuel venturi 0.052"
(O/F) = 0.658
Pressure (PSIG)
Volts (V) (He-Ne Laser)
Time (s)
P_ox Choke
P_fuel venturi
P_ox Low
P_fuel Low
P_chamber
He-Ne Voltage

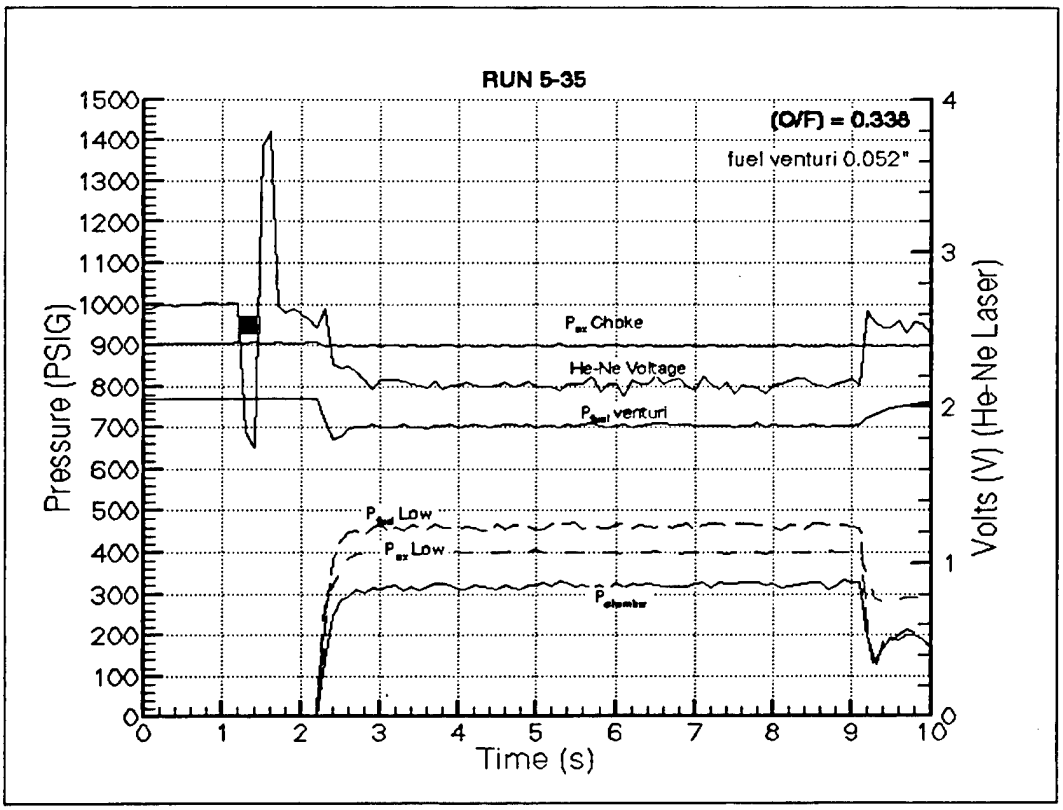
RUN 5-35
(O/F) = 0.338
fuel venturi 0.052"
Pressure (PSIG)
Volts (V) (He-Ne Laser)
Time (s)
P_ox Choke
He-Ne Voltage
P_fuel venturi
P_fuel Low
P_ox Low
P_chamber

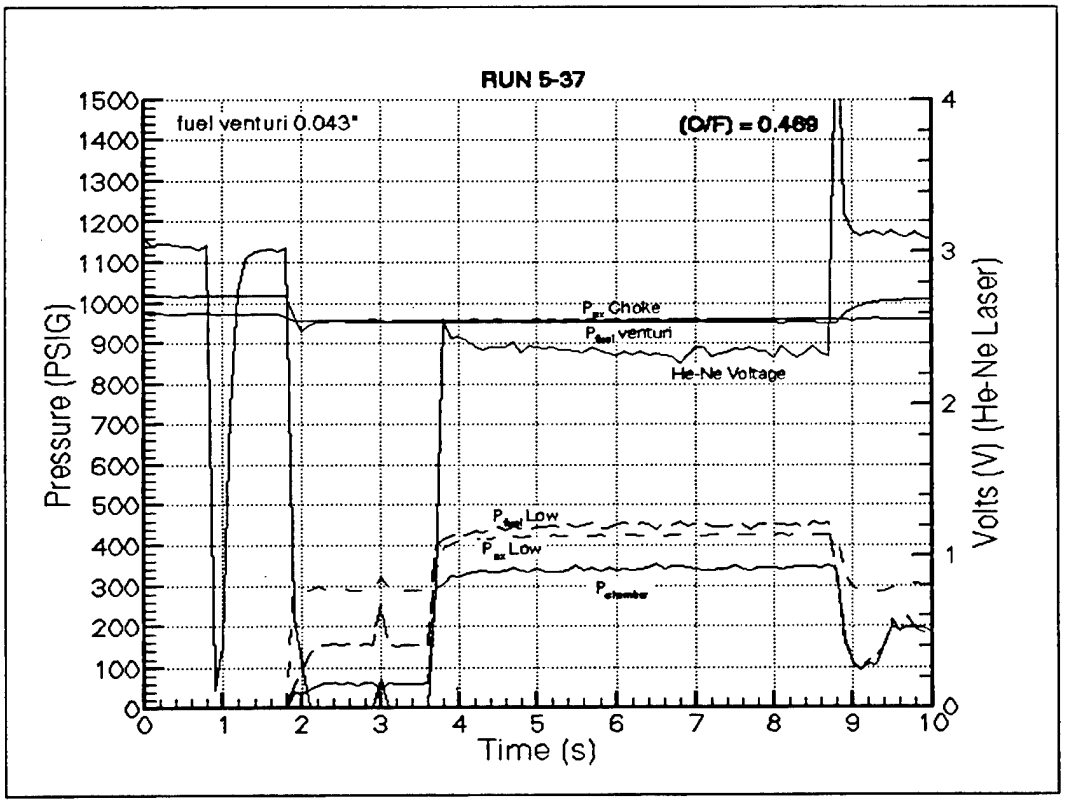
RUN 5-37
fuel venturi 0.043"
(O/F) = 0.469
Pressure (PSIG)
Volts (V) (He-Ne Laser)
Time (s)
P_ox Choke
P_fuel venturi
He-Ne Voltage
P_fuel Low
P_ox Low
P_chamber

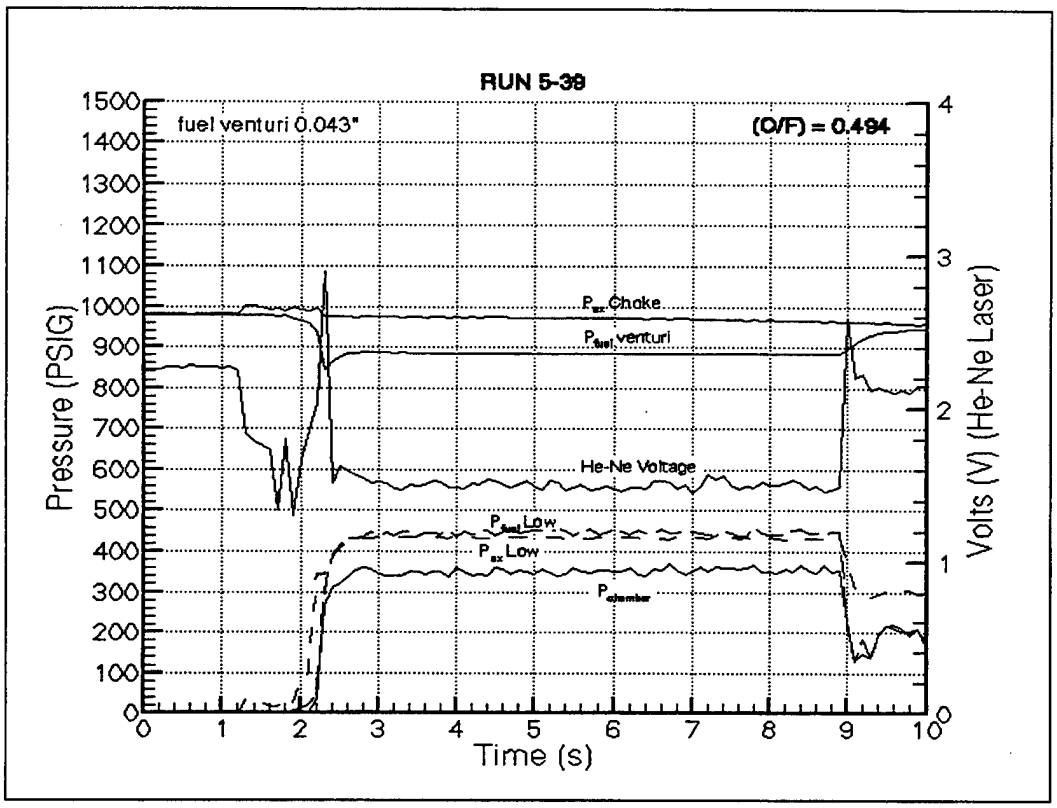
RUN 5-39
fuel venturi 0.043"
(O/F) = 0.494
Pressure (PSIG)
Volts (V) (He-Ne Laser)
Time (s)
P_ox Choke
P_fuel venturi
He-Ne Voltage
P_fuel Low
P_ox Low
P_chamber

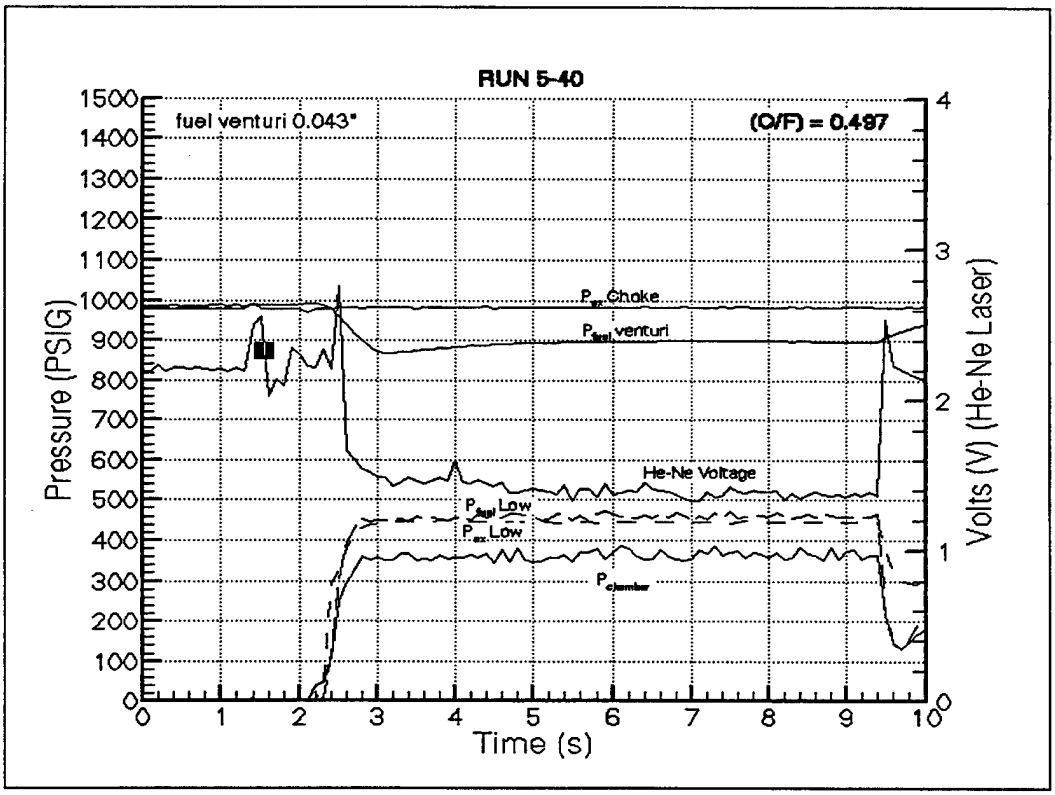
RUN 5-40
fuel venturi 0.043"
(O/F) = 0.497
Pressure (PSIG)
Volts (V) (He-Ne Laser)
Time (s)
P_ox Choke
P_fuel venturi
He-Ne Voltage
P_fuel Low
P_ox Low
P_chamber

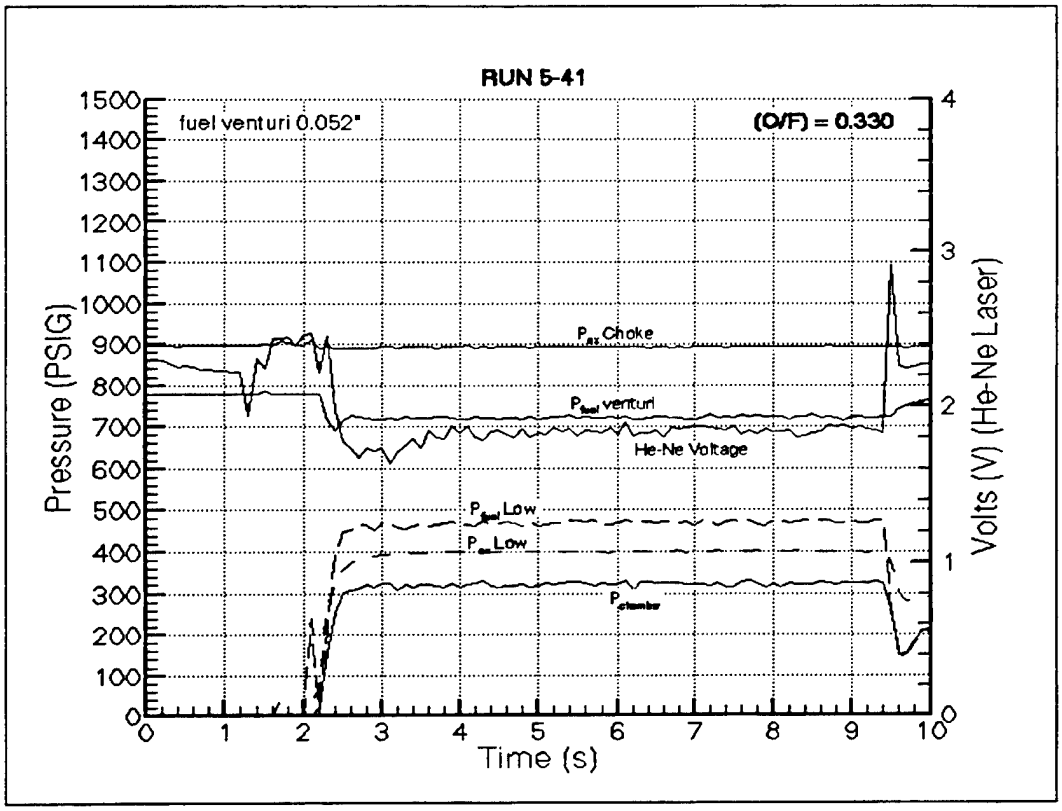
RUN 5-41
fuel venturi 0.052"
(O/F) = 0.330
Pressure (PSIG)
Volts (V) (He-Ne Laser)
Time (s)
He-Ne Voltage
Low
Low

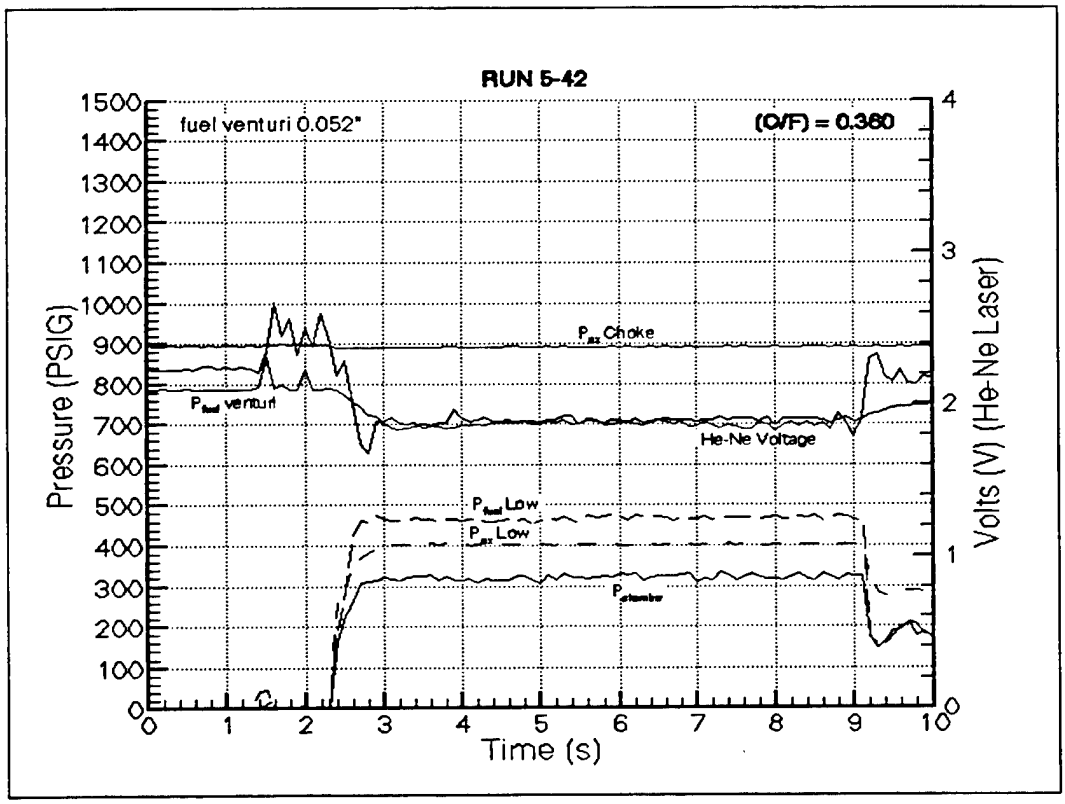
RUN 5-42
fuel venturi 0.052"
(O/F) = 0.360
Pressure (PSIG)
Volts (V) (He-Ne Laser)
Time (s)
He-Ne Voltage
Low
Low

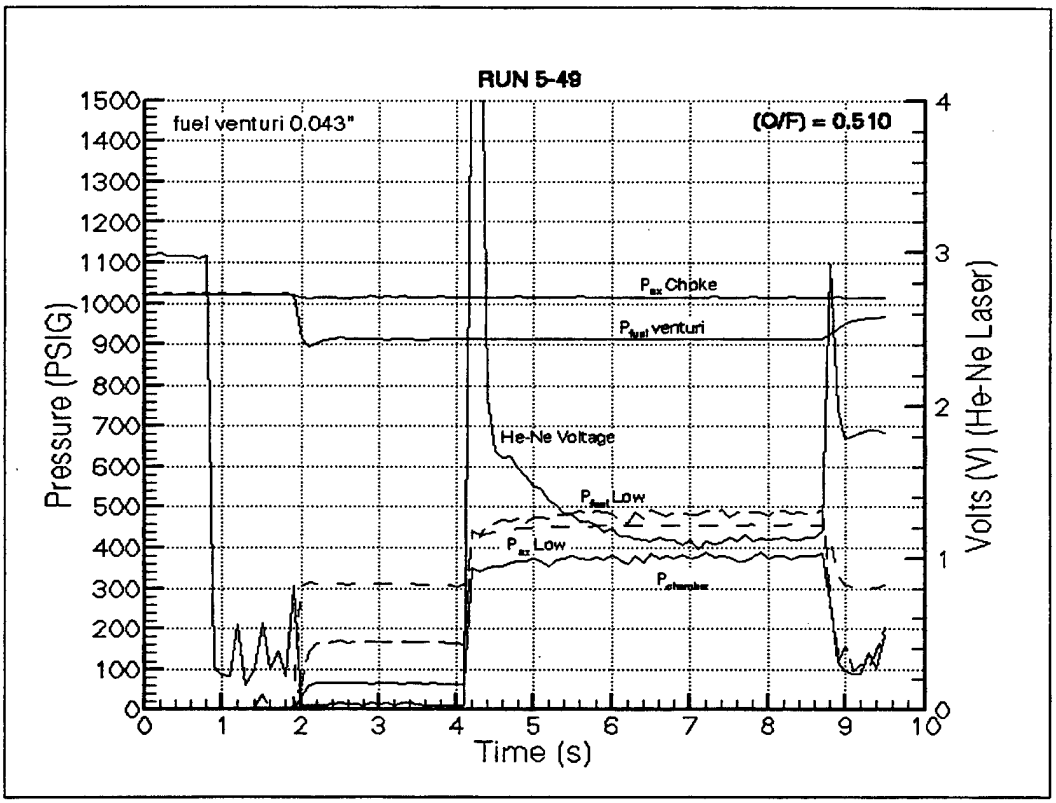
RUN 5-49
fuel venturi 0.043"
(O/F) = 0.510
Pressure (PSIG)
Volts (V) (He-Ne Laser)
Time (s)
He-Ne Voltage

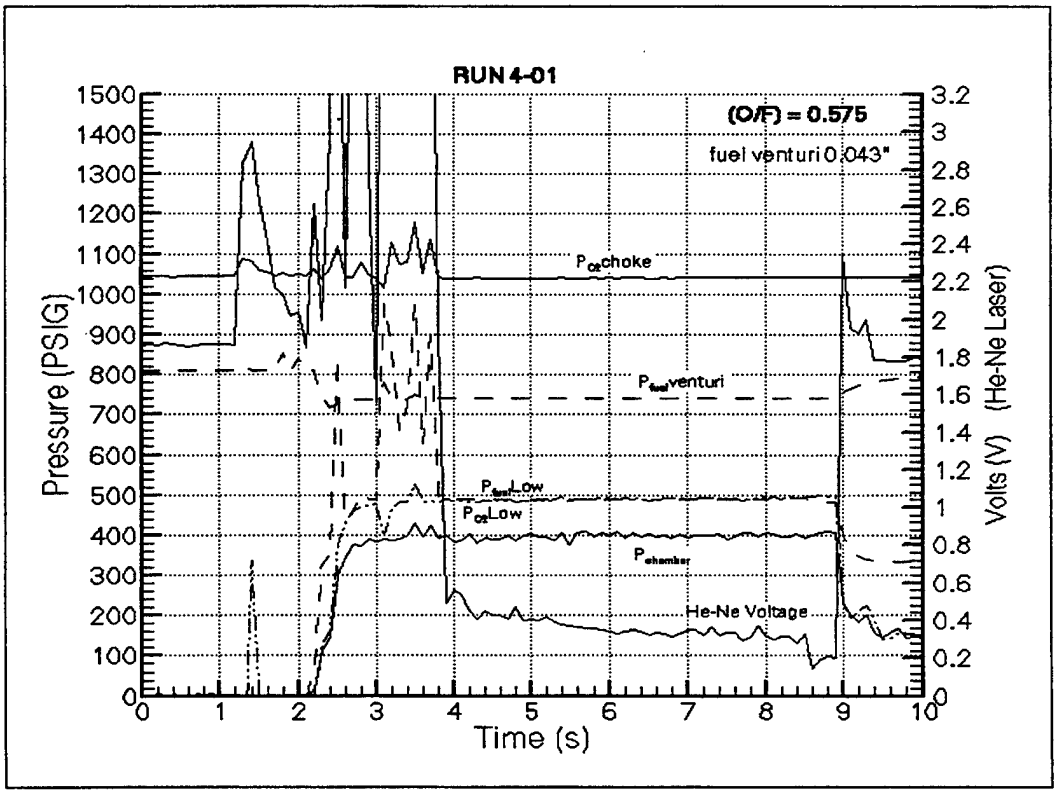
RUN 4-01
(O/F) = 0.575
fuel venturi 0.043"
Pressure (PSIG)
Volts (V) (He-Ne Laser)
Time (s)
He-Ne Voltage

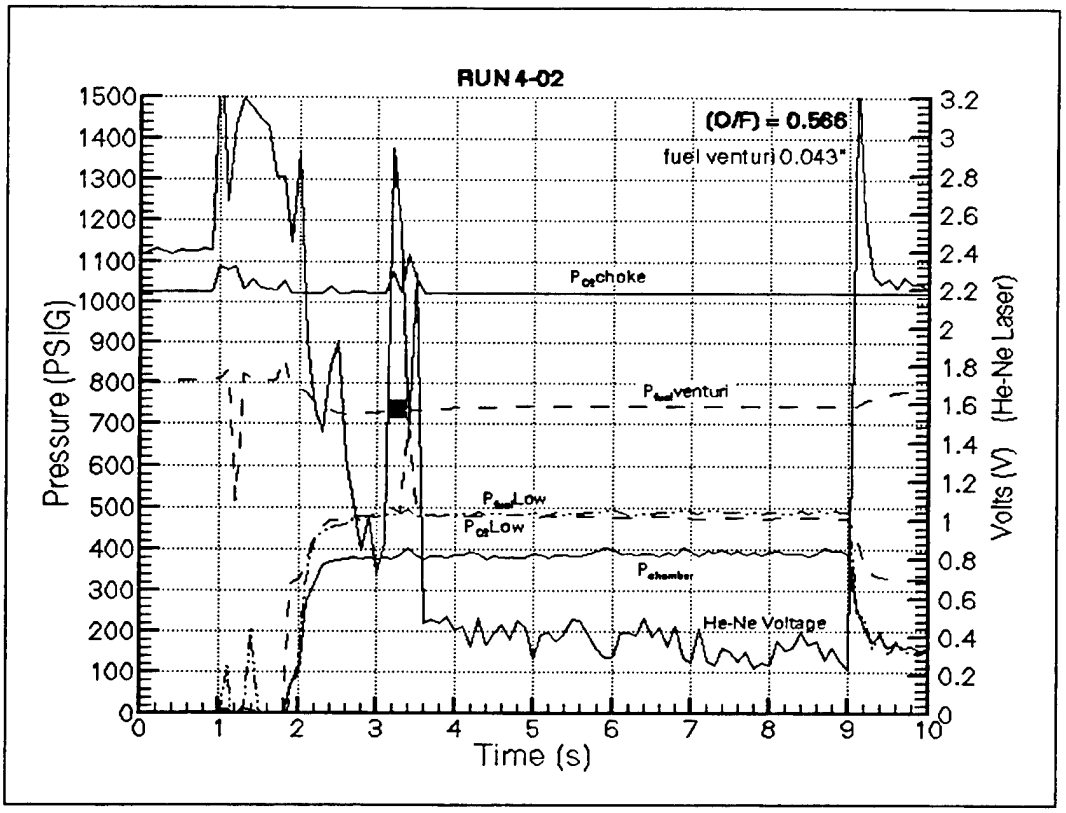
RUN 4-02
(O/F) = 0.566
fuel venturi 0.043"
P_{ox}choke
P_{fuel}venturi
P_{fuel}Low
P_{ox}Low
$P_{chamber}$
He-Ne Voltage
Pressure (PSIG)
Volts (V) (He-Ne Laser)
Time (s)

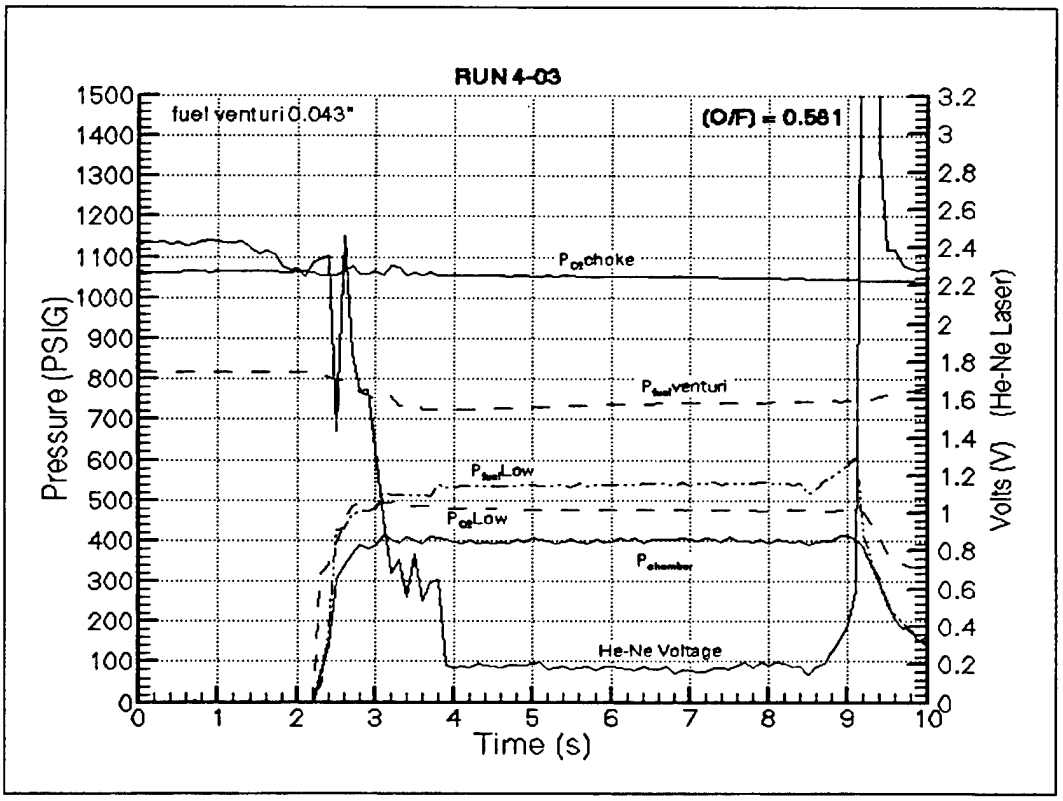
RUN 4-03
fuel venturi 0.043"
(O/F) = 0.581
P_{ox}choke
P_{fuel}venturi
P_{fuel}Low
P_{ox}Low
$P_{chamber}$
He-Ne Voltage
Pressure (PSIG)
Volts (V) (He-Ne Laser)
Time (s)

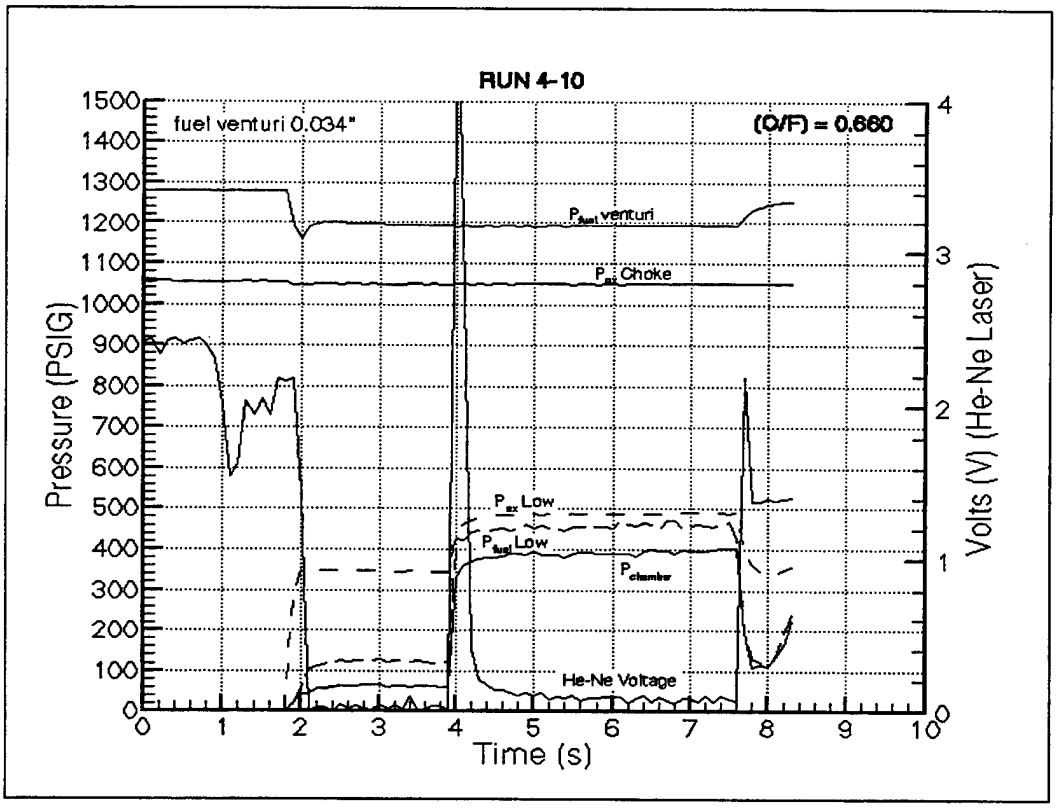
RUN 4-10
fuel venturi 0.034"
(O/F) = 0.660
P_fuel venturi
P_ox Choke
P_ox Low
P_fuel Low
P_chamber
He-Ne Voltage
Pressure (PSIG)
Volts (V) (He-Ne Laser)
Time (s)

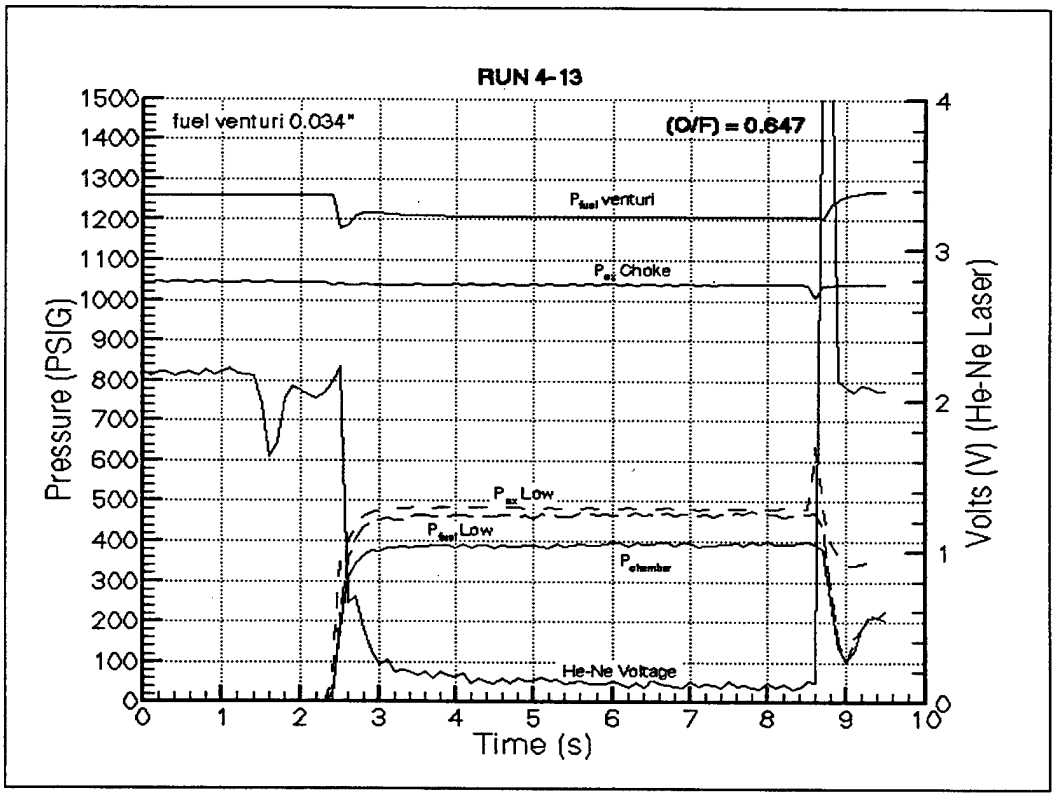
RUN 4-13
fuel venturi 0.034"
(O/F) = 0.647
P_fuel venturi
P_ox Choke
P_ox Low
P_fuel Low
P_chamber
He-Ne Voltage
Pressure (PSIG)
Volts (V) (He-Ne Laser)
Time (s)

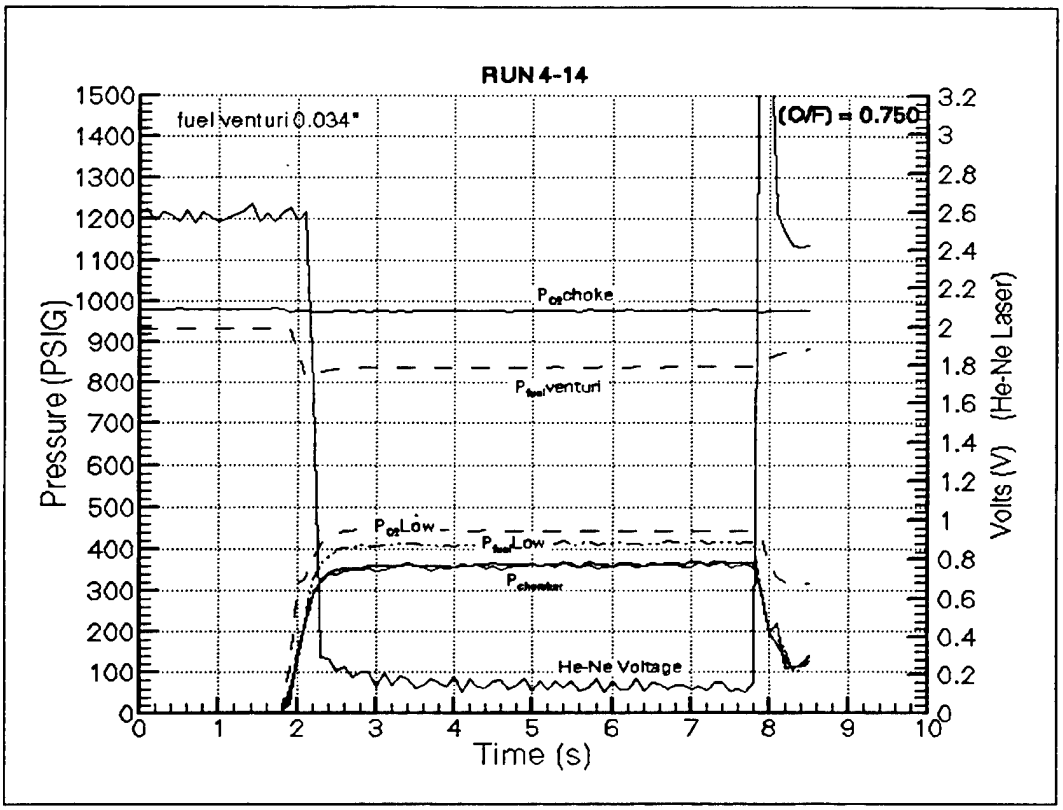
RUN 4-14
fuel venturi 0.034"
(O/F) = 0.750
P_{O2}choke
P_{fuel}venturi
P_{O2}Low
P_{fuel}Low
$P_{chamber}$
He-Ne Voltage
Pressure (PSIG)
Volts (V) (He-Ne Laser)
Time (s)

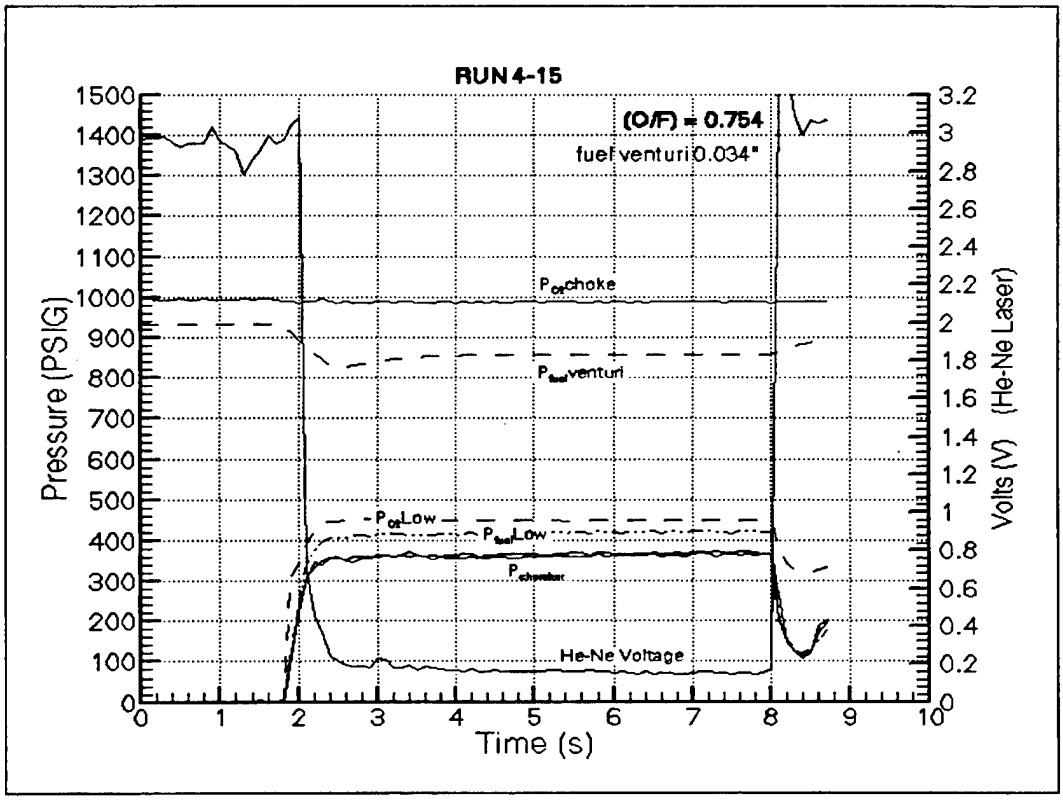
RUN 4-15
(O/F) = 0.754
fuel venturi 0.034"
P_{O2}choke
P_{fuel}venturi
P_{O2}Low
P_{fuel}Low
$P_{chamber}$
He-Ne Voltage
Pressure (PSIG)
Volts (V) (He-Ne Laser)
Time (s)

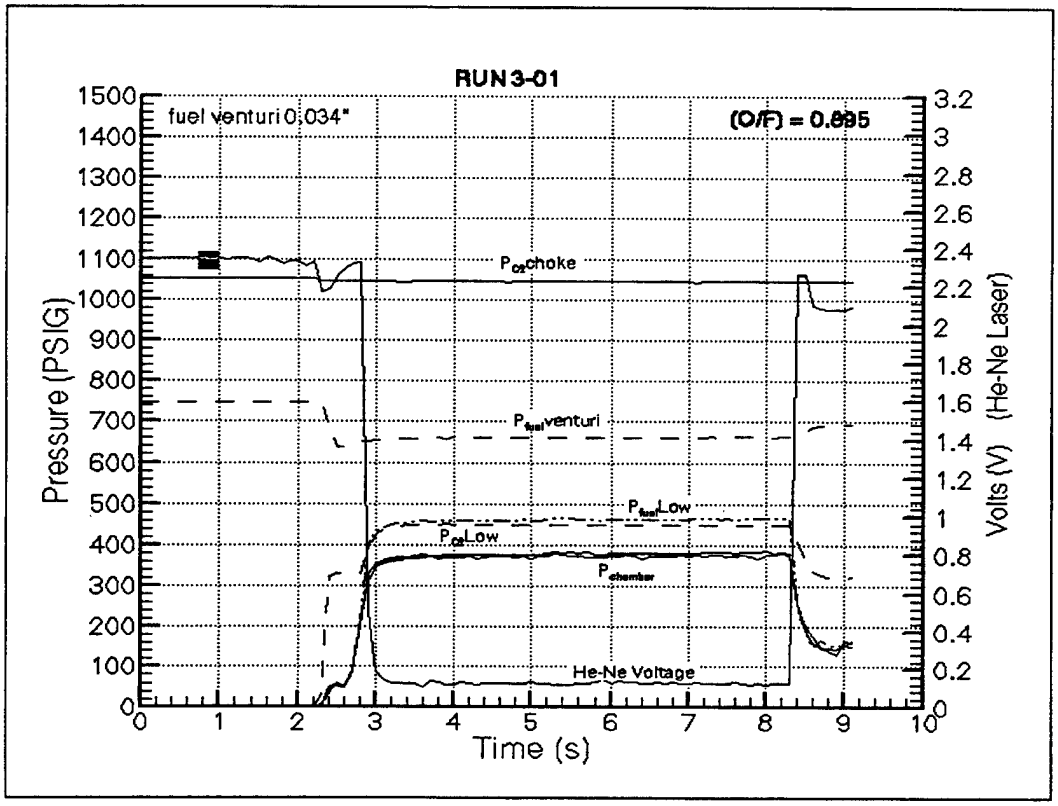
RUN3-01
fuel venturi 0.034"
(O/F) = 0.895
P_{O2}choke
P_{fuel}venturi
P_{fuel}Low
P_{O2}Low
$P_{chamber}$
He-Ne Voltage
Pressure (PSIG)
Volts (V) (He-Ne Laser)
Time (s)

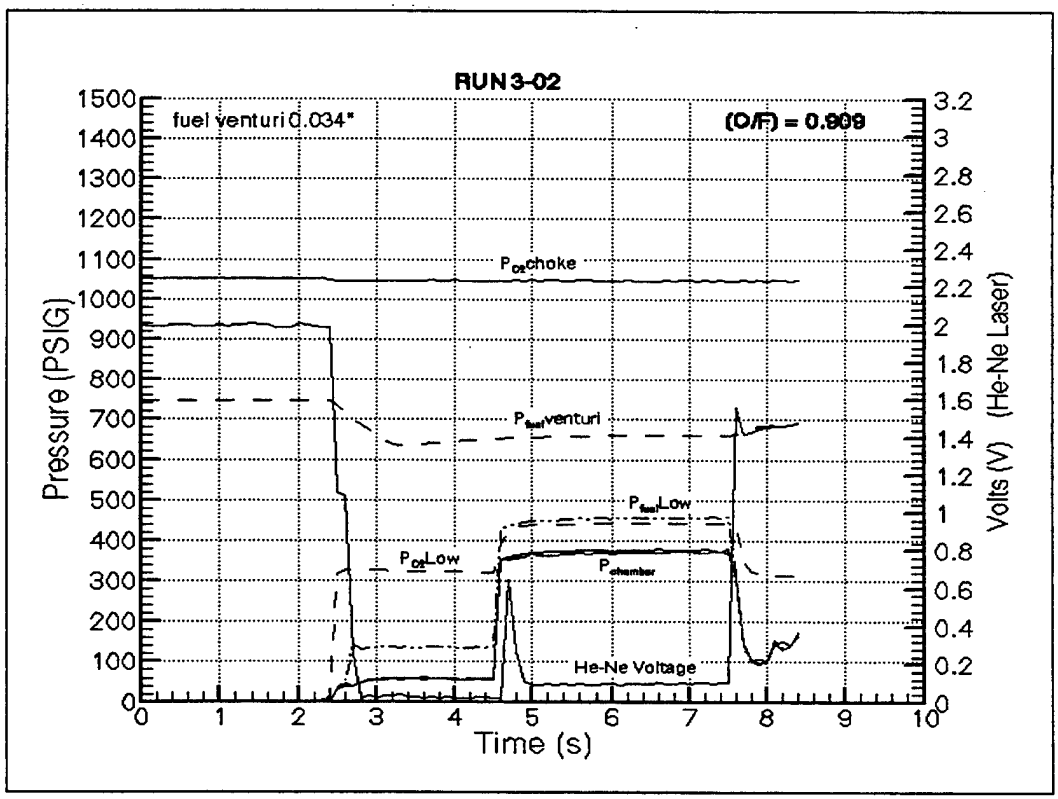
RUN3-02
fuel venturi 0.034"
(O/F) = 0.909
P_{O2}choke
P_{fuel}venturi
P_{fuel}Low
P_{O2}Low
$P_{chamber}$
He-Ne Voltage
Pressure (PSIG)
Volts (V) (He-Ne Laser)
Time (s)

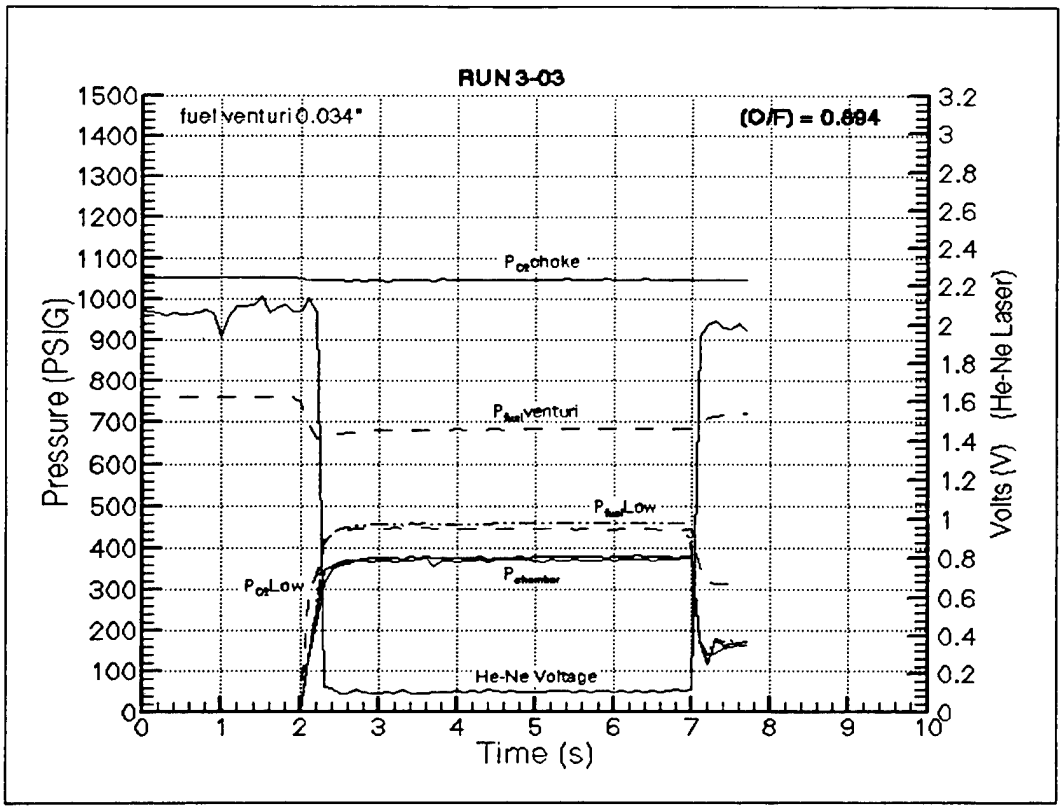
RUN 3-03
fuel venturi 0.034"
(O/F) = 0.884
P_{ox}choke
P_{fuel}venturi
P_{fuel}Low
P_{ox}Low
$P_{chamber}$
He-Ne Voltage
Pressure (PSIG)
Volts (V) (He-Ne Laser)
Time (s)

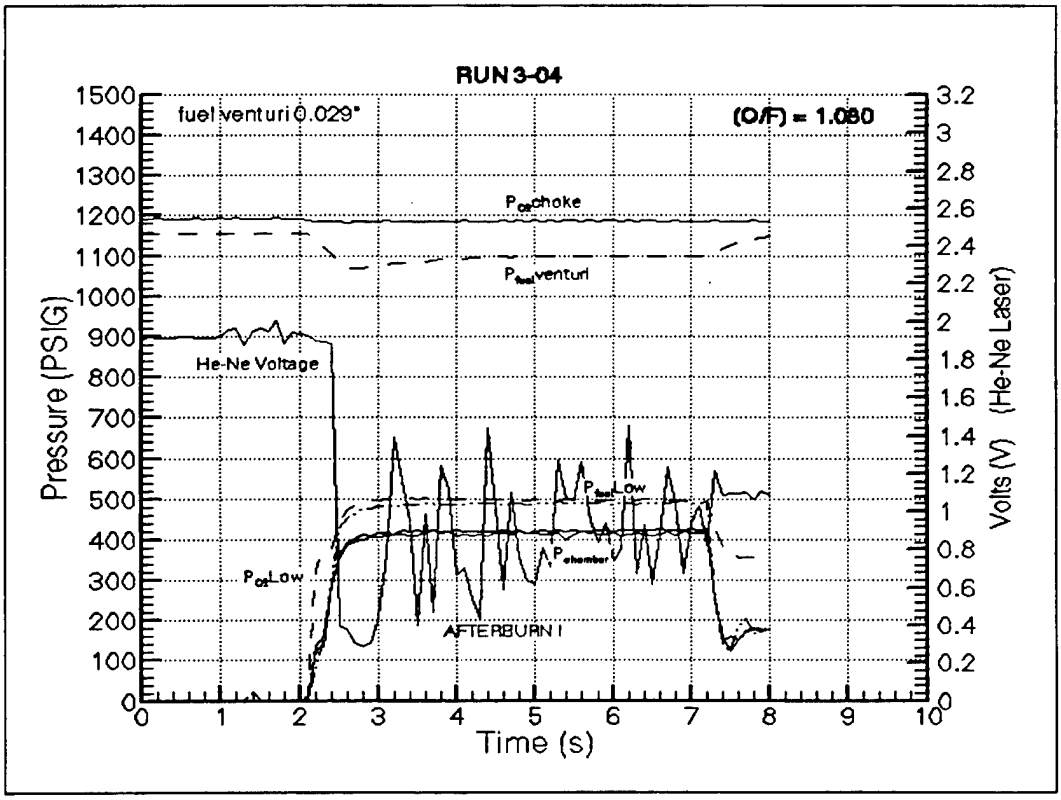
RUN 3-04
fuel venturi 0.029"
(O/F) = 1.080
P_{ox}choke
P_{fuel}venturi
He-Ne Voltage
P_{fuel}Low
$P_{chamber}$
P_{ox}Low
AFTERBURN I
Pressure (PSIG)
Volts (V) (He-Ne Laser)
Time (s)

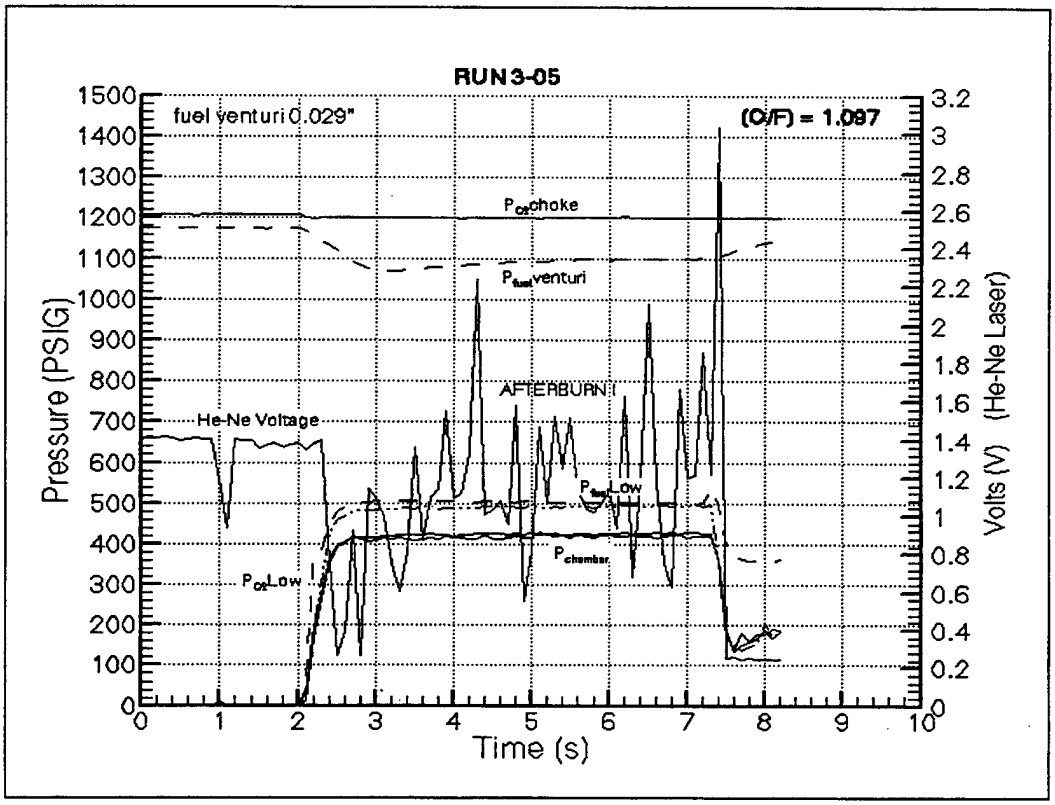
RUN 3-05
fuel venturi 0.029"
(O/F) = 1.097
P_{ox}choke
P_{fuel}venturi
AFTERBURN I
He-Ne Voltage
P_{fuel}Low
$P_{chamber}$
P_{ox}Low
Pressure (PSIG)
Volts (V) (He-Ne Laser)
Time (s)

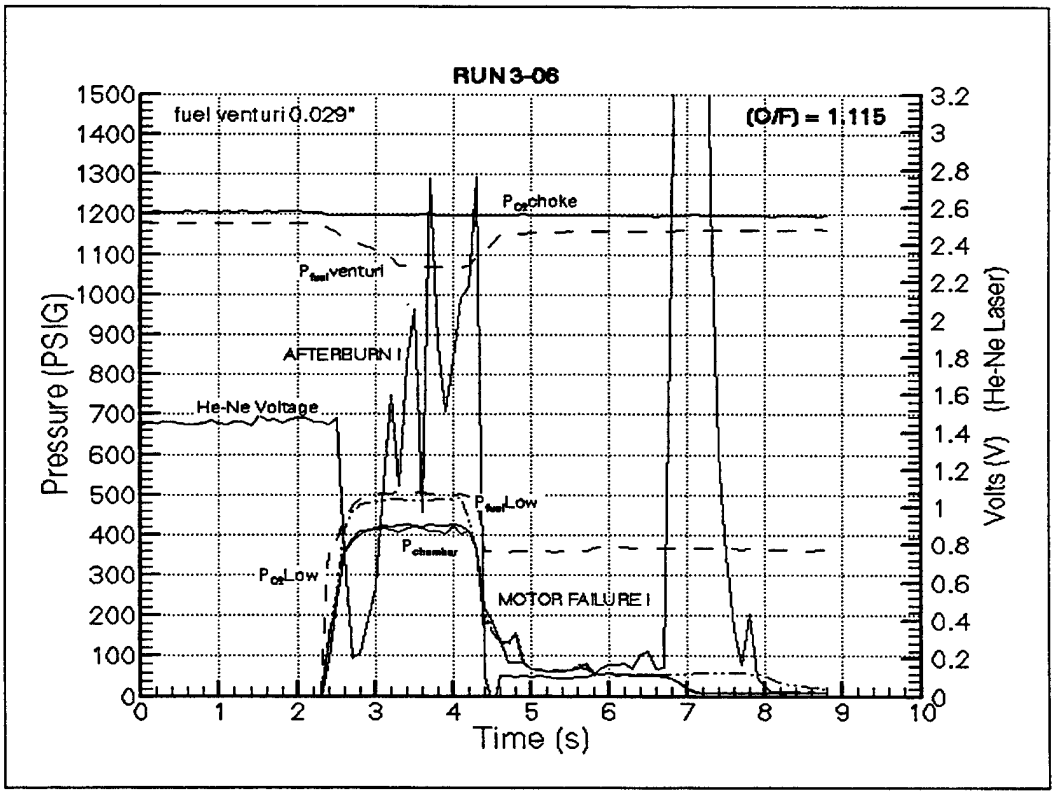
RUN 3-06
fuel venturi 0.029"
(O/F) = 1.115
P_{ox}choke
P_{fuel}venturi
AFTERBURN I
He-Ne Voltage
P_{fuel}Low
$P_{chamber}$
P_{ox}Low
MOTOR FAILURE I
Pressure (PSIG)
Volts (V) (He-Ne Laser)
Time (s)

APPENDIX D. WHITE LIGHT TRANSMISSIONS TRACES

The following five-wavelength power peak white light traces represent the main (O/F) ratios whose soot concentration results were relatively repeatable, since most of these kind of traces are similar.

Runs whose transmissions traces are shown are:

5-41 -- O/F = 0.333,	5-39 -- O/F = 0.494,	4-01 -- O/F = 0.575,
4-15 – O/F = 0.754,	3-02 -- O/F = 0.909,	3-05 -- O/F = 1.097.

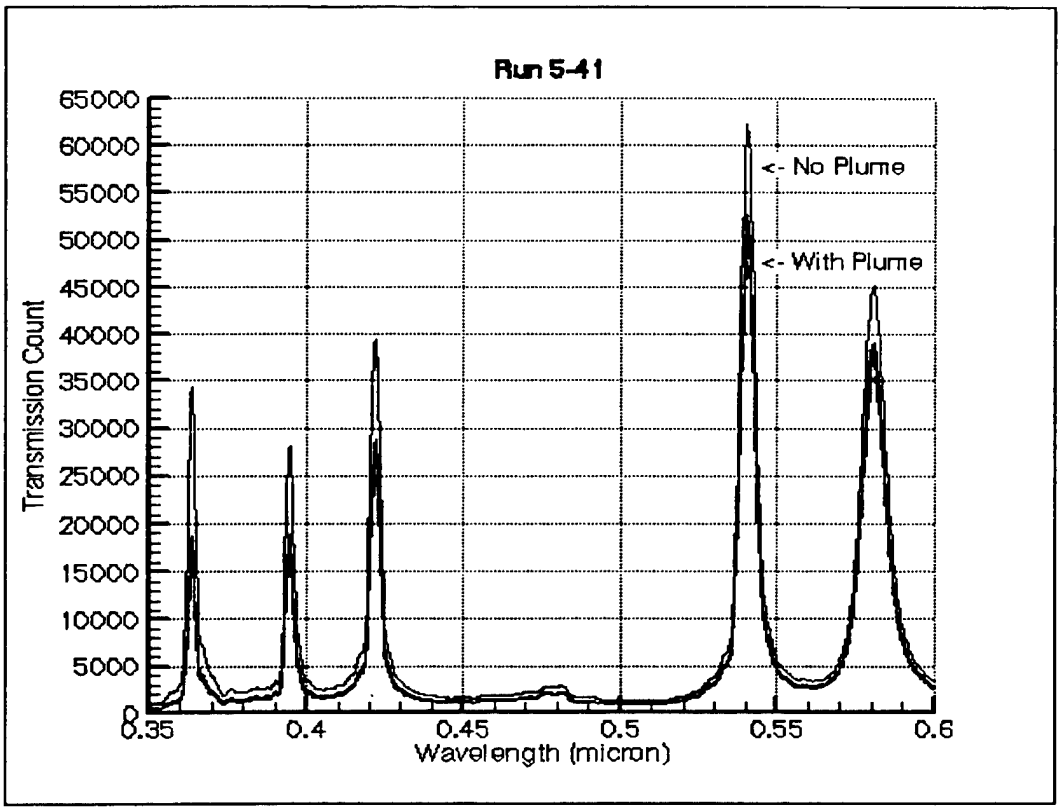
Run 5-41
65000
60000
55000
50000
45000
40000
35000
30000
25000
20000
15000
10000
5000
0
Transmission Count
0.35
0.4
0.45
0.5
0.55
0.6
Wavelength (micron)
<- No Plume
<- With Plume

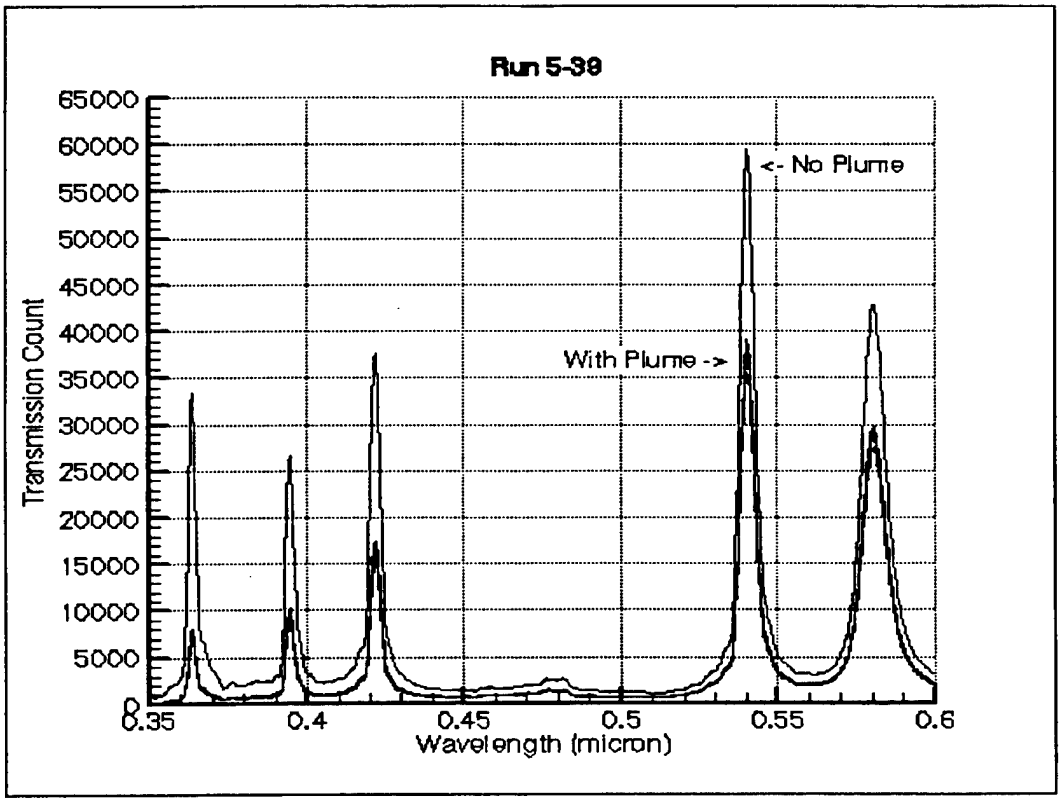
Run 5-39
65000
60000
55000
50000
45000
40000
35000
30000
25000
20000
15000
10000
5000
0
Transmission Count
0.35
0.4
0.45
0.5
0.55
0.6
Wavelength (micron)
<- No Plume
With Plume ->

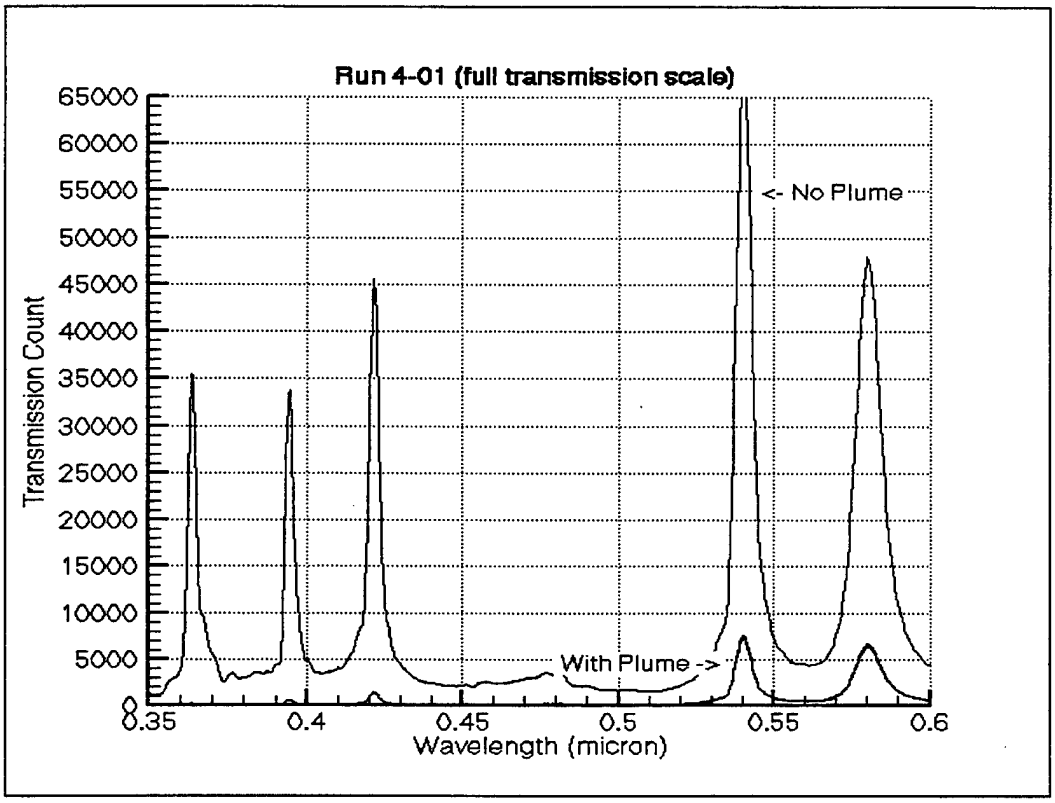
Run 4-01 (full transmission scale)
Transmission Count
65000
60000
55000
50000
45000
40000
35000
30000
25000
20000
15000
10000
5000
0
<- No Plume
With Plume ->
0.35
0.4
0.45
0.5
0.55
0.6
Wavelength (micron)

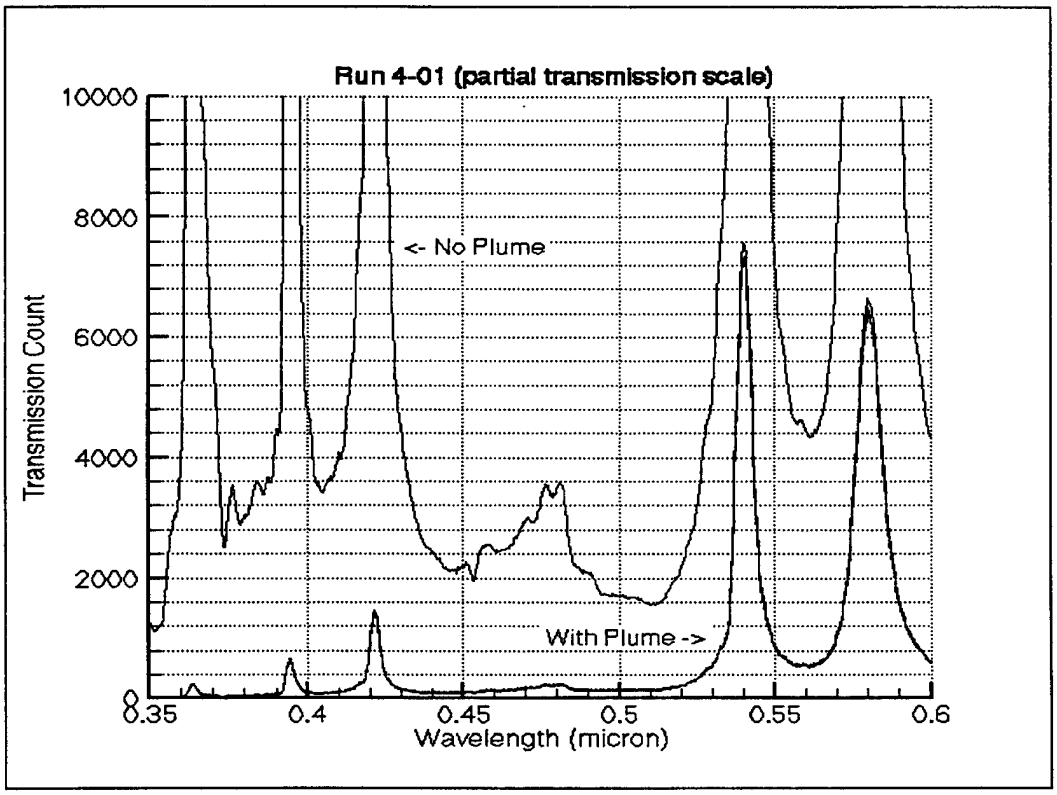
Run 4-01 (partial transmission scale)
Transmission Count
10000
8000
6000
4000
2000
0
<- No Plume
With Plume ->
0.35
0.4
0.45
0.5
0.55
0.6
Wavelength (micron)

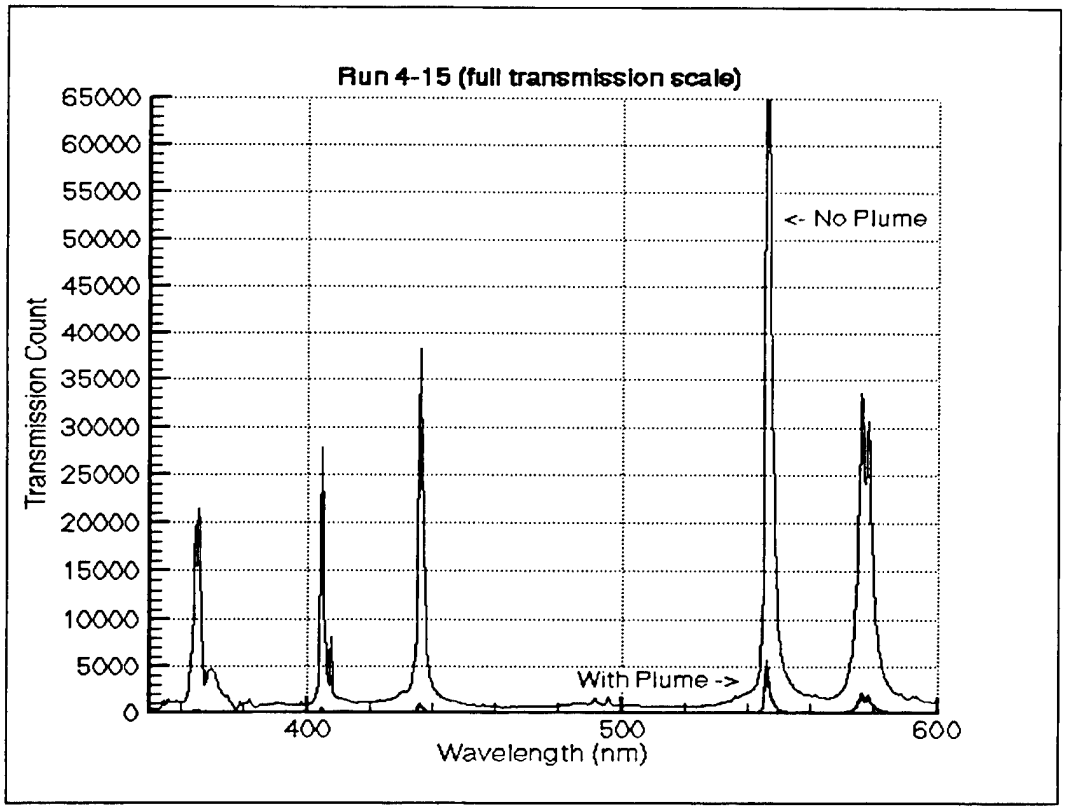
Run 4-15 (full transmission scale)
Transmission Count
65000
60000
55000
50000
45000
40000
35000
30000
25000
20000
15000
10000
5000
0
<- No Plume
With Plume ->
400
500
600
Wavelength (nm)

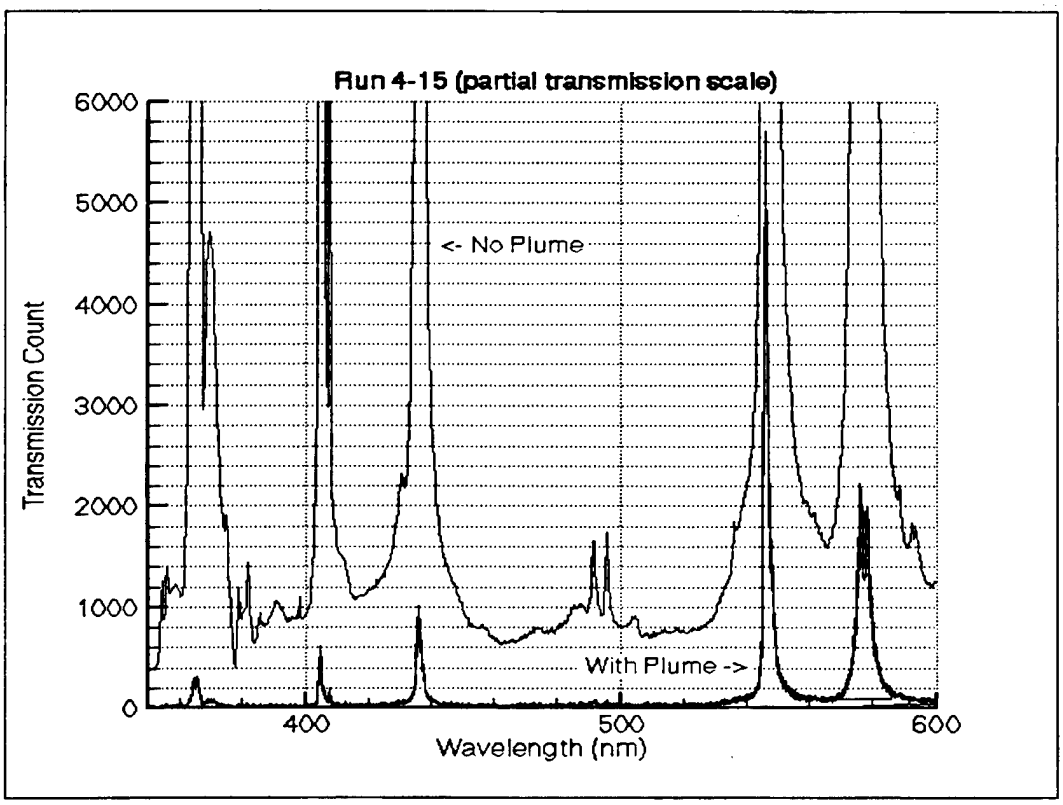
Run 4-15 (partial transmission scale)
Transmission Count
6000
5000
4000
3000
2000
1000
0
<- No Plume
With Plume ->
400
500
600
Wavelength (nm)

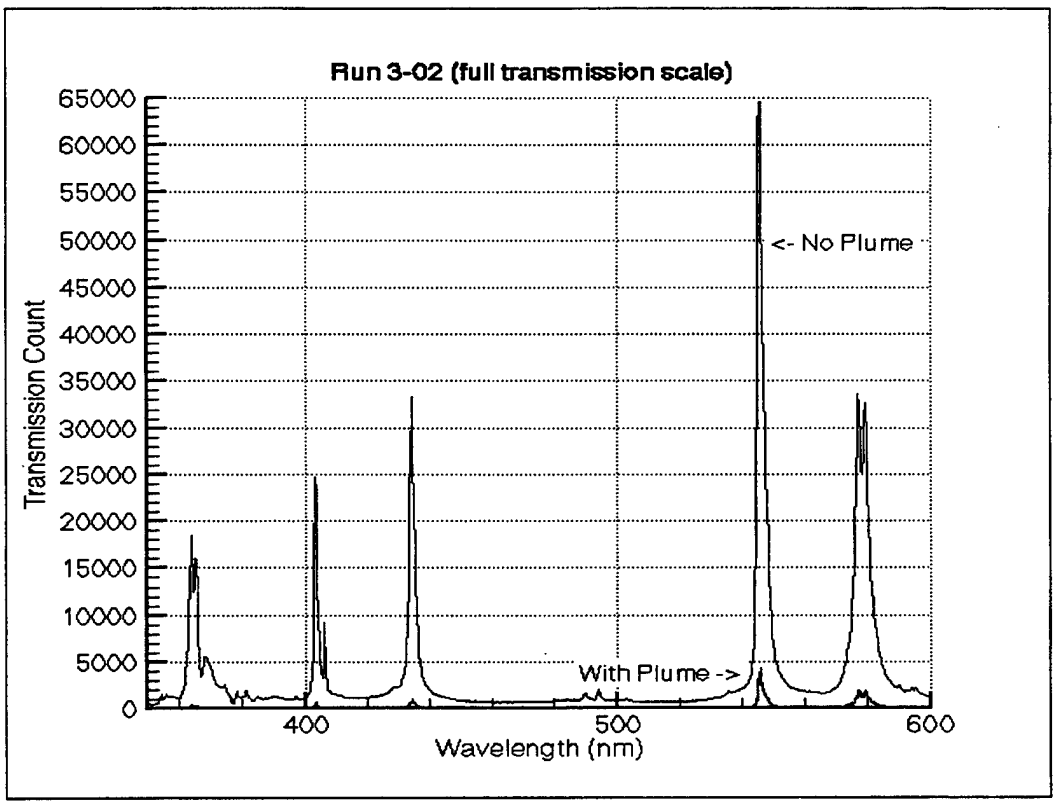
Run 3-02 (full transmission scale)
Transmission Count
65000
60000
55000
50000
45000
40000
35000
30000
25000
20000
15000
10000
5000
0
400
500
600
Wavelength (nm)
<- No Plume
With Plume ->

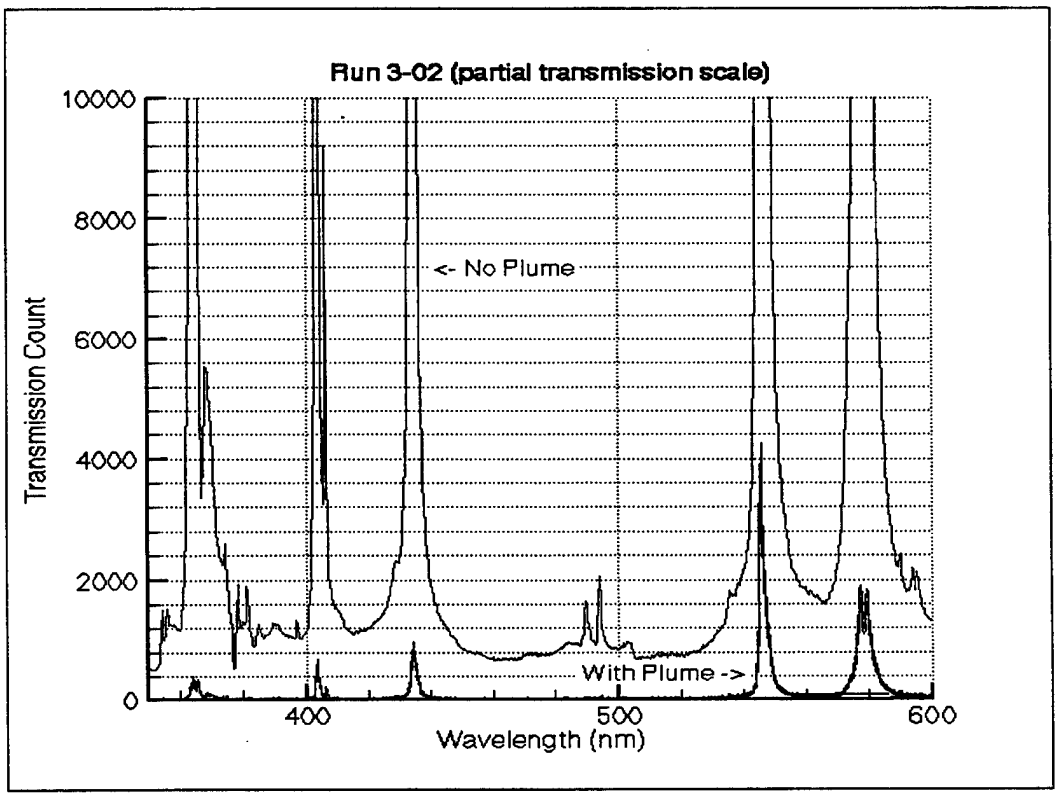
Run 3-02 (partial transmission scale)
Transmission Count
10000
8000
6000
4000
2000
0
400
500
600
Wavelength (nm)
<- No Plume
With Plume ->

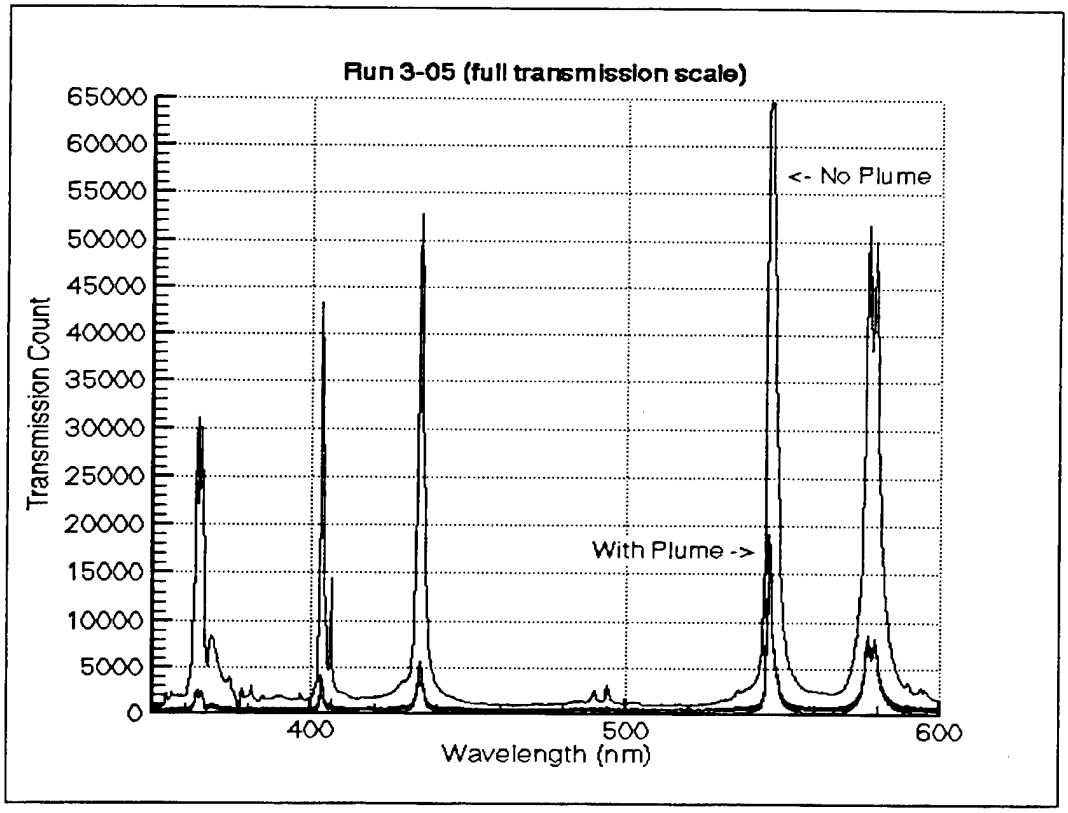
Run 3-05 (full transmission scale)
Transmission Count
65000
60000
55000
50000
45000
40000
35000
30000
25000
20000
15000
10000
5000
0
400
500
600
Wavelength (nm)
<- No Plume
With Plume ->

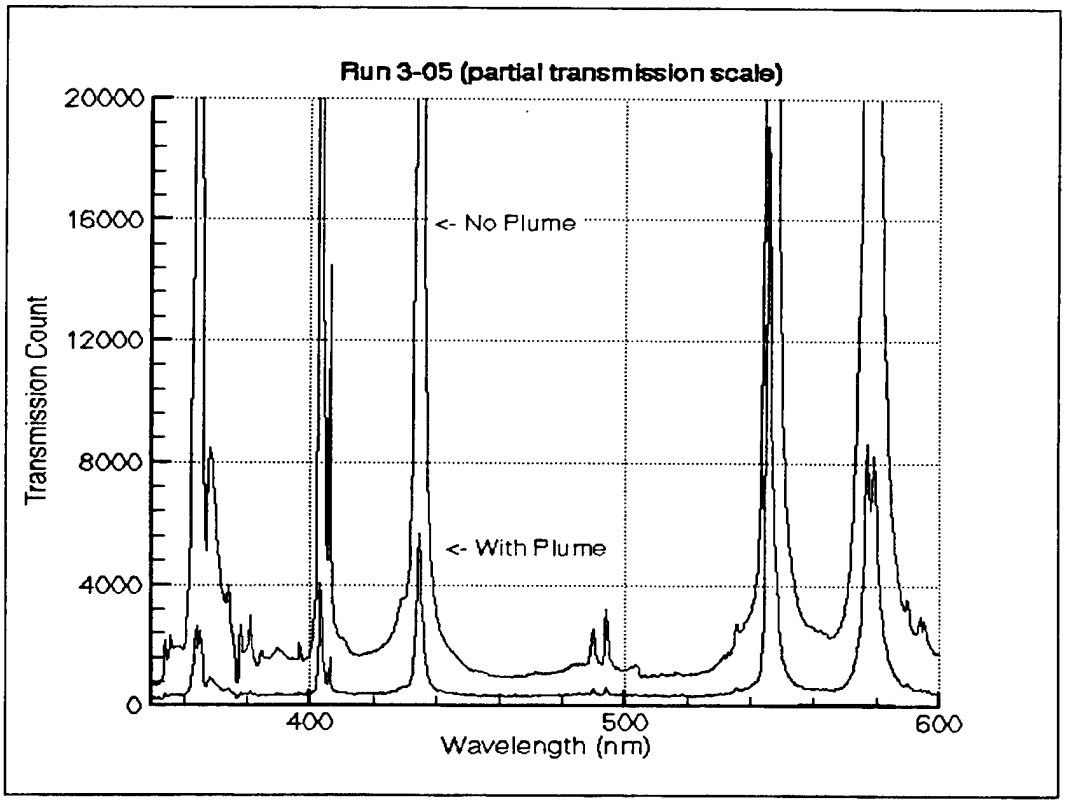
Run 3-05 (partial transmission scale)
Transmission Count
20000
16000
12000
8000
4000
0
400
500
600
Wavelength (nm)
<- No Plume
<- With Plume

LIST OF REFERENCES

1. Kuo, K.K., "Principles of Combustion", John Wiley & Sons, Inc., Chapter 8, 1986.

2. Cashdollar, K.L. , Lee, C.K. , and Singer, J.M., "Three Wavelength Light Transmission Technique to Measure Smoke Particle Size and Concentration", Applied Optics, 18, page 1763, June 1979.

3. Swenson, A. W. , "Liquid Hydrocarbon Fuel Composition Effects on Plume Characteristics", M.S. Thesis, Naval Postgraduate School, 55 pages, Dec 1995.

4. Haynes, B.S., "Soot and Hydrocarbons in Combustion", in Fossil Fuel Combustion, John Wiley & Sons Inc.., Chapter 5, pages 291-320, 1991.

5. Glassman, I., "Combustion", Academic Press, Inc. , New York, Chapter 6 & 8, 1977.

6. Stull, R.V. and Plass, G.N., "Emissivity of Dispersed Carbon Particles", J. Opt. Soc. Am. , 50, pp. 121, February 1960.

7. Manser, J. R. , "Solid Rocket Motor Plume Particle Size Measurements Using Multiple Optcal Techniques in a Probe", M.S. Thesis, Naval Postgraduate School, 111 pages, March 1995.

8. Powell, E. A., et al, "Combustion Generated Smoke Diagnostics by Means of Optical Measurement Techniques", AIAA Paper No. 76-67, presented at the 14th AIAA Aerospace Sciences Meeting, Washington D.C. , January 1976.

9. Dobbins, R.A. and Jismagian, G.S., "Optical Scattering Cross Sections for Polydispersions of Dielectric Spheres", Journal of the Optical Society of America, Vol. 56, No. 10, pp. 1345, October 1966.

10. *TEP*[R] for Windows – A Combustion Analysis Tool, Version 1.0, User's Manual, Software and Engineering Associates, Inc., Carson City, Nevada.

11. Hodkinson, J.R., "The Optical Measurement of Aerosols", Aerosol Science, C.N. Davies, Ed., Chapter 10, pages 290-297, Academic Press, New York, 1966.

12. Lawver, B.R., "Testing of a Fuel/Oxidizer Rich High Pressure Preburner", NASA CR 165609, prepared by Aerojet Tech Systems Corporation, Contract NAS 3 22647, May 1982.

13. Powell, E.A., and Zinn, B.T.,"In Situ Measurement of the Complex Refractive Index of Combustion Generated Particulates", Combustion Diagnostics by Nonintrusive Methods, Ed. by McCay, T.D. and Roux, J.A., AIAA Progress in Astronautics and and Aeronautics, Vol. 92, pp 238-251.

14. Santoro, R.J., Semerjian, H.G., and Dobbins, R.A., "Interpretation of Optical Measurements of Soot in Flames", AIAA paper 83-1516, AIAA 18th Thermophysics Conference, June 1983.

INITIAL DISTRIBUTION LIST

1. Defense Technical Information Center 2
   8725 John J. Kingman Rd., STE 0944
   Ft. Belvoir, VA 22060-6218

2. Dudley Knox Library 2
   Naval Postgraduate School
   411 Dyer Rd.
   Monterey, CA 93943-5000

3. Professor David W. Netzer 2
   Naval Postgraduate School - Code 09
   Monterey, CA 93943

4. Professor Oscar Biblarz 1
   Naval Postgraduate School - Code AA/BI
   Monterey, CA 93943

5. Associate Research Professor Christopher M. Brophy 1
   Naval Postgraduate School - Code AA/BR
   Monterey, CA 93943

6. Chairman of the Department of Aeronautics and Astronautics 1
   Professor Gerald H. Lindsey
   Naval Postgraduate School - Code AA/LI
   Monterey, CA 93943

7. Mr. Tom Smith 1
   U.S. Air Force Phillips Laboratory
   10 East Saturn Blvd.
   Edwards AFB – CA 93524-7680

8. Mr. Marty Venner 1
   U.S. Air Force Phillips Laboratory
   10 East Saturn Blvd.
   Edwards AFB – CA 93524-7680

9. Mr. Curtis Johnson 1
   Johnson Rockets
   318 North Carson Street, Suite 203
   Carson City – NV 89701

10. Centro Tecnico Aeroespacial 1
    ITA – Biblioteca Central
    Praca Mal. Eduardo Gomes, 50.
    S. Jose dos Campos – SP – BRASIL - 12228-900

11. Instituto de Atividades Espaciais 1
    Divisao de Sistemas Belicos – Biblioteca
    Praca Mal. Eduardo Gomes, 50.
    S. Jose dos Campos – SP – BRASIL - 12228-904

12. Major Silvino Luiz Carvalheiro da Silva 1
    CTA-IAE- Divisao de Sistemas Belicos
    Praca Mal. Eduardo Gomes, 50.
    S. Jose dos Campos – SP – BRASIL - 12228-904